

Aus dem Zentrum für Translationale Knochen-, Gelenk- und Weichgewebeforschung
Leiter: Herr Prof. Dr. Michael Gelinsky

**Pine oil mixed with hydroxyapatite for coating on CoCr alloy under heat treatment as a
biomaterial for bone replacement application**

D i s s e r t a t i o n s s c h r i f t
zur Erlangung des akademischen Grades
Doctor of Philosophy (Ph.D.),
vorgelegt
der Medizinischen Fakultät Carl Gustav Carus
der Technischen Universität Dresden

von

M.Sc. Fernanda Albrecht Vechietti

aus São Luiz Gonzaga, Brasilien

Dresden 2019

From the Laboratory of Biomaterials & Advanced Ceramics
Head: Prof. Dr. Luís Alberto Loureiro dos Santos
From the Center for Translational Bone, Joint and Soft Tissue Research
Head: Prof. Dr. Michael Gelinsky

Pine oil mixed with hydroxyapatite for coating on CoCr alloy under heat treatment as a biomaterial for bone replacement application

PhD thesis for obtaining the academic degree of
Doctor of Engineering of the Graduate Program in Mining, Metals and Materials Engineering
– PPGE3M of the Universidade Federal do Rio Grande do Sul, Brasil, and
Doctor of Philosophy (Ph.D.) of the Faculty of Medicine Carl Gustav Carus of the Technische
Universität Dresden, Germany

Agreement for joint supervision of doctoral studies leading to the award of a joint or a dual
doctoral degree.

Submitted by:
M.Sc. Fernanda Albrecht Vechietti
Born in São Luiz Gonzaga, Brazil

Porto Alegre - Brazil/Dresden - Germany,
2019

1. Gutachter: Herr Prof. Dr. rer. nat. Michael Gelinsky – Medizinische Fakultät Carl Gustav Carus der Technischen Universität Dresden

2. Gutachter:

3. Gutachter:

Tag der mündlichen Prüfung:

(Verteidigungstermin) gez: -----

Vorsitzender der Promotionskommission

Contents

List of Figures	vi
List of Tables	ix
List of Abbreviations	x
Summary	xi
1. Introduction	1
1.1 Objective	3
2. Literature review	4
2.1 Metallic biomaterials	4
2.1.1 Co-based alloys	5
2.1.2 Corrosion of CoCr alloys	7
2.2 Surface of metallic implants	11
2.3 Interface between substrate and coating	12
2.4 Cell-surface interaction	13
2.5 Calcium phosphates (CaP)	15
2.5.1 Hydroxyapatite	15
2.6 HAp coating	16
2.6.1 HAp coating methods	16
3. Materials & methods	27
3.1 Synthesis and characterization of HAp powder	27
3.2 Preparation of metallic substrate	27
3.3 Thermal behavior of the Pine Oil	28
3.4 HAp/pine oil slurry preparation and coating process	28
3.5 Characterization of the coating	29
3.6 Surface topography and wettability	29
3.7 Scratch resistance of the coating	29
3.8 Corrosion tests	30

3.8.1 Cyclic voltammetry	31
3.8.2 Potentiodynamic polarization	31
3.9 <i>In vitro</i> bioactivity analyses	33
3.10 Cell culture	34
4. Results & Discussion	36
4.1 Characterization of HAp powder	36
4.2 Thermal characterization of the pine oil	38
4.3 Characterization of the coating surface	40
4.3.1 X-ray diffraction and FTIR analyses	43
4.4 Surface properties	45
4.4.1 Topography, roughness and wettability	45
4.5 Scratch resistance of the coating	50
4.6 In vitro bioactivity and morphology	53
4.7 Metallography of the Co-15Cr-15W-10Ni alloy	62
4.8 Corrosive behavior	63
4.8.1 Effect of heat treatment on corrosion resistance	66
4.9 Cell Proliferation and osteogenic differentiation	68
5. Conclusions	73
5.1 Future perspectives	74
6. References	75
Acknowledgements	90

List of Figures

Figure 1. Metallic materials and their applications in human body as biomaterial devices. _____	5
Figure 2. Electrochemical cell shows how the chemical reaction occurs on the metallic biomaterials exposed to an aqueous environment (into human body). _____	8
Figure 3. (A) Revision surgery of a hip joint with soft tissue reaction to metal ions around the implant. (B) Photograph shows the base of the modular neck with severe wear and (C) parts of a hip prosthesis with severe signs of wear at the base of modular neck. _____	10
Figure 4. Representation of the adhesion and cohesion forces within an adhesive and between an adhesive and substrate. _____	13
Figure 5. Demonstration of the sequential reactions that occurs after the implantation of a biomaterial into a living system. _____	14
Figure 6. (A) Coating of joint prostheses by plasma spray process on titanium substrate [87] and (B) commercial coatings of HAp obtained by plasma spray process [88]. _____	17
Figure 7. Schematic of an electrochemical process for deposition of HAp on 316L nanostructured stainless steel. _____	19
Figure 8. Nano-HAp coating on Ti6Al4V substrates obtained by EPD process: Fig 8-A shows the deposition at a time of 10 min. at different potentials: (A) 5 V, (b) 10 V, (C) 15 V and (D) 20 V and Fig 8-B shows the deposition at 10 V at different time points: (A) 5 min, (B) 10 min. (C) 15 min. and (D) 20 min.. _____	22
Figure 9. Morphology of the HAp coating fabricated by biomimetic method, using two SBF solutions (SBF-A 5x more concentrated than solution SBF-B): (A) SBF-A coating, (B) SBF-B coating after 5 h of soaking, (C) SBF-B coating after 6 h of soaking, and (D) SBF-B coating after 24 h of soaking on a Ti6Al4V plate. _____	26
Figure 10. Pencil hardness tester (PH-5800, BYK-Gardner GmbH, Geretsried, Germany) and scale of hardness from softer to harder pencil. _____	30
Figure 11. Representation of a potentiodynamic polarization curve. _____	32
Figure 12. X-ray diffraction spectrum of HAp powder obtained by wet route and sintered at 1110 °C (PDF 01-072-1243; 01-084-1998). _____	36
Figure 13. The FTIR spectrum of the HAp powder sintered at 1110 °C. _____	37
Figure 14. Particle size distributions of the HAp powder sintered at 1100 °C for 1 h (A) and appearance in scanning electron microscopy (B). _____	38
Figure 15. Weight loss of the PO (TGA). _____	39
Figure 16. DSC thermogram of the PO. _____	39
Figure 17. (A) Metallic substrate with slurry before to be fully brushed and (B) after brush coating with HAp/PO slurry. _____	40
Figure 18. (A) Optical microscopy and (B) SEM images of HAp coating after sintering. _____	41
Figure 19. Coated metallic substrate after sintering (A) and SEM micrograph of the cross-section (B). _____	42
Figure 20. (A) Coated metallic substrate and (B) SEM micrograph of the coating after scratch test with 4H pencil. _____	42

Figure 21. SEM micrograph of the HAp coating (A) and EDS spectra of the coating (B).	43
Figure 22. XRD pattern of HAp coating on CoCr alloy prepared by brushing method (PDF 01-072-1243; 01-084-1998).	43
Figure 23. FTIR spectra of the HAp/PO slurry before and after sintering.	44
Figure 24. Image of brushing coated samples on surfaces with different treatments (passivated (A), polishing (B), heat treated (C) and untreated) (D) after heat treatment.	46
Figure 25. Surface roughness images for uncoated samples: (a) heat treated surface ($R_a = 0.825 \pm 0.060 \mu\text{m}$); (b) surface untreated ($0.550 \pm 0.009 \mu\text{m}$); (c) polished surface ($0.274 \pm 0.033 \mu\text{m}$); (d) passivated surface ($0.477 \pm 0.018 \mu\text{m}$).	46
Figure 26. Surface roughness images for brush-coated samples: (a) coated heat treated surface ($R_a = 2.20 \pm 0.14 \mu\text{m}$); (b) coated untreated surface ($1.47 \pm 0.12 \mu\text{m}$); (c) coated polished surface ($1.48 \pm 0.03 \mu\text{m}$) and (d) passivated coated surface ($1.05 \pm 0.06 \mu\text{m}$).	48
Figure 27. Evaluation of the wettability tested with different liquids (water, PO and HAp/PO) on roughness properties of the uncoated substrates: polished, passivated, untreated and heat treated.	49
Figure 28. Effect of the different surface treatments on the contact angle values for the coated samples.	50
Figure 29. SEM micrographs of the coated CoCr substrates with different surface treatment: (A) heat treated, (B) untreated, (C) passivated, (D) polished.	51
Figure 30. Optical microscopy and SEM images of surface morphology after pencil scratch with different types of surface modification: Polished (A,B,C), passivated (D,E,F), untreated (G,H,I), heat treatment (J,K,L).	52
Figure 31. Coated passivated (left) and polished (right) substrate before of immersion in SBF.	53
Figure 32. SEM micrographs of the coated passivated substrate before and after soaking in SBF solution: (A) before soaking, after (B) 3 days, (C) 7 days, (D) 14 days, and (E) 21 days of soaking.	55
Figure 33. SEM micrographs of the coated polished substrate before and after soaking in SBF solution: (A) before soaking, after (B) 3 days, (C) 7 days, (D) 14 days, (E) 21 days of soaking.	56
Figure 34. SEM micrographs of HAp coated passivated substrate before and after immersion in SBF: (A) before soaking, after immersion for (A) 3 days, (C) 7 days, (D) 14 days and (E) 21 days.	57
Figure 35. SEM micrographs of HAp coated polished substrate before and after immersion in SBF: (A) before soaking, after immersion for (B) 3 days, (C) 7 days, (d) 14 days and (e) 21 days.	58
Figure 36. Surface morphologies of the coated passivated substrate before and after soaking in SBF: (A) before soaking, after soaking for (B) 3 days, (C) 7 days, (D) 14 days and (E) 21 days.	60
Figure 37. Surface morphologies of the coated polished substrate before and after soaking in SBF: (A) before soaking, after soaking for (B) 3 days, (C) 7 days, (D) 14 days and (E) 21 days.	61
Figure 38. Optical micrograph of the untreated (as-received) Co-15Cr-15W-10Ni alloy.	62

Figure 39. Optical micrograph of the Co-15Cr-15W-10Ni alloy after heat treatment at 800 °C for 1 h.	63
Figure 40. Comparison of cyclic voltammetry curves for Co-15Cr-15W-10Ni alloy samples in the as polished state (black) and after additional passivation in HNO ₃ (red) for the valence oxide states (I,II,III peaks), recorded in Ringer's solution.	64
Figure 41. Comparison of open circuit potentials of Pol, Pol_Pas_coa_800, Pol_Pas_coa_300, Pol_coa_800, developing upon 30 min immersion in Ringer's solution.	65
Figure 42. Linear potentiodynamic polarization plots made in duplicates for Co-15Cr-15W-10Ni alloy samples in the as polished state (Pol) and after additional passivation in HNO ₃ (Pol_Pas) recorded in Ringer's solution.	66
Figure 43. Linear potentiodynamic polarization plots for Co-15Cr-15W-10Ni alloy samples after HAp coating of the as polished state immersed in Ringer's solution.	67
Figure 44. Linear potentiodynamic polarization plots for Co-15Cr-15W-10Ni alloy samples after HAp coating of the passivated state, measured in Ringer's solution.	68
Figure 45. Development of cell numbers in indirect (left) and direct contact (right) to uncoated and coated polished substrates 1, 7, 14 and 21 days after cell seeding. Cell numbers were determined by quantification of the LDH activity.	70
Figure 46. Cell response to the adhesion assay (DNA) on coated polished substrate after 1, 7, 14 and 21 days of culturing.	70
Figure 47. Specific ALP activity of cells cultivated in presence (indirect, left) or directly on (right) uncoated and coated polished substrates after 7, 14 and 21 days. Enzyme activity was normalized to the cell number using the values achieved by DNA quantification.	71
Figure 48. Cell response of the differentiation assay of ALP (LDH) activity on coated polished substrate after 7, 14 and 21 days for the indirect and direct method achieved by LDH activity quantification.	72

List of Tables

<i>Table 1. Different deposition techniques of HAp and some main characteristics and process parameters.</i>	24
<i>Table 2. Characteristics of the Pine oil 65% for the slurry preparation.</i>	29
<i>Table 3 Description of the surface treatment and coating parameters of the CoCr disc samples.</i>	31
<i>Table 4. Purity and reagents quantity to prepare 1000 mL of SBF [129].</i>	33

List of Abbreviations

ALP:	Alkaline phosphatase
ACP:	Amorphous calcium phosphate
CaO:	Calcium oxide
ASTM:	American Society for Testing and Materials
CaP:	Calcium phosphate
CV:	Cyclic voltammetry
DSC:	Differential Scanning Calorimetry
DNA:	Deoxyribonucleic acid
E_{corr} :	Corrosion current density
EDS:	Energy-dispersive X-ray spectroscopy
EPD:	Electrophoretic deposition
FCC:	Centered cubic structure
FCS:	Fetal calf serum
FDA:	Food and Drug Administration
FTIR:	Fourier-transform infrared spectroscopy
HAp:	Hydroxyapatite
HC:	Hexagonal crystalline structure
IBAD:	Ions beam assisted deposition
I_{corr} :	Lower corrosion density
ISO:	International Organization for Standardization
LDH:	Lactate Dehydrogenase
OCP:	Open circuit potential
PBS:	Phosphate buffered saline
PLD:	Pulsed laser deposition
PO:	Pine Oil
SBF:	Simulated body fluid
SEM:	Scanning Electron Microscopy
TGA:	Thermogravimetric analysis
TTCO:	Tetracalcium phosphate
XRD:	X-ray diffraction

Summary

CoCr alloys have been used for orthopedic implants as they allow combining high strength, corrosion resistance and biocompatibility. Since 1985 metallic implants coated with calcium phosphates have been widely studied to improve the biocompatibility and adequate bonding to the adjacent bones, but despite of advances and development of many technologies, rate of failure of such implants still are a problem. In the present work, a novel and simple route was developed to obtain hydroxyapatite (HAp) coating on CoCr alloy from a slurry of eco-friendly pine oil (PO) mixed with HAp particles. The HAp coating was deposited onto CoCr substrates using a paint brushing followed by heat treatment at 800°C for 1 h in order to improve the adhesion between the substrate and coating. Several substrate surface morphologies made by polishing, passivation, heat treatment and remaining the substrate untreated were tested, and then coated to evaluate the influence of the roughness on the interaction between substrate and coating. Wettability tests were carried out by sessile drop method; the contact angle of water on the metal implant surfaces was much higher (68°) than that of PO (23°), allowing a more homogeneous coating process when PO was used for HAp suspension. Scanning Electron Microscopy (SEM), X-ray diffraction (XRD) and Fourier-transform infrared spectroscopy (FTIR) analyses indicated a substrate fully covered by pure HAp. The interaction between substrate and coating was analyzed by SEM, optical profilometer and pencil scratch tests. Good particle distribution and tight bonding to the substrate were found for all surfaces morphologies tested. The bioactivity tests *in vitro* performed in simulated body fluid (SBF) showed high resistance to degradation and a decreased formation of cracks was observed on the surfaces after 21 days of soaking. Potentiodynamic polarization and cyclic voltammetry analyses corroborated that the coated and uncoated samples showed good corrosion resistance. The HAp coating on the passivated substrate presented a superior corrosion resistance compared to uncoated ones and it can be assumed that the HAp coating improve the surface protection against corrosion. However, the high temperature treatment promoted decrease of corrosion resistance in case of the coated polished substrate, which also affected the growth of human primary bone-derived cells which were used for *in vitro* cytocompatibility tests of the different surface modifications. In order to overcome the high costs and complexity of the conventional deposition methods and the risk of phase transformation of HAp, related to those, this thesis presents a straightforward and efficient route to coat HAp onto metallic substrates as a potential alternative for improvement of bone implants.

Zusammenfassung

CoCr-Legierungen wurden und werden für orthopädische Implantate verwendet, da sie eine Kombination aus hoher Festigkeit, Korrosionsbeständigkeit und Biokompatibilität ermöglichen. Seit 1985 wurden metallische Implantate umfassend untersucht, die mit Calciumphosphaten beschichtet sind, um die Biokompatibilität und die Anbindung an das angrenzende Knochengewebe zu verbessern. Trotz des Fortschritts und der Entwicklung vieler Technologien ist die Ausfallrate solcher Implantate immer noch ein Problem. In der vorliegenden Arbeit wurde ein neuer und einfacher Weg entwickelt, um eine Hydroxylapatit (HAp) -Beschichtung auf einer CoCr-Legierung mittels einer Suspension aus umweltfreundlichem Kiefernöl (PO), das mit HAp-Partikeln gemischt ist, zu erhalten. Die HAp-Beschichtung wurde unter Verwendung eines Pinsels auf den CoCr-Substraten aufgebracht, gefolgt von einer Wärmebehandlung bei 800°C für 1 Stunde, um die Haftung zwischen dem Substrat und der Schicht zu verbessern. Verschiedene durch Polieren, Passivieren und einer Wärmebehandlung hergestellte Oberflächenmorphologien sowie ein unbehandeltes Substrat wurden getestet und dann beschichtet, um den Einfluss der Rauheit auf die Wechselwirkung zwischen Substrat und Beschichtung zu bewerten. Die Benetzbarkeit wurde durch Kontaktwinkelmessungen bestimmt. Der Kontaktwinkel von Wasser auf den Metallimplantatoberflächen war viel höher (68°) als der von PO (23°), was einen homogenen Beschichtungsprozess ermöglichte, wenn PO für die HAp-Suspension verwendet wurde. Rasterelektronenmikroskopie- (REM), Röntgenbeugungs- (XRD) und Fourier-Transform-Infrarotspektroskopie (FTIR) -Analysen ergaben, dass die Substrate vollständig mit reinem HAp bedeckt waren. Die Wechselwirkung zwischen Substrat und Beschichtung wurde mittels REM, optischem Profilometer und Bleistift-Kratztest analysiert. Es wurde eine gute Partikelverteilung und für alle getesteten Oberflächenmorphologien eine stabile Bindung zum Substrat nachgewiesen. Die in vitro in simulierter Körperflüssigkeit (SBF) durchgeführten Bioaktivitätstests zeigten eine hohe Beständigkeit gegen Abbau und es wurde eine verringerte Bildung von Rissen auf den Oberflächen nach 21 Tagen Auslagerung beobachtet. Potentiodynamische Polarizations- und Cyclovoltammetrieanalysen bestätigten, dass die beschichteten und unbeschichteten Proben eine gute Korrosionsbeständigkeit zeigten. Die HAp-Beschichtung auf dem passivierten Substrat zeigte im Vergleich zu unbeschichteten Proben eine überlegene Korrosionsbeständigkeit, und es kann angenommen werden, dass hierbei die HAp-Beschichtung den Oberflächenschutz gegen Korrosion verbessert. Die Hochtemperaturbehandlung förderte jedoch die Abnahme der Korrosionsbeständigkeit im Falle des beschichteten, polierten Substrats, was auch das Wachstum von menschlichen primären Zellen aus Knochengewebe beeinflusste, die für in vitro-

Zytokompatibilitätstests der verschiedenen Oberflächenmodifikationen verwendet wurden. Um die hohen Kosten und die Komplexität der konventionellen Abscheidungsverfahren und das damit verbundene Risiko einer Phasenumwandlung von HAp zu überwinden, bietet diese Arbeit eine einfache und effiziente Möglichkeit, HAp als mögliche Alternative zur Verbesserung von Knochenimplantaten auf metallische Substrate aufzutragen.

Resumo

Ligas de CoCr têm sido empregadas em implantes ortopédicos por permitirem a combinação de alta resistência mecânica, resistência a corrosão e biocompatibilidade. Implantes metálicos revestidos com fosfatos de cálcio têm sido estudados desde 1985 devido a sua capacidade de aumentar a biocompatibilidade e promover a ligação adequada com os ossos adjacentes. No entanto, apesar de todos os avanços e o desenvolvimento de muitas tecnologias, a taxa de falha destes implantes ainda é um problema. No presente trabalho, uma nova e simples rota foi desenvolvida para revestir a liga de CoCr com hidroxiapatita (HAp) a partir de uma mistura óleo de pinho (PO) ecológica com partículas de HAp. O revestimento de HAp foi depositado sobre o substrato de CoCr usando uma pincel de pintura seguido de tratamento térmico a 800 °C por 1 h a fim de aumentar a adesão entre o substrato e o revestimento. Foram testadas diversas morfologias de superfície do substrato, sendo estas polidas, passivadas, tratadas termicamente, além de um substrato não tratado, e em seguida foram revestidas para avaliar a influencia da rugosidade na interação entre substrato e revestimento. Testes de molhabilidade foram realizados pelo método de gota sêssil; o ângulo de contato da água na superfície metálica do implante foi muito maior (68°) que os com PO (23°), permitindo uma maior homogeneidade no processo de revestimento quando utilizado PO na suspensão de HAp. Análises por Microscopia Eletrônica de Varredura (MEV), difração de raio-x (DRX) e espectroscopia infravermelha por transformada de Fourier (FTIR) indicaram que o substrato foi completamente coberto com a HAp pura. A interação entre o substrato e o revestimento foi analisada por MEV, perfilômetro óptico e teste de arrancamento, os quais demonstraram uma boa distribuição de partículas e uma próxima ligação para todas as morfologias de superfície testadas. Testes in vitro de bioatividade foram realizados com fluido corpóreo simulado (SBF) e apresentaram alta resistência a degradação e uma redução da formação de trincas na superfície foi observada após 21 dias de imersão. Análises de polarização potenciodinâmica e voltametria cíclica comprovaram uma boa resistência à corrosão nas amostras revestidas e não revestidas. O revestimento de HAp no substrato passivado apresentou uma resistência à corrosão superior aos não revestido e pode ser assumido que o revestimento de HAp melhorou a proteção da superfície contra corrosão. No entanto, o tratamento térmico com alta temperatura promoveu uma diminuição da resistência à corrosão no caso do substrato polido revestido, no qual afetou o crescimento de células primárias derivadas de osso humano que foram usadas nos testes de citocompatibilidade in vitro nas diferentes superfícies modificadas. A fim de solucionar o alto custo e a complexidade no método convencional de deposição, além dos riscos da transformação de fase da HAp, esta tese apresenta uma direta e eficiente rota de revestimento

de HAp em substratos metálicos como uma potencial alternativa para o melhoramento de implantes ósseos.

1. Introduction

Metallic biomaterials were introduced in the 19th century and their main application was designated to bone repair, typically internal fracture fixation of long bones. Over the years, a range of metallic materials have been developed for orthopedic surgery as temporary devices (e.g. bone plates, pins, screws and permanent implants (e.g. total joint replacements) and in orthodontic procedure (e.g. tooth filling and roots) (Chen and Thouas, 2015).

The aging of the population is growing rapidly and it has been resulted in an increasing of the healthcare demand, where more than 21% of adults in the United States, more than 100 million people in Europe, and about 16.7% of the population in Australia, have arthritis or have suffered from arthritis (Zhang et al., 2009). In 2017, it was estimated that the number of total hip replacements could increase in 174% (572.000 procedures) and the number of total knee arthroplasties would reach in 673% (3.48 million of procedures) only in the U.S. by the end of 2030 (Kurtz. S et al., 2007). In order to attempt replacing the arthritic hip joint with an artificial one, thousands of hip joint prosthesis have been implanted around the world every year. However, many efforts have been carried out to improve both biological and mechanical properties, and prevent aseptic loosening.

Aiming at an achieving successful of an implant, both bulk and surface properties are crucial. Bulk properties of an implant are chosen according to the functional characteristics, such as, high mechanical strength, flexibility, optical transparency and surface properties are modified in order to improve biocompatibility and biofunctionality. Thus, several metals and metallic alloys have been studied as bulk biomaterial, where among them the most used are: (a) titanium and their alloys that applied for dental and orthopedic implants; (b) CoCr alloys for bearing surfaces and used in hip and knee joint replacement, heart valves parts and stents; (c) Nitinol (Ti-Ni alloys) for shape memory applications and stainless steel for stents and orthopedic implants (Tiwari et al., 2016).

In order to improve osseointegration, in the late 1970s, porous coatings were added to implant surfaces, but high incidence of thigh pain, bead shedding and loosening were diagnosed (Herrera et al., 2015). Thus, researches to find a coating capable of enhancing implant osseointegration boosted the interest in calcium phosphate ceramics (Herrera et al., 2015), but it was only in 1985 that Fulong and Osborn began developing clinical trials with hydroxyapatite coating on Ti-6Al-4V substrate (Fulong and Osborn, 1991). Biomedical coating is a relatively new area in the biomaterial field and in the last two decades the medical industry has

experienced a rapid growth, which improved the quality and expectance of life of thousands of people.

Hydroxyapatite (HAp) is the most common and well-known calcium phosphate, mainly due to its similarity with the mineral phase of bone, and its osteoinductive ability to promote bone ingrowth, osseointegration and bone bonding (Shojaee and Afshar, 2015). However, artificial HAp is brittle, while metallic implants have better mechanical properties due to their suitable mechanical strength. Several deposition techniques have been employed looking for combining the good mechanical strength and ductility of the metal with outstanding biocompatibility and bioactivity of the HAp. Among these techniques, sol-gel (Romonji et al., 2016), biomimetic coating (Habibovic et al., 2002), pulsed laser deposition (Capuccini et al., 2008), hot isostatic pressing (Onoki and Hashida, 2006), sputter coating (Chen et al., 2006), electrochemical (Eliaz et al., 2009), electrophoretic deposition (Wei et al., 2001) and plasma spray (Vahabzadeh et al., 2015) have been extensively studied. However, plasma spray is the only technique approved by the Food and Drug Administration (FDA), therefore it is a dominant coating technique for implant application due its good adhesion between metal-coating, high deposition rates, low substrate temperature and variable coating porosity (Mohseni et al., 2014).

Plasma spray is a thermal spray coating technique that consist in using high temperatures, such as 20.000 °C or more (Gomez et al., 2009), high heat source, a relatively inert spraying medium (argon, hydrogen or helium) and high particle velocities (Crivella, 2018). The need to use these complex parameters may result in limited coatings for biomaterial applications. The main limitation of plasma sprayed HAp coatings is the formation of amorphous calcium phosphates, which promote degradation and compromise the integrity of the bone-implant interface (Furlong and Osborn, 1991). The dissolution of unstable phases is undesirable because it leads to decrease in the mechanical strength and biocompatibility. One of the most important parameters of hydroxyapatite coatings for orthopedic implants is adequate wear resistance, allowing for stable, secure bone attachment and promoting elasticity and strength. Furthermore, the use of nanotechnology with hydroxyapatite coating might enhance bioactivity and provide good implant-bone adhesion (Yang et al., 2005). Although HAp coatings have been more widely studied on titanium substrates, CoCr alloys are of great interest due to their superior mechanical properties. Until now, there has been no consensus about which material is more suitable, (Shojaee and Afshar, 2015) or a coating technique that ensures the integrity of the implant for different metallic materials.

However, more than 30 years have passed since the introduction of HAp coating as biomaterial, and still numerous researches have been performed to improve HAp coating,

combining good coating-metal adhesiveness, mechanical properties and biocompatibility. Thus, this work aims at contributing to the field of biomaterials, seeking to employ an environmentally friendly coating technique based on pine oil mixed with HAp in order to promote the interaction between substrate and coating as an alternative to complex and expensive, already established techniques.

1.1 Objective

The main objective of this work was to coat a CoCr alloy using a mixture of environmentally friendly pine oil (PO) with HAp via brushing method and to assess the effect of the oil on the interaction between the metallic substrate and ceramic coating as a novel and simple alternative coating method for biomedical applications.

Specific objectives were:

- a) To prepare the slurry of the HAp/PO and to coat the metallic substrate via brushing method, testing different proportions and heat treatment temperatures, in order to achieve the best interaction between substrate and coating and to obtain a pure HAp;
- b) To employ PO in order to improve wettability of the coating and to evaluate its influence on adhesiveness properties of different surface morphologies of the CoCr alloy;
- c) To determine the adequate morphology and to evaluate the influence of the metallic substrate roughness on the metal-coating interaction by the scratch resistance using different treatments for modification of metallic surfaces;
- d) To evaluate the *in vitro* bioactivity of the coatings during soaking in SBF (simulated body fluid) solution at 37 °C for 3, 7, 14 and 21 days;
- e) To investigate the influence of heat treatment on the corrosion resistance by potentiodynamic cyclic polarization test;
- f) To determine the biological effects of the obtained coatings on human primary bone-derived cells (OB10) by investigating cell proliferation and osteogenic differentiation.

2. Literature review

2.1 Metallic biomaterials

In 1984, the National Institute of Health Consensus Development Conference defined biomaterial as being “Any substance (other than a drug) or combination of substances, synthetic or natural in origin, which can be used for any period of time, as a whole or as a part of a system which treats, augments, or replaces any tissue, organ, or function of the body” (Patel and Gohil, 2012).

The history of biomaterials started with ancient civilizations, where registers of Egyptian mummies showed that artificial eyes, ears, teeth, and noses were already used by them. Registers of Chinese and Indians civilizations revealed the utilization of waxes, glues, and tissues for reconstruction of missing or defective parts of the body. With century's, synthetic materials advancements, surgical techniques, and sterilization methods have been introduced to improve the quality of life of patients and to allow the use of biomaterials in several ways (Patel and Gohil, 2012).

Metallic materials have been used since the 19th century, when the metal industry began to expand during the industrial revolution, and its development started due to demands for bone repair and internal fracture fixation of long bones (Zheng et al., 2017). Currently, a few metals and alloys such as stainless steels, cobalt-based alloys, titanium-based alloys, NiTi shape memory and magnesium-based alloys have been used in medical industry as orthopedic implants, in dental applications, as intravascular stents and prosthetic heart valves due their biocompatibility and long-term capacity as an implant material (Fig 1) (Yang et al., 2005). The key requirements for biomaterial design involve excellent mechanical properties, corrosion resistance and biocompatibility. Metallic biomaterials compared with non-metallic biomaterials, possess superior mechanical properties such as yield strength, fatigue strength and fracture toughness, which results in the use of these biomaterials in different applications in the body, as for example in artificial hip and knee joints, bone plates, and dental implants (Zheng et al., 2017).

For metallic biomaterials, good corrosion resistance is one of the most important parameters determining their biocompatibility (Chen and Thouas, 2015). However, when a metallic biomaterial (inert or passive) is implanted, the physically and chemically conditions inside the human body are different from ambient conditions, which can promote a severe corrosion. The degradation of metallic products (release of metallic ions) during the post-implantation period,

different pH values and oxygen concentration in the body can compromise the integrity and life of an implant device through its corrosion (Zheng et al., 2017). According to Jacobs. J et al (Jacobs et al., 1998) there are two main reasons that determine why and how a metal corrode. The first are thermodynamic forces that conduct the oxidation and reduction reactions (corrosion reactions) and correspond to the energy required or released during a reaction. The second are the kinetic barriers, which limit the rate of the oxidation and reduction reactions to prevent corrosion.

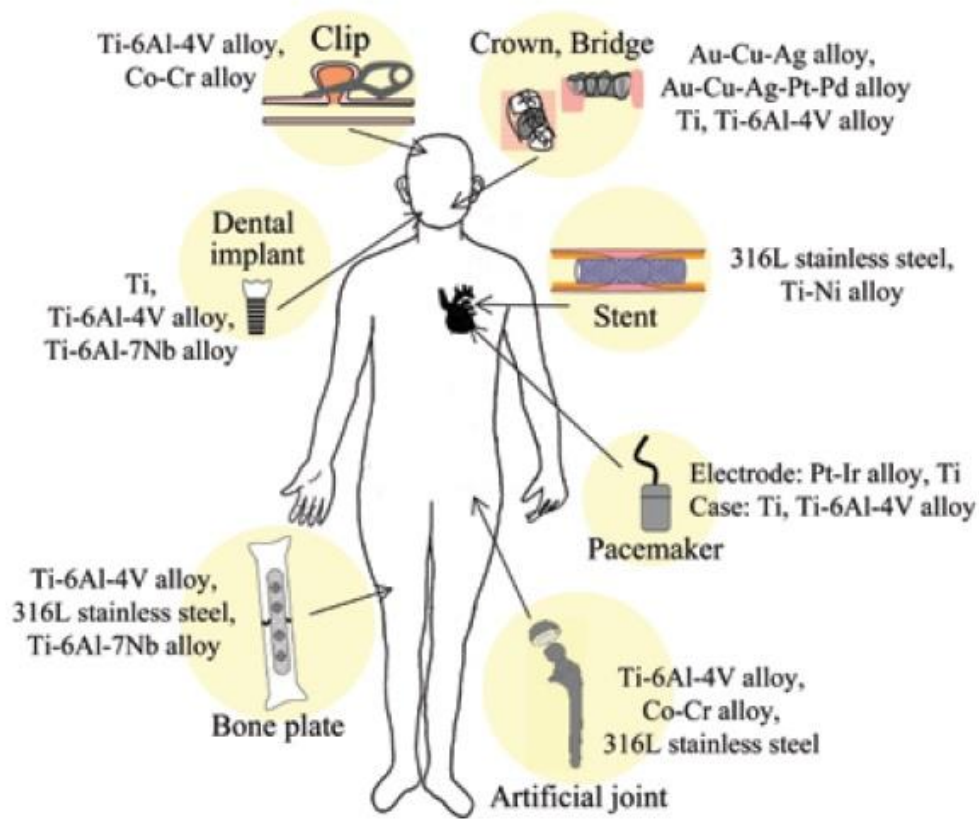


Figure 1. Metallic materials and their applications in human body as biomaterial devices (Hiromoto, 2008).

2.1.1 Co-based alloys

In the early 1900s, Elwood Haynes (Yao et al., 2005) was the first researcher to investigate cobalt alloys for biomedical applications. Initially, he discovered that a strengthening effect and corrosion resistance could be achieved by usage of Cr in Co. Then, he discovered that the use of tungsten (W) and molybdenum (Mo) in CoCr alloys increase its strengthening effect, and so the first ternary cobalt alloys got patented (Disegi et al., 1999). Co is an allotropic element at

temperatures below 417°C and it presents a compact hexagonal crystalline structure (HC), whereas between 417°C and 1193°C (melting point), Co presents a face centered cubic structure (FCC) (Royse, 2010). Co-based alloys exhibit a dendritic α -FCC metastable matrix due to the sluggish nature of the FCC→HCP (hexagonal close-packed) transformation and the addition of alloying elements such as Cr and W increases the transformation temperature (Giacchi et al., 2011). For the application of Co-based alloys, they are classified into three groups: (i) wear-resistant alloys: Co-Cr-W are characterized by the carbon content and tungsten (W); (ii) high temperature resistant alloys: low carbon amount and nickel addition (establish FCC structure) and W (promotes hardening of the solid solution and formation of carbides); (iii) corrosion resistant alloys: they exhibit high tenacity and low carbon amount to the minimize formation of carbides (Royse, 2010).

The high mechanical properties of these alloys are due to the solid-solution strengthening (with Cr, W and Mo) and the formation of metal carbides, while the good corrosion properties result from the addition of chromium in the alloy (Favre et al., 2013). In the CoCr alloys the combination of solid-solution hardening and carbide precipitation by the addition of carbon, chromium, molybdenum, tungsten or nickel in the pure cobalt matrix are introduced to improve their mechanical properties (Matković et al., 2004). On the other hand, heat treatment is also responsible for an improvement of the mechanical properties by dissolving the large network and producing a homogenous structure (Giacchi et al., 2011).

According to ASTM four types of Co-based alloys are recommended for surgical implant applications: (i) F75: cast CoCrMo alloy, (ii) F90 wrought CoCrWNi alloy, (iii) F562: wrought CoNiCrMo alloy and (iv) F563: wrought CoNiCrMoFe. Among these alloys, only cast CoCrMo and CoCrWNi are extensively employed in implants fabrication (Jabobs et al., 1998). Thus, the Co-Cr alloys have a long history consisting of more than 80 years of use as dental and medical materials, and when compared to steels, these alloys exhibit both higher mechanical properties and corrosion resistance (Kadlec and Onderka, 2013; Niinomi et al., 2015)].

2.1.1.1 L605 alloy

Co-20Cr-15W-10Ni alloy L605, well-known as “Haynes 25”, is a non-diamagnetic Co-based alloy with Cr, W and Ni as main alloying elements and its high temperature-resistance, corrosion-resistance mechanical-resistance make it an attractive material for biomedical applications as well (Favre, 2012). In 2004, Guidant Corporation introduced a vascular stent manufactured from L605 and it opened a wide opportunity for L605 applications in vascular implants (Aihara, 2009).

Such as the other CoCr alloys, the CoCrWNi alloy is also primarily strengthened by carbide precipitation and the mechanical properties are strongly affected by their deformation microstructure and high performances are results of its microstructural characteristics (Lee et al., 2011). The microstructure of the L-605 alloy is composed of a single FCC γ -phase with alloying elements in solid solution. Commercially, the L-605 alloy has a grain size between 50 and 100 μm and its homogeneous microstructure is obtained by plastic deformation at high temperature, followed by a treatment solution above than 1200 °C, in order to remove precipitates, undesired phases, and to give the final shape of the product. For this alloy, laves phases are predicted to be formed during aging treatment below than 700 °C and between 700 °C and 1100 °C carbide formation is expected. Above than 1100 °C precipitates are dissolved, and hence the material becomes a single FCC phase. Co-20Cr-15W-10Ni alloy has two main FCC carbides: the first one is M_6C and the second one is M_{23}C_6 , being M is one or several metallic elements of the alloy (Favre et al., 2013).

2.1.2 Corrosion of CoCr alloys

CoCr alloys have been widely used as metallic biomaterial due to their beneficial combination of superior wear behavior and corrosion resistance, good mechanical properties and suitable biocompatibility (Luo et al., 2013). However, when a metallic material is implanted its find conditions non-environment in the body as highly oxygenated saline electrolyte at a pH of around 7.4, temperature of 37°C, chloride solutions (high corrosive to metals), ionic composition and protein concentration in body fluids that contribute to accelerate the corrosion process of metal (Hansen, 2008).

Failures and loosing of the artificial joints and bone fixation devices are often evidenced after 5-10 years of implantation. It occurs due to the mechanical degradation that is caused by the fatigue, fretting fatigue and wear. The contact of the material surface to the surrounding tissue influences the corrosion of the material over the year, which accelerates material degradation even further (Hiromoto, 2008).

Corrosion is defined as being a destructive attack of a metal by chemical or electrochemical reaction with its environment (Niinomi, 2010; Revie, 2008) and its occurrence in metallic biomaterials results in the loss of the structural integrity and surface function in the metallic biomaterials and a very small amount of released metallic ions may promote allergic response and carcinogenesis in the human body (Niinomi, 2010). For these reasons, many attempts have been performed to evaluate corrosion resistance of implant materials using quantitative electrochemical test such as potentiodynamic polarization and impedance spectroscopy (Legat

et al., 2006; Reclaru et al., 2005 Tsyntsar et al., 2007), and qualitative *in vivo* implantation of devices in animals (Hansen, 2008). Metals and their alloys (usually, except for gold) have a tendency to react with the environment and form a native oxide layer thin on surface that protects the material against corrosion. However, some metals and alloys are more resistant to corrosion and it is due to phenomenon of passivity that protects the surface, which prevents that the metal corrode earlier or when it would be expected (Al-Subai, 2011). CoCr alloys have superior corrosion resistance due to the addition of chromium in the alloy (Favre, 2012). Chromium is the most important element added to alloys to improve the corrosion resistance, which also increase the resistance to pitting, oxidizing environments and crevice attack through the forming of a passive film on the surface (Al-Subai, 2011).

When a metallic alloy is implanted, the body fluid corresponds to electrolyte, which contains negatives ions (anions) that migrate towards the anode, and the positive ions (cations) that migrate toward the cathode in solution. This solution is an electrolyte that is used to complement the circuit, as shows Figure 2. The electrical potential is measured by an electrical component (Figure 2), which can be a voltmeter or a battery, which is an unwanted corrosion cell for a biomaterial in the body (Park and Lakes, 2007).

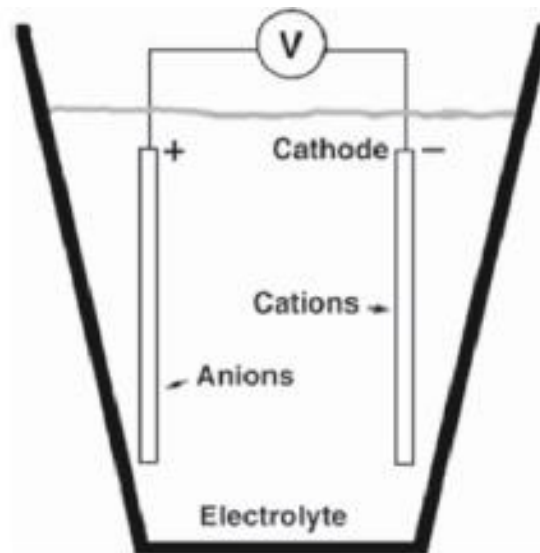


Figure 2. Electrochemical cell shows how the chemical reaction occurs on the metallic biomaterials exposed to an aqueous environment (into human body).

2.1.2.1 Biological effect of CoCr alloys

In the biomaterials field, CoCr alloys have been used in different applications such as artificial hip, knee joints, dentistry (Lu et al., 2015) and cardiovascular stent applications (Sojitra et al.,

2009). However, for each application, these alloys have a particular cellular response, which has been studied extensively. One the most concern of a material implanted is about the soluble metal ions release, like aluminum (Al), chromium (Cr), vanadium (V), cobalt (Co) and titanium (Ti), because these ions bind to proteins, remain in solution, and then are scattered by the surrounding tissues, bloodstream, and remote organs (Hallab and Jacobs, 2009).

There are two ways for an implant to corrode: electrochemically or mechanically, and as consequence metal ions or metal particles are released which may influence biological functions: adverse tissue reaction, cytotoxicity and metal sensitivity are related as main effects. Furthermore, many studies have reported that large particles (more than 150 nm to 10 μ m), can be phagocytosed by several type of cells, such as osteoblast, fibroblasts, endothelial cells, and macrophages (Yunpeng. J et al, 2013). Cobalt, chromium, vanadium, and possibly nickel trace elements are essential for a normal growth, development, and physiology of the organism (Siddiqui et al., 2014), but in excessive amounts, cobalt has been reported to promote polycythemia, hypothyroidism, cardiomyopathy, and carcinogenesis; chromium can also promote to nephropathy, hypersensitivity, and carcinogenesis; nickel can promote eczematous dermatitis, hypersensitivity, and carcinogenesis; and vanadium can lead to cardiac and renal dysfunction (Bitar and Parvizi, 2015). Also, it has been associated with hypertension and manic-depressive psychosis (Lu et al., 2015). Figure 3 depicts a per-operative view of an old patient (81 years) with a severe corrosion in a titanium hip joint after 4 years of implantation and increase of Co ions release. Such corrosion promotes intermittent pain in the groin and trochanteric area about two years post-implantation in the patient (Vundelinckx et al., 2013).

Influence of the interaction of dental cast metallic alloys with living tissues and effects of bacterial adhesion and toxicity on target tissues (soft tissues in the mouth) were reported by Schmalz and Garhammer (Schmalz and Garhammer, 2002). Controlling bacterial adhesion is essential in dental applications, since inadequate oral hygiene may lead to plaque accumulation and cause gingival inflammation. However, high levels of free energy surface and rough surfaces of dental metallic alloys may also influence oral bacterial adhesion (Schmalz and Garhammer, 2002). The toxicity of dental metallic is the main requirement to determine toxic potential of metal ions in cell culture systems, since have been reported problems with inflammations of the gingiva in patients with excellent oral hygiene (Schmalz and Garhammer, 2002). Co-based alloys have proved as pursuing different biological responses, which were reported by Berstein et al. (Berstein et al., 1992) to inhibit the growth of the primary fibroblasts, but tests performed with permanent cell cultures (human lymphoma cells) showed no inhibition and alteration of cell growth (Berstein et al., 1992).



Figure 3. (A) Revision surgery of a hip joint with soft tissue reaction to metal ions around the implant. (B) Photograph shows the base of the modular neck with severe wear and (C) parts of a hip prosthesis with severe signs of wear at the base of modular neck (Vundelinckx et al., 2013).

Tsaousi et al. showed that CoCr alloys promote dose-dependent cytotoxicity and genotoxicity on human fibroblasts. In patients exposed to worn CoCr hip replacements an increase of chromosome anomalies in the bone marrow adjacent to the implant was observed as well as chromosome translocations and aneuploidy in the peripheral blood. Behl et al., 2013 evaluated the response of porcine dural fibroblasts and epithelial cells to CoCr nanoparticles and ions. These studies showed a decrease of viability of the dural epithelia after one day of culture, but it was not observed for dural fibroblast.

On the other hand, Savarino et al. (Savarino et al., 1999) analyzed levels of Co and Cr and Ni in serum of several patients and the variation among some white blood cells, namely leucocytes, myeloid cells, lymphocyte subpopulation in patients with aspect loosening of hip prostheses and toxic effects from implant metal ions were observed. According to the authors, among 22 investigated patients, 54% presented normal levels of Co and Cr ions and 18.2% presented high levels of Co and Cr ions and the number these cell cultivated had a higher decrease when both ions were increased. The cell behavior of the Co, Cr and CoCr alloy was studied by Allen et al. (Allen et al., 1997) using osteoblast cell lines. Tests with Co presented toxicity (0.1 mg/mL) and inhibited the production of type-I collagen, osteocalcin and alkaline phosphatase by osteoblast both cell lines cell lines (SaOS-2 and MG-63), while for the Cr (1.0 mg/mL) and Co-Cr alloy (1.0 mg/mL) there was no cytotoxicity or inhibition of type-I collagen synthesis of both cell lines.

2.2 Surface of metallic implants

Metallic materials, such as stainless steel, titanium and cobalt-chromium and their alloys with appropriate surface modification have been suggested for biomedical application, in order to accelerate bone healing (Liu et al., 2015) and promote direct attachment to bone (Vasilescu et al., 2011).

The implant surface, which is the first component to interact with the host and surface modification, has been extensively studied and modified in order to increase the biocompatibility and osseointegrative properties, which in turn may enhance the bone healing and apposition, and consequently, ensure a rapid biological fixation of implants. Surface modification of biomaterials is an important parameter in the development of biocompatible coating and metal oxides. It has been widely recognized that the native oxide layer (chemically passive surface) confers corrosion resistance and is usually less reactive than the biological media, which results in enhanced biocompatibility of the metallic surfaces (Silva-Bermudez and Rodil, 2013).

Adhesion is a surface phenomenon, in which two surfaces are kept in contact by interfacial forces (valence forces and/or interlocking actions) and the substrate adherent determines the adhesion conditions. Surface preparation is the most critical step to control the adhesive bonding (Wegman and Twisk, 2012) and in order to achieve a strong adhesive bond, some features are essential, such as: surface roughness, contact angle, good wetting and cleaning of the surface (Marshall et al., 2010). Independent of the coating technique cleaning, roughening and condensate elimination are essential to ensure the adhesive bonding and bond durability. Cleaning is the first step that consist to remove the contaminants, such as oil, greases, paint,

rust, scale and moisture (Fauchais et al., 2014). As a second step, the roughening provides asperities or irregularities to enhance coating adhesion to the substrate (Fauchais et al., 2014), whereas the surface roughness is achieved by abrasive or mechanical blasting (Paredes et al., 2006). Third step is the elimination of adsorbents and condensates, which consist in a pre-heating of the substrate, being responsible for volatilization and burning of oil, greases, paint, rust, scale and moisture retained on the metal surface (Paredes et al., 2006). Pre-heating may contribute to residual thermal stress reduction to improve adhesion of the layer. To occur the substrate heating in the plasma spray process there must be absorption of the kinetic energy of the impact and also of the energy transferred by the flame/plasma, however, this pre-heating can promote a negative influence on the tensile stresses of the substrate–coating interface (Paredes et al., 2006).

2.3 Interface between substrate and coating

One of the main requirements for a coated metallic implant to be successful is enhancing the bonding strength between the substrate and the coating. The overall bonding effectiveness is determined by combining adhesive and cohesive forces in every situation involving a substrate and the adhesive (Fig 4). Adhesion is defined as an attraction process between different molecular materials, which when in direct contact promotes that the adhesive “clings” or binds to the applied surface or substrate (Fraunhofer and Anthony, 2012). Whereas the cohesion is the internal strength responsible to keep the particles attached within of the adhesive (Harun et al., 2017). Therefore, separation of the adhesive from the substrate is necessary to prevent, which could occur from bond fail or internal breakdown of the adhesive, e.g. arising from cohesive failure (Fraunhofer and Anthony, 2012).

Many theories have been proposed to explain the adhesion phenomenon, but they are at the same time complementary and contradictory. For instance, mechanical interlocking, electronic theory, diffusion theory, theory of boundary layers and interphases, adsorption (thermodynamic) theory, and chemical bonding theories are considered. Among these theories, chemical bonding represents the best explanation of adhesion phenomena, which consist in the formation of covalent, ionic or hydrogen bonds across the interface (Marshall et al., 2010; Roa et al., 2011),. Hence, it is understood that the chemical bond formed across the adhesive–substrate interface may greatly participate on the adhesion between the materials (Roa et al., 2011). These bonds are categorized as primary bonds and present strong bonding forces (Marshall et al., 2010), but

when compared to physical interaction with weak bonding (van der Waals), it is called secondary interaction forces (Marshall et al., 2010).

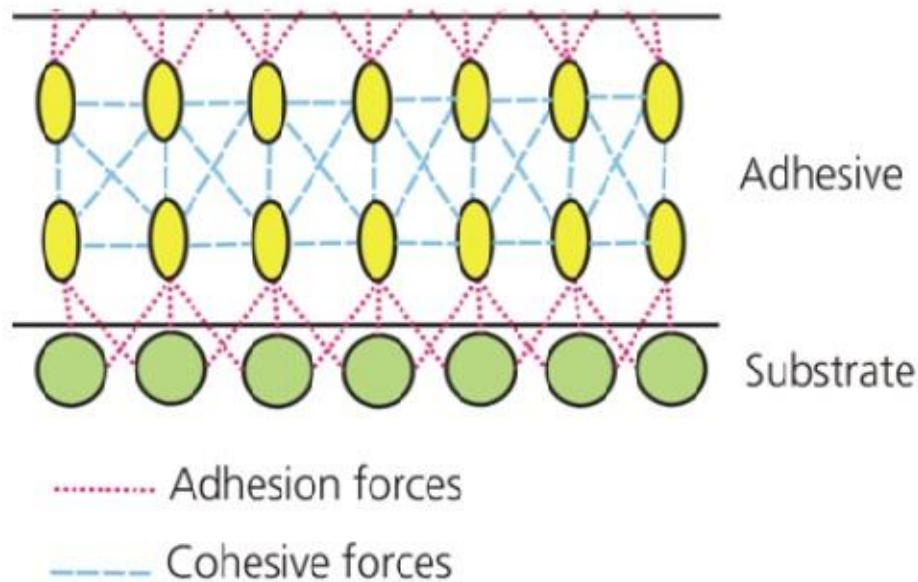


Figure 4. Representation of the adhesion and cohesion forces within an adhesive and between an adhesive and substrate (Adhesives.org, 2017).

2.4 Cell-surface interaction

As already mentioned in the requirements above, a successful orthopedic implant has to provide suitable mechanical properties and good biocompatibility to allow osseointegration. According to Huliang (Cao and Liu, 2013), osseointegration refers to as being a structural and functional connection between bone tissue and the surface of an implant for load carrying, which involves a cascade of cellular and extracellular biological events that take place at the bone/implant interface.

Although the material surface properties have been studied intensively, there is still the necessity of a better understanding about cytocompatibility of an implant, which is influenced by its chemical composition, since surface topography plays a vital role for cell-surface interaction (Jäger et al., 2007).

Another important aspect when a material is implanted into the body is the protein adsorption, because the protein would be instantaneously adsorbed by its surface and can significantly influence its biocompatibility (Wang et al., 2017). Figure 5 presents a scheme of the sequential reactions that may occur at the interface of the implant after implantation. Initially, the interaction

of proteins with the metallic surface occurs immediately upon the metal contact with the blood, and then platelets attach the surface (Tanaka et al., 2009). When a biomaterial is implanted, within a few seconds a thin layer of proteins is formed on its surface and consequently the cells will respond to these proteins. This film is important responsible to control the bioreaction, in which the cells multiply and organize into several forms of complex tissue (Paital and Dahotre, 2009).

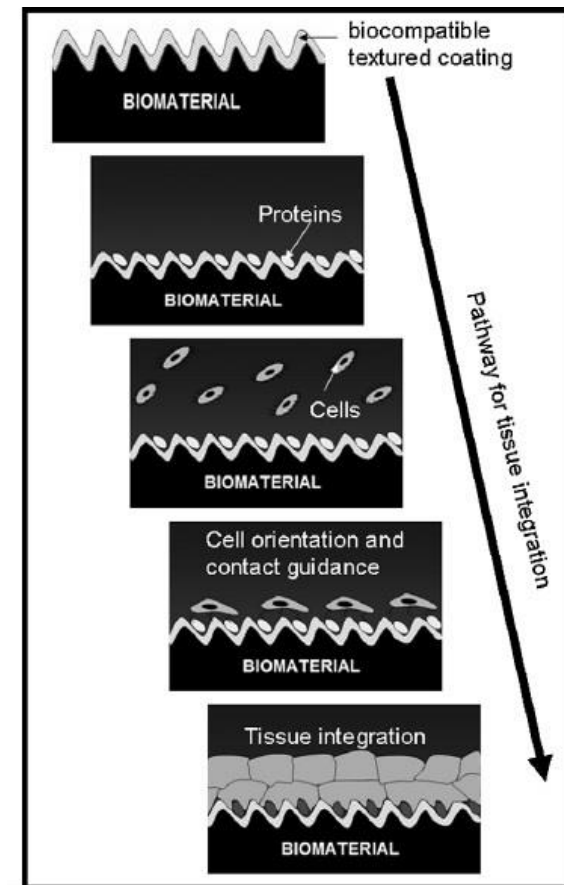


Figure 5. Demonstration of the sequential reactions that occurs after the implantation of a biomaterial into a living system (Paital and Dahotre, 2009).

Biomaterials and medical devices, prior to interacting with host cell, immediately and spontaneously form a layer of host protein (Anderson et al., 2008) and it can be determinant for the osseointegration process, because proteins encountered by the cells must support or actively promote activities for the attachment and proliferation (Wilson et al., 2005). Furthermore, protein adsorption can influence the corrosion rate, bone cell attachment and proliferation of a metallic implant surface (Tanaka et al., 2009). The rough surface is also determinant for metallic implants, because it promotes its friction and bacterial adhesion process. Surfaces irregularities

can lead to bacterial adhesion and colonization. For metallic implants, a rough surface is usually below than 10 nm and for CoCrMo alloys it is established that minimum level is around 12 nm (Tan, 2016).

Surface wettability is a property to enhance cell response and it is widely observed that cells have superior adhesion on hydrophilic surfaces (Wilson et al., 2005). According to Voglers (Vogler, 1998) definitions, hydrophobic surfaces are those where attractive forces are detected exhibiting water contact angles above 65° and hydrophilic surfaces repulsive forces are detected exhibiting water contact angles below 65°. Moreover, cleaning and sterilization might promote significant changes, such as, changes in surface chemistry or energy, and ion release, subsequent to affect cellular activity. Thus, the use of ethanol or butanol to disinfection the material can create a more hydrophobic surface and autoclaving contributes to (non-biological) surface contamination (Wilson et al., 2005).

2.5 Calcium phosphates (CaP)

The first recognized CaP was the apatite in 1786, when Abraham Gottlob (Canillas et al., 2017), well-known as father of geology, discovered this mineral, but Nicolas Louis Vauquelin (Dorozhkin, 2013) is the one who discovered the acidic calcium orthophosphates. Apatite as a mineral group name corresponds to minerals with the same crystallographic structure and the term “apatite” involves CaP ratio within 1.5-1.67 for the calcium phosphate group (Canillas et al., 2017; Dorozhkin, 2013; Eliaz and Metoki, 2017). CaP are the main inorganic constituents found in bone (≈60% w.t.), principal constituent of enamel in the tooth (ca. 90%) and its name presents a common family of minerals containing calcium cations (Ca^{2+}), together with orthophosphate (PO_4^{3-}), metaphosphate (PO_3^{3-}) or pyrophosphate ($\text{P}_2\text{O}_7^{4-}$) anions, and occasionally hydrogen (H^+) or hydroxide (OH^-) ions (Eliaz and Metoki, 2017). The applications of biomaterial based on CaPs were introduced in 1920 for fracture treatment. However, it was in the 1970s that research about CaPs had a large growth in the orthopedic and dental fields (Habracken et al., 2016).

2.5.1 Hydroxyapatite

Among CaP's, hydroxyapatite (HAp, $\text{Ca}_{10}(\text{PO}_4)_6(\text{OH})_2$) is the most common phase due to its quite similar chemical composition to the mineral phase of bones (Chen and Thouas, 2015) and excellent biocompatibility with hard and soft tissues, such as skin and muscle (Shi, 2006). The structure of pure HAp belongs to the monoclinic system with space group P21/b, and at temperature above than 250°C there is a monoclinic to hexagonal transition (space group

P63/m). However, some impurities, like partial substitution of hydroxide by fluoride or chloride ions, stabilize the hexagonal structure of HAp at room temperature and due to this, the very rare single crystals of natural HAp presents a hexagonal space group (Dorozhkin and Epple, 2002).

Bone is a ceramic-organic bio-nanocomposite with a complex structure that is composed mainly by a major mineral phase of calcium phosphate (ca. 69% w.t.), an organic matrix (ca. 22% w.t.), mostly collagen type I [66] and water (ca. 9% w.t.) (Kattimani et al., 2016). The main function of collagen is to provide elasticity and support, whereas the CAPs (HAp and amorphous calcium phosphates) provide stiffness to the bone tissue (Shi, 2006). HAp is widely used as a coating for orthopedic (hip-joint prosthesis) and dental implants (Dorozhkin and Epple, 2002).

2.6 HAp coating

Metallic materials have good mechanical properties and corrosion resistance, however, their biocompatibility is limited. Thus, bioactive materials such as HAp have been used to coat metallic substrate surfaces to enhance the implant bioactivity (Asri et al., 2016). In the late 1960's, the use of bioactive HAp and CaP coatings was proposed for biological fixation of load-bearing as an alternative to cement fixation (Yang et al., 2005). Nevertheless, it was only in 1985 that Furlong and Osborn (Yang et al., 2005) began employing clinical trials with HAp coated implants, which were successful from the clinical point of view, having a failure rate less than 2% during a mean follow-up study of 10 years.

HAp coatings allow a faster, more stable and stronger implant-to-bone fixation. They generate a uniform bone-implant interface and act as a protective layer to prevent the release of metal ions from the implant to the body (Lu et al., 2004). HAp coatings have a common level of crystallinity of about 60-70% and thicknesses between 30-300 μm are considered suitable for biomedical applications. High degrees of crystallinity show low dissolution rates *in vitro*, less resorption and more direct bone contact *in vivo*. Coatings with high amorphous contents promote a rapid weakening and disintegration of the coating, which can result in an inflammatory response from surrounding tissue (Tsui et al., 1998).

2.6.1 HAp coating methods

2.6.1.1 Plasma spray

A large number of techniques have been developed to produce HAp coatings on metallic implants, such as sol-gel dip coating, electrochemical deposition, electrophoretic deposition, plasma spray process, hot isostatic pressing, pulsed laser deposition and biomimetic deposition.

Among these techniques, only plasma spray is commercially approved by the FDA from USA for use as biomedical coating on implants (Asri et al., 2016). Figure 6 (A) shows the process of coating by plasma spray of prosthesis with HAp and (B) metallic implants coated with HAp for different applications.

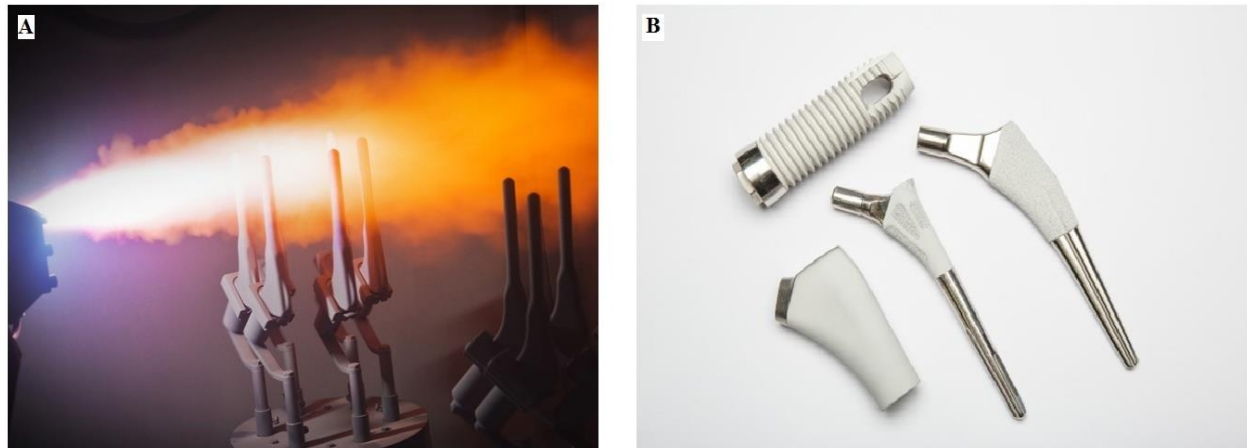


Figure 6. (A) Coating of joint prostheses by plasma spray process on titanium substrate (Medicoat, 2018.) and (B) commercial coatings of HAp obtained by plasma spray process (APS Materials, 2018).

Plasma spray coating has been widely used to coat mainly titanium alloy with HAp in orthopedic surgery to reconstruct hip and knee joints. This is a complex process that involves several parameters, which achieves temperatures around 13 000 K. It is based in the deposition of a stack of successive melted HAp particles on the substrate that are transported by gas (hydrogen and/or argon), followed by cooling that allows obtaining thickness between 15 and 200 μm with a lamellar structure (Demnati et al., 2014).

Despite the plasma spray coating process has shown excellent clinical performance, some intrinsic drawbacks resulted in limitations of this method (Yang et al., 2005), including poor coating-metal adhesion strength, non-uniform thickness, and changing of structural and chemical properties (Chen et al., 2006). Likewise, this process requires high temperature, which can lead to partial decomposition of the HAp, resulting in the limitation of this process (Demnati et al., 2014). The most common limitation of plasma sprayed HAp coating is the formation of secondary phases, such as tricalcium phosphate (α/β form), calcium oxide (CaO), and tetracalcium phosphate (TTCP) along with amorphous calcium phosphate (ACP) and the presence of these undesirable phase increases dissolution of the coating (Vahabzadeh et al.,

2015). Due to these limitations associated to plasma spray process, experimental deposition procedures have been investigated to overcome them.

2.6.1.2 Electrodeposition

Another coating technique that has been drawing attention is electrodeposition, essentially due to the possibility to be conducted at mild temperature and its applicability to complex substrates. The electrodeposition technique allows a high production rate (Shadanbaz and Dias, 2012) and the thickness and chemical composition can be controlled by adjusting electrodeposition conditions (Song et al., 2008) (current density, temperature, pH and electrolyte composition) (Mali et al., 2016).

Electrodeposition method has been used to coat different metallic alloys for biomedical applications (Coşkun et al., 2014; Manso et al., 2000; Thanh et al., 2013), due to their homogeneity and among other characteristics mentioned above (Coşkun et al., 2014). This technique is carried out using a negative charge against a substrate in a three-electrode electrochemical cell (Arshanapalli, 2013) coupled to a galvanostat/potentiostat system, which allows to control the thickness of the coating by controlling the deposition time (Mali et al., 2016). The system of an electrochemical cell is shown in Figure 7, where for HAp coating, a SBF solution with near-physiological conditions is used as an electrolyte for conduction of ions to carry out the deposition of the CaP coating, and CaP phases are precipitated out of solution on the substrate (Shadanbaz and Dias, 2012). The counter electrode (cathode) and working electrode (anode) are where the electrochemical reactions take place.

Coşkun et al. (Coşkun et al., 2014) deposited HAp on a CoCrMo substrate by electrodeposition using different solution concentrations and a computational technique was proposed to optimize electrolyte concentrations. A simple and cost-effective method was established by Thanh et al. (Thanh et al., 2013a), investigating the influence of experimental conditions (precursor concentration, temperature and H₂O₂ content) on the electrodeposition process of the HAp coating onto 316L stainless steel. For coating metallic substrates like the 316L stainless steel by electrodeposition process, it is important to investigate the electrochemical reactions that generate gaseous hydrogen which can attack the surface and reduce the adhesion of the HAp coating to the substrate surface (Thanh et al., 2013a).

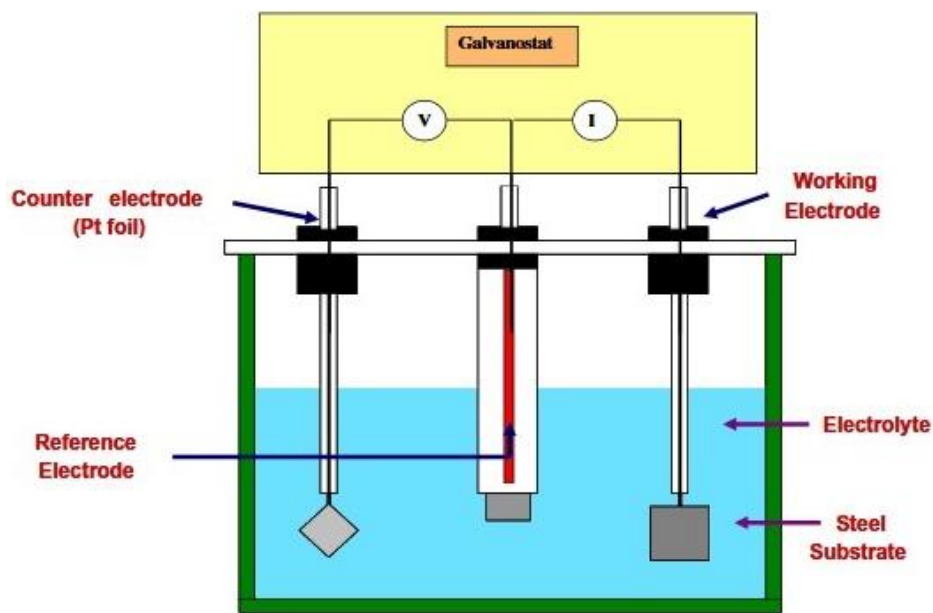


Figure 7. Schematic of an electrochemical process for deposition of HAp on 316L nanostructured stainless steel (Mali et al., 2016).

The effects of low constant voltages on coating morphology, micro-structure and composition of HAp deposition on Ti substrate were studied by Manso et al. (Manso et al., 2000), resulting in a well-crystallized HAP coating through electrical activation of spontaneous deposition. However, this technique has two main limitations: the first one is the low adhesion and second one is the high dissolution rate of the formed coating.

2.6.1.3 Ion beam-assisted deposition

Ion beam assisted deposition (IBAD) technique utilizes an ion beam to coat the surface of a material with a thin film (Paital and Dahotre, 2009a). Ions are accelerated to a determined energy and directed toward the surface of the target material (Cui and Luo, 1999). This technique is a vacuum process that combines physical vapor deposition with ion beam bombardment (Hamdi and Ide-Ektessabi, 2003), allowing the production of coatings with exact processing control, low temperature, versatility of ion species and a good adhesive bond. For making coatings by IBAD method, many parameters, such as evaporation rate or sputtering rate, ion species, ion energy and ion beam current density can affect the composition, structure and chemical properties of coating, with the ion bombardment being the key factor (Hamdi and Ide-Ektessabi, 2003). HAp coatings incorporated with different concentrations of Ag, used as an antibacterial component, were deposited using IBAD with *in situ* heat treatment. After that, and

over a total period of 6 h, where the substrate temperature was 550 °C for the first 4 h and 450 °C for the subsequent 2 h, a coating was obtained with three different layers, showing a “mixed” crystalline interface layer adjacent to the metallic substrate, a crystalline inferior layer and a mostly amorphous layer on the top surface (Bai et al., 2010).

IBAD simultaneous vapor deposition was used by Hamdi and Ektessabi (Hamdi and Ide-Ektessabi, 2003) to prepare HAp layers from CaO and P₂O₅ powders used as Ca and P precursors and then heated at 650 °C for 6 h and submitted to annealing for another 2 h at 1400°C. In order to increase the crystallinity and, hence, biostability, post-deposition heat treatments at 700, 1000 and 1200 °C for 2 h were performed on the deposited films. Luo et al. (Luo et al., 2000) studied the *in vitro* and *in vivo* degradability of Ti surfaces coated with HAp by IBAD in rabbits, and after 12 weeks no significant degradation of the coating was observed. Furthermore, post deposition treatment has been applied to improve the crystallinity of the coating. Nonetheless, IBAD process is expensive and involves a vacuum chamber and plasma treatment based on ionized particle bombardment (Paital and Dahotre, 2009a).

2.6.1.4 Sol–gel deposition

Sol-gel is a method that allows sintering ceramic and nanostructured materials at a relatively low temperature, using simple equipment. Furthermore, dense and uniform coating layers with a thickness lower than 1 mm can be obtained from sol-gelled materials (Salehi et al., 2015). This deposition technique involves a series of steps: (i) preparation of a homogenous solution; (ii) aging of the sol/gel at a suitable temperature to achieve desired properties (e.g. optimum viscosity); (iii) the sol/gel is submitted to casting, spinning, drawing, coating, emulsification, dipping, or spraying, for example for obtaining the required gel form coating through sol–gel transition; and (iv) the specimen is submitted to drying, followed by heating to obtain the desired product. In addition, each step is guided by a set of experimental parameters in order to control the chemistry of the process and the quality of the final product (Paital and Dahotre, 2009). Sol-gel deposition technique was introduced as a promising alternative to coating methods such as plasma spraying, electrophoretic deposition, sputter coating, pulsed-laser deposition and dip coating into a powder suspension to produce thin bioactive layers (Chai and Ben-Nissan, 1999), which was combined with dip-coating technique to coat metallic biomaterials to improve adhesion (substrate/coating) (Asri et al., 2016).

Many researchers developed new alternatives to improve the adhesion strength and biocompatibility properties of the sol-gel coating. For instance, Romonți et al. (Romonți et al., 2016) prepared fluorohydroxyapatite and fluoroapatite coatings and deposited those on CoCrMo

substrates by the sol-gel method looking for achieving a better performance of fluoro-substituted apatite on the optimization of biocompatibility properties. A study reporting the synthesis of hybrid (silica and organic chains) networks with a mixture of two alkoxysilanes (methyltrimethoxysilane and 3-glycidoxypropyl-trimethoxysilane) in different proportion via sol-gel method was proposed by Diaz et al. (Juan-Díaz et al., 2016). In this study, they proposed to develop a coating for complex surfaces which promotes good adhesiveness, biodegradability and biocompatibility on titanium dental screws. The results showed that it was possible to coat the dental screws, however, when changing the composition of the sol-gel coating the biodegradability was highly affected. On the other hand, Burnat et al. (Burnat et al., 2017) studied titanium dioxide (TiO_2) to improve anticorrosion and bioactivity properties, which proved that coating doped with the highest concentration of calcium ions showed the best anticorrosion properties.

2.6.1.5 Electrophoretic deposition

Electrophoretic deposition (EPD) allows production of relatively homogeneous coatings with controlled microstructure, thickness and morphology on complex shaped materials (Besra and Liu, 2007; Jugowiec et al., 2017). EPD technique is a colloidal process applied in ceramic production (Besra and Liu, 2007) and also offers advantages in relation to high purity of deposits and room temperature processing. There are two key steps required: (i) electrophoresis, where the charged particles dispersed in a colloidal solution or suspension moves through an electric field; and (ii) deposition, which occurs with accumulation and coagulation process of charged particles on the surface of opposite charged electrodes (Jugowiec et al., 2017). Despite these advantages, EPD involves parameters that influence the process and are grouped into two categories: The first category is related to suspension parameters (dielectric constant, viscosity, temperature, particle size and morphology, content of the dispersant in the suspension, electrokinetic properties of particles), and the second category includes parameters referent to the electric field of EPD (applied voltage, deposition time, distance between electrodes, area of electrodes submerged in the suspension, as well as material of the counter electrode) (Jugowiec et al., 2017).

In the EPD process, the use of additives is necessary to obtain stable suspensions and to promote the desired level of electrophoretic mobility. However, Zhitomirski and Gal-Or (Zhitomirsky and Gal-Or, 1997) deposited HAp on Ti6Al4V surgical alloy substrates by EPD technique and pointed out a problem associated to the use of additives, which can increase the chance of contamination and decrease chemical stability of HAp. As an alternative, many

studies have reported the addition of different organic solvents to HAp suspensions. Isopropyl alcohol as a suspension medium was studied by Zhitomirski and Gal-Or (Zhitomirsky and Gal-Or, 1997) to coat metallic substrate. Afterwards, Xiao et al. (Xiao and Liu, 2006) developed optimum conditions to prepare a dense, uniform and adherent coating using primary aliphatic alcohols (C1–C4) as medium. The addition of polyvinyl alcohol and N,N-dimethylformamide to HAp suspensions was also reported in order to improve the adherence and strength of the coatings and to prevent cracking of the deposits after drying (Boccaccini et al., 2010). Figure 8 shows nano-HAp coatings obtained by EPD process with variation of the potential and the deposition time (Drevet et al., 2016).

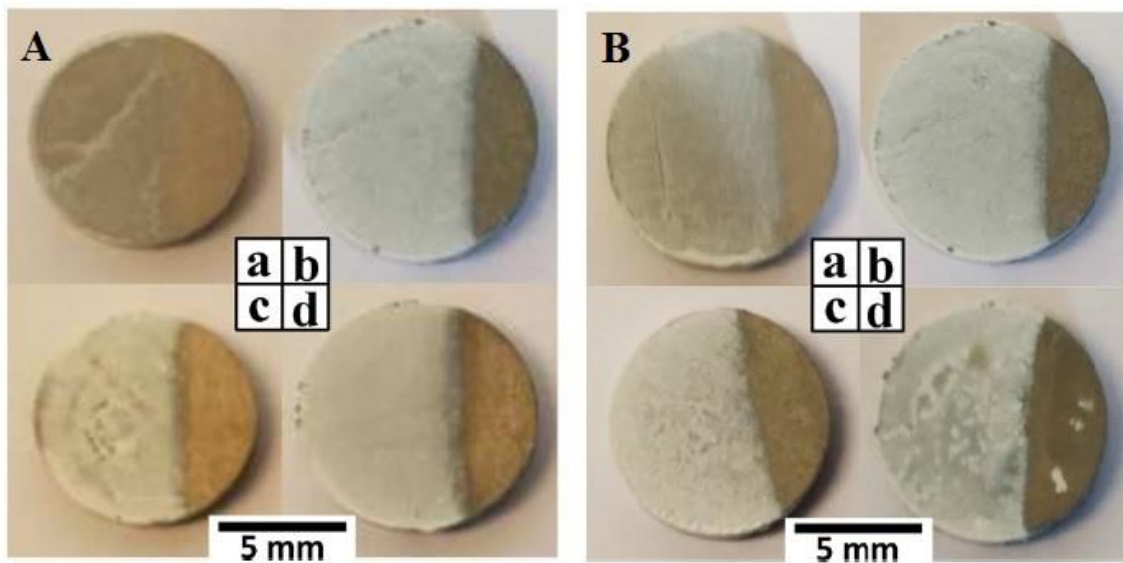


Figure 8. Nano-HAp coating on Ti6Al4V substrates obtained by EPD process: Fig 8-A shows the deposition at a time of 10 min. at different potentials: (A) 5 V, (b) 10 V, (C) 15 V and (D) 20 V and Fig 8-B shows the deposition at 10 V at different time points: (A) 5 min, (B) 10 min. (C) 15 min. and (D) 20 min (Drevet et al., 2016).

Looking for optimization of the EPD technique, numerical simulation has been employed providing insights into local variations of particle interaction processes during deposition (Boccaccini and Zhitomirsky, 2002). Particularly, numerical modeling seems to be a promising way to understand the lack between predictive models linking EPD process parameters and deposit properties (Boccaccini and Zhitomirsky, 2002), but then a robust mathematical model is required. Moreover, disadvantages include difficulty to produce crack-free coatings and suitable

bonding strength between the coating and metallic implant are frequent in this process (Asri et al., 2016).

2.6.1.6 Pulsed laser deposition

Pulsed laser deposition (PLD) has been used to create thin films through energetic condensation of atomic and molecular species (Koch et al., 2007). In the PLD deposition, a laser is used to vaporize a target that contains materials of the desired film. Thus, the surface of the target absorbs the radiation and electromagnetic energy is converted into electronic excitation, chemical energy, mechanical energy, and thermal energy (Koch et al., 2007). György et al. (György et al., 2004) proposed a PLD deposition of HAp enriched with carbonate and manganese ions on Ti substrate, using high vacuum, oxygen pressure at 10 Pa and post treatment for 6 h at 300 – 400°C in a water flow of vapor to promote crystallization. A pure, adherent and crystalline HAp coating was reported by Dinda and Mazumder (Koch et al., 2007), using PLD deposition followed by post annealing for 4 h at different temperatures (290, 300 and 310°C) to restore the initial crystalline structure. Despite this technique is a promising method to produce pure, crystalline and adherent HAp coatings (Dinda et al., 2009), several parameters and requirements, such as vacuum control (like medium vacuum (10^{-3} - 10^{-5} Torr), high vacuum (10^{-6} - 10^{-8} Torr), or ultra-high vacuum ($<10^{-9}$ Torr) (Koch et al., 2007), high temperature of substrate, laser radiation, laser operational frequency (Kassing et al., 2006) and post deposition heat treatment (to improve the crystallinity and adhesion) are necessary to be controlled and achieved (Dinda et al., 2009; Kassing et al., 2005).

2.6.1.7 Biomimetic coating

Biomimetic coating process was developed between the 1990s and 2000s (Surmenev et al., 2014) and consist in the immersion of metal implants in SBF at physiological pH conditions, temperature and ion concentration approximately equal to the human blood plasma (Surmenev et al., 2014). Initially, a substrate surface preparation involving alkali, acid or heat treatment is required. Then the substrate is soaked into SBF and several reactions occur. As an example, titanium and their alloys may be used to describe this process in five steps: (i) during the alkali pre-treatment a layer of amorphous sodium titanate is formed on the Ti surface; (ii) sodium titanate layer allows the formation of Ti-OH groups on its surface during SBF soaking; (iii) a layer of amorphous calcium titanate is formed with the interaction of the Ti-OH groups and local calcium ions from SBF; (iv) conversion of amorphous calcium titanate takes place to amorphous calcium phosphate with a Ca/P ratio of approximately 1.4; and (v) as the last step, the

amorphous calcium phosphate is converted into bonelike calcium deficient carbonated hydroxyapatite with a Ca/P ratio close to the value of mineral bone (≈ 1.65) (Koju et al., 2017).

The biomimetic coating process involves low temperatures to produce coatings (Rigo et al., 2004) with high bioactivity, good resorption characteristics which allows deposition on porous or complex geometries (Habibovic et al., 2002) and for this reason many studies have been published on this method.

Bharati et al. (Bharati et al., 2005) developed a CaP coating by biomimetic process through immersion of Ti substrate into a concentrated SBF with and without the use of CaO-SiO₂ glass as a source of nucleating agent for apatite formation. The results showed that it is possible to obtain a uniform and relatively thick coating with the surface of the substrate completely covered. Titanium substrates were coated with HAp by a new biomimetic route proposed by Habibovic et al. (Habibovic et al., 2002). The authors obtained a thick and homogeneous calcium phosphate coating after a few hours (4-48 h) of immersion and without any chemical pretreatment, using two biomimetic procedure steps: (i) the substrates were soaked in a solution that was 5 times more concentrated than normal SBF, (ii) the substrate was soaked into another solution with similar composition of the initial solution, but with decreased contents of crystal growth inhibitors (i.e., Mg²⁺ and HCO₃⁻). Figure 9 shows SEM micrographs of the coating morphology obtained after soaking in SBF solution on titanium substrate. Table 1 shows a brief summary of the main characteristics and parameters of the deposition techniques described in this chapter.

Table 1. Different deposition techniques of HAp and some main characteristics and process parameters.

Deposition technique	Thickness	Advantage	Disadvantage	Ref.
Plasma spray	<20 μm	Rapid deposition, a wide range of materials can be deposited, low degradation	Coating with lack uniformity (thickness, phase composition and microstructure), scarcely adherent	(Harun et al., 2017) (Graziani et al., 2017) (ASM Handbook, 2013)

Electrodeposition	0.1-0.5 mm	Low cost, can coat complex shapes and can produce uniform thickness	Bonding strength is not suitable between substrate and coating	(Harun et al., 2017)
Ion beam-assisted deposition	From a few angstroms to 2-4 μm	Uniform coating thickness; high reproducibility and control over micro-structure and chemical composition	Expensive; the coating-deposited is amorphous, crystalline coating can be difficult to deposit	(Surmenev, 2012)
Sol-gel	<1 μm to 15 mm	Low-coat, low processing temperature, high purity and thin film	High sintering temperatures; thermal expansion mismatch non-uniformity in thickness, lack of adherence to substrate	(Harun et al., 2017) (Asri et al., 2016) (Koju et al., 2017)
Electrophoretic	0.1-0.2 mm	Low equipment cost, can coating of complex shape, can control the microstructure and thickness by simple adjustment of process parameters	Difficult to obtain crack-free coatings; high sintering temperatures	(Harun et al., 2017) (Wang et al., 2002) (Farrokhi-Rad, 2018)
Pulsed laser deposition	0.05-5 μm	Coating dense, porous, crystalline and amorphous	Requires surface treatment, limited uniformity and splashing or particle deposition	(Harun et al., 2017) (Asri et al., 2016)
Biomimetic	<30 μm	Low processing temperatures, can cover complex shaped implants	Replenishment is required, Time-consuming and a constant pH (SBF)	(Asri et al., 2016) (Fatehi et al., 2008)

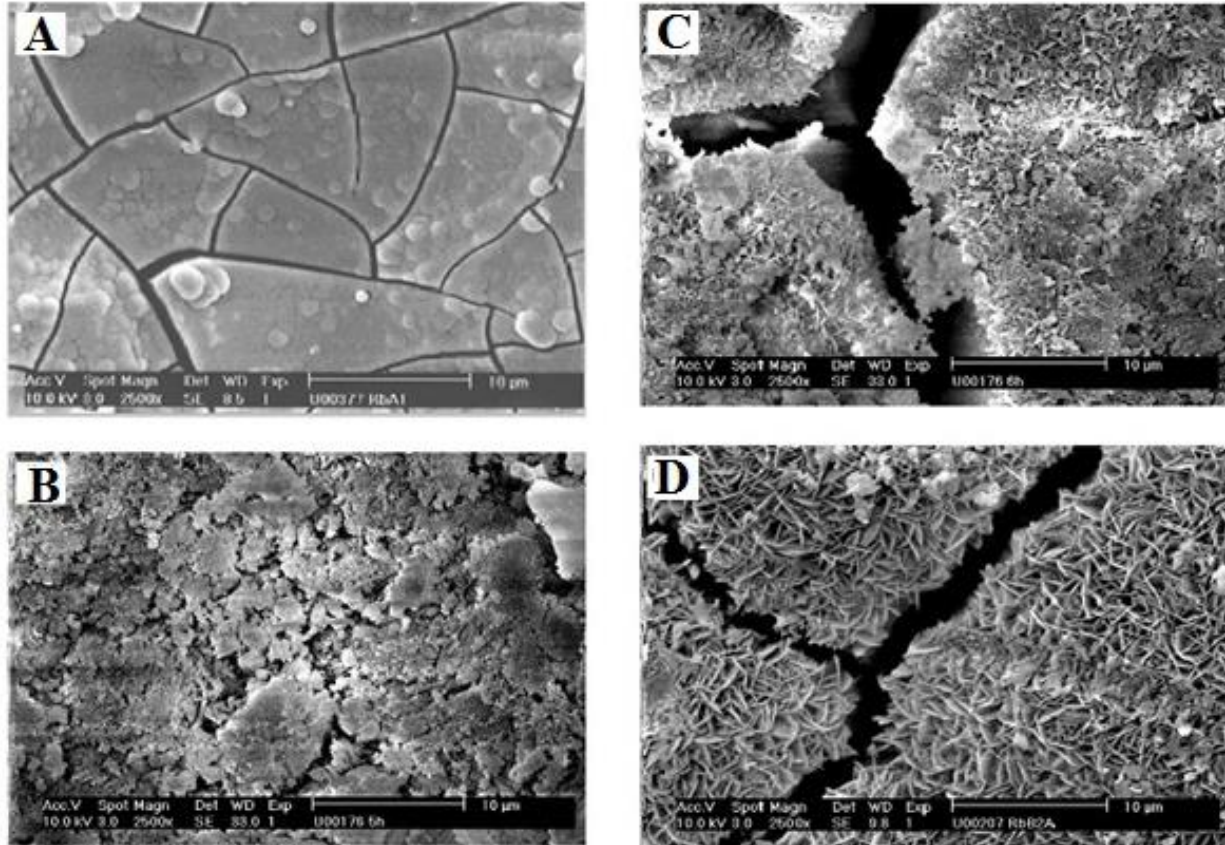


Figure 9. Morphology of the HAp coating fabricated by biomimetic method, using two SBF solutions (SBF-A 5x more concentrated than solution SBF-B): (A) SBF-A coating, (B) SBF-B coating after 5 h of soaking, (C) SBF-B coating after 6 h of soaking, and (D) SBF-B coating after 24 h of soaking on a Ti6Al4V plate (Habibovic et al., 2002).

3. Materials & methods

3.1 Synthesis and characterization of HAp powder

The HAp powder synthesis was carried out by precipitation technique through a wet chemical route using phosphoric acid (H_3PO_4 , Vetec 85%) and calcium hydroxide ($\text{Ca}(\text{OH})_2$, Synth[®]) according to the protocol described by Ramesh et al. (Ramesh et al., 2007). The $\text{Ca}(\text{OH})_2$ was added to water under mechanical stirring and heating; when the temperature reached $90 \pm 2^\circ\text{C}$ the H_3PO_4 was added. The solution obtained by mixing the reagents was maintained at a temperature of $90 \pm 2^\circ\text{C}$ for 24 h. After this period, the resulting precipitate was filtrated and dried in an oven at $110 \pm 2^\circ\text{C}$ for 24 h and calcined at 1100°C for 1 h. Then, the reaction product was crushed using a pestle and mortar and then sieved a # 325 ($<45\ \mu\text{m}$).

The crystalline phases of the resulting powder were identified by XRD using a Phillips X'Pert diffractometer MPD with copper tube ($K\alpha$ radiation = $1.5418\ \text{\AA}$). The voltage and current used in the tube were 40 kV and 40 mA, respectively, and XRD patterns were recorded in the 2θ range of 20° – 60° with a step duration of $0.05^\circ/\text{s}$.

FTIR was carried out with a Perkin Elmer model Spectrum at room temperature in the range of 400 – $4000\ \text{cm}^{-1}$ with the HAp powder being dispersed in a KBr matrix, in order to determine the functional groups PO_4^{3-} and/or OH^- . Particle size distribution analysis was performed through laser particle size analysis, using a laser diffractometer Cilas 1180 with a detection range of the instrument from 0.04 to $2500\ \mu\text{m}$. The particle morphology of the obtained powder was observed by SEM (JOEL - model JSM 6060).

3.2 Preparation of metallic substrate

A Co-15Cr-15W-10Ni alloy (Fort Wayne Indian Company, USA), according to ASTM F-90, was used as substrate for coating of HAp/PO by brushing method. The substrates were cut by wire electroerosion from the as-received raw material in discs with a diameter of $11.00\ \text{mm}$ and a thickness of $1.00\ \text{mm}$. Four types of surfaces modifications were prepared to investigate the interaction of the coating with different substrates of varying roughness: polished, passivated, heat treated and untreated. Untreated samples served as a control and one untreated sample with a diameter of $24.62\ \text{mm}$ and a thickness of $14.16\ \text{mm}$ was used to perform XRD analysis and for a better substrate observation, in order to attend the size dimensions of the XRD device. The polished substrate were ground using SiC paper with different grit sizes including 400, 600,

800, 1000, 1200 grit and then polished using 3 μm and 1 μm diamond pastes. The samples were polished before passivation and heat treatment to remove an oxide layer and impurities formed during the wire electroerosion cut. Passivation treatment was carried out in a solution of 20% nitric acid for 30 min at room temperature, following the practice for surface preparation of metallic surgical implants (ASTM F86-13). The “heat treated” samples were prepared by treatment in a furnace (NABERTHERM) at 800 °C for 1 h with a heating rate of 5 °C/min under N_2 and O_2 atmosphere, followed by cooling to room temperature. Untreated samples served as a control and samples untreated with a diameter of 24.62 mm and thickness 14.16 mm were used as received for a better observation of the coating and substrate. Finally, all samples were cleaned in each solution of acetone, ethanol and distilled in a water ultrasonic bath for 15 min.

3.3 Thermal behavior of the Pine Oil

Thermogravimetric analysis (TGA) analysis was performed using a TA Instruments, model TGAQ5000.IR with a rate of 10 °C/min, in the range from 30 °C to 650 °C under N_2 atmosphere and a gas flow of 25 mL/min. Differential scanning calorimetry (DSC) analysis was performed in a TA Instruments DSC (Q20) under nitrogen flow of 50 mL/min within the temperature range between -60 °C and 60 °C and a heating rate of 10 °C/min.

3.4 HAp/pine oil slurry preparation and coating process

The HAp powder and pine oil (proportion of 1:5 w:v) were mixed using a magnetic stirrer for 24 h at room temperature to achieve a homogeneous slurry. From preliminary tests, obtaining coating with different proportions (e.g. 1:2 w:v and 3:3 w:v) is also possible. PO was provide from Quimicamar-Brazil and its characteristics are summarized in Table. 1. Then, the metallic surfaces were completely coated with slurry using a paint brush (Condor - Brazil) of synthetic bristle and a width of 4 mm. A preliminary study was performed using temperatures in a range of 400 °C – 800 °C (in intervals of 100 °C) in order to determine the optimum temperature to promote adhesiveness between alloy and coating. Based on the results, the coated samples were heat treated in a high vacuum using a Graphite hot Zone furnace (Model 1000-2560-FP20) at 800 °C for 1 h, with a heating rate of 5 °C/min. The temperature used was chosen based on previous work by Khalid (Khalid et al., 2013), who reported about an improved adhesion and crystallization of HAp between 800 °C and 900 °C.

Table 2. Characteristics of the Pine oil 65% for the slurry preparation.

Commercial name	Chemical name	Composition	Extracted
Pine oil 65%	Alpha Terpineol or mix of terpene alcohols and terpene hydrocarbons	Terpene alcohols (total terpene alcohols 40%) and terpene hydrocarbons (alpha-pinene, beta-pinene, limonene, terpinolene and others).	From gum-resin of the pine tree

3.5 Characterization of the coating

After burnt out of PO under heat treatment, the crystalline phases present in the coating were analyzed by XRD using an Ultima IV type III diffractometer (Rigaku, Tokyo, Japan) equipped with cross beam optics (CBO) with Cu K α radiation and scanning speed of 0.05 °/s and in the 2 θ range of the scan interval from 10 to 70 °/s. The HAp/PO coating was removed from the substrate and dispersed in a KBr matrix for the FTIR investigation before and after sintering to evaluate its chemical structure in a range of 4000-400 cm⁻¹.

3.6 Surface topography and wettability

Surface topography and roughness were examined by SEM (Camscan Series 2, Obducat CanScan Ltd., Cambridgeshire, United Kingdom) and optical profilometer (Plu 2300, Sensofar Technology, Terrassa, Spain) in triplicates to measure the surface roughness value (R_a) for uncoated and coated samples. The surface tension of the coated and uncoated samples was measured by sessile drop method using a digital microscope (Keyence, VHX 600 dso) and then evaluated in the ImageJ software. Five liquid drops (diameter 10 μ m) of water, PO and HAp/PO were deposited on each sample and the contact angle was measured using a video camera linked to a microscope. The contact angle was measured by calculating the slope of the tangent to the drop at the liquid-solid interface.

3.7 Scratch resistance of the coating

The hardness and scratch resistance of the coating (Fig. 10) were measured by a pencil hardness tester (PH-5800, BYK-Gardner GmbH, Geretsried, Germany) following the ISO 15184 standard recommendations (Pardun et al., 2015). The pencil hardness tester is a constant-load

scratch test that deals with different scale of hardness grades (9B-9H). The test starts from soft grades (9B) to harder grades (9H) and the same load is applied on the surfaces of the coated samples with indenters of different hardness grades. The hardest pencil grade that did not cause damage to the coated specimen was considered as the pencil hardness of the coating (Lakshmi et al., 2011).

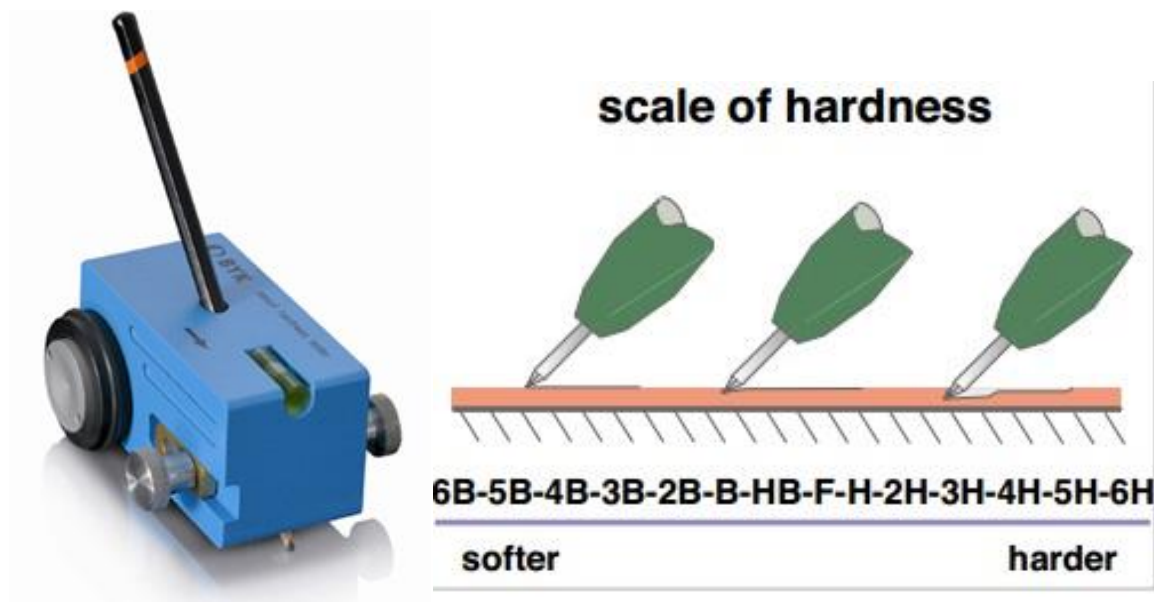


Figure 10. Pencil hardness tester (PH-5800, BYK-Gardner GmbH, Geretsried, Germany) and scale of hardness from softer to harder pencil.

3.8 Corrosion tests

In order to evaluate the effect of heat treatment on corrosion resistance, samples uncoated and coated with different surface and heat treatments were investigated. Table 3 shows specifications of the samples studied. CoCr disc samples were used as working electrode and electrically connected by using a sample holder for sheets with O-ring isolation and Cu back-contact. Electrochemical polarization tests have been performed by means of a Solartron SI 1287 electrochemical interface which was connected to a three-electrode cell with a saturated calomel electrode (SCE) reference electrode ($E = 0.241 \text{ V vs. normal hydrogen electrode (NHE)}$) and a Pt net as counter electrode. The measurements were conducted in Ringer's solution (8 g/L NaCl, 0.2 g/L KCl, 0.2 g/L CaCl_2 and 1 g/L NaHCO_3) with $\text{pH} = 7.4$ at 37°C . After immersion of the samples under open circuit potential (OCP) conditions for 30 min for establishing steady conditions, for cyclic voltammetry the potential was swept at a rate of 5 mV/sec from the OCP

firstly in anodic direction up to a value of 1 V vs. SCE, then in cathodic direction up to the OCP value and two 2 cycles were recorded. Linear potentiodynamic polarization measurements were conducted after 30 min of OCP adjustment with a slow sweep rate of 0.5 mV/s starting from the cathodic regime (OCP-150 mV) and sweeping up to 1 V vs. SCE. Electrochemical measurements on uncoated samples were repeated to ensure a high level of reproducibility.

Table 3 Description of the surface treatment and coating parameters of the CoCr disc samples.

Sample	Surface treatment	Coating	Heat treatment (°C)
Pol	Polished	-----	-----
Pol_Pas	Polished & Passivated*	-----	-----
Pol_Pas_coa_300	Polished & Passivated	HAp + PO**	300
Pol_coa_800	Polished	HAp + PO	800
Pol_Pas_coa_800	Polished & Passivated*	HAp + PO	800

* Polishing and passivation of the CoCr disc were carried out as described in section 3.2.

** Preparation and coating of the CoCr disc were carried out as described in section 3.4.

3.8.1 Cyclic voltammetry

Cyclic voltammetry (CV) is a useful technique for acquiring information about electrochemical reactions (reduction and oxidation), where reversible and irreversible oxidations are investigated. This method consist in applying a time varying potential to an electrochemical system and as response the current is measured (Örnberg, 2007). The circuit system is formed by a three electrode cell: working, counter and reference electrode that are placed close to each other in an electrolytic solution under an inert atmosphere (Brubaker, 2014). During CV analysis reduction and oxidation events are measured through the recording of the current between the working and counter (or auxiliary) electrode, which results in a data plotted as current (i) vs. potential (E). Reduction events occur with the reduction potential and are measured by increasing current values. Oxidation events are observed at potentials that favors the loss of electrons by decrease of current values (Jove Science Education, 2018).

3.8.2 Potentiodynamic polarization

Potentiodynamic polarization is a direct current technique usually highly to determinate corrosion rate, passivity and breakdown, and susceptibility to pitting (localized corrosion) (Örnberg, 2007). In this technique normally three electrodes are used: (i) working electrode that

is the metallic sample to be investigated; (ii) reference electrode is a conductor with a well-known potential that complete the system and; (iii) counter electrode is responsible to provide current to the working electrode (Bakrachevska, 2014). To perform the measurements, electrochemical potential (voltage) is applied between the electrodes (Bakrachevska, 2014) and a potentiostat device controls the driving force of the electrochemical reactions that occurs on the working electrode (Örnberg, 2007). During potentiodynamic polarization, the potential applied to the working electrode increases with time and measured variable is the current. Thus, a graph is plotted as result: current vs. potential (Bakrachevska, 2014). A typical potentiodynamic polarization curve is shown in Figure 11. This OCP circuit corresponds to the corrosion potential E_{corr} , where two features also are important for analysis: Breakdown potential ($E_{\text{Breakdown}}$) occurs when the potential applied increase significantly the anodic current. The repassivation potential (E_{Repass}) corresponds to the protection potential at which hysteresis loop is completed when a reverse polarization scan is applied (Örnberg, 2007). In Figure 11 a dashed line represents where the local corrosion occurs.

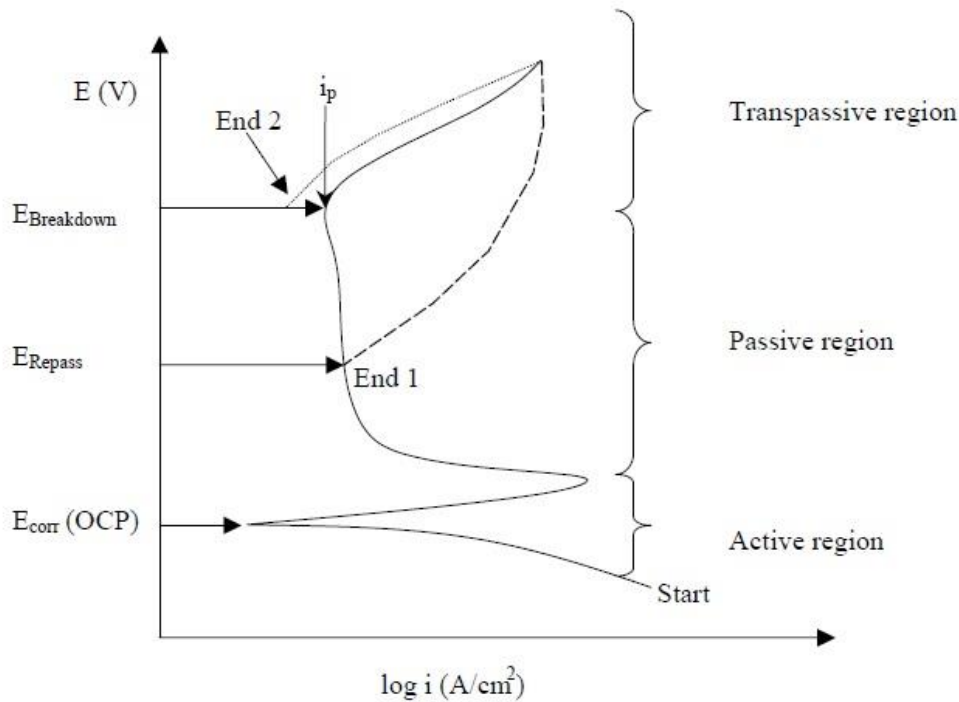


Figure 11. Representation of a potentiodynamic polarization curve (Örnberg, 2007).

Fig. 11 shows a potentiodynamic polarization curve with three regions: active, passive and transpassive region. When the potentiodynamic polarization scan starts the potential progress for

a positive region and three regions (Fig. 11). The active region corresponds to the susceptible corrosion in which the metal begins to corrode with an increase of the potential that increase the current density and which is observed above E_{corr} . The current density has a sharp decrease with the increase of potential and then the passive region starts and a critical state for the formation of the oxide film. These regions will reclaim until a complete oxide formation, where the current density is stabilized and a low or no increases of the current density are observed with a further increase of the potential. The metal will keep passivated until a determined high potential that causes a significantly increase of the current density, which affects the transpassive region and the corrosion enables again (La, 2014).

3.9 *In vitro* bioactivity analyses

The coated polished and passivated substrates were immersed in SBF solution and incubated (CO_2 incubator/Queue Stabil Therm) at 37 °C for 3, 7, 14 and 21 days. The SBF solution was prepared according to Oyane et al. (Oyane et al., 2003) and buffered to pH 7.4 with 1 M NaOH at 37 °C. The composition of the SBF solution is similar to human blood plasma and its composition for 1 L can be seen in Table 4. The SBF solution was refreshed every 2 days. For analysis, the samples were rinsed with deionized water to remove the inorganic ions and dried in a desiccator for 24 h. Then, the samples were characterized by SEM (Leica EM SCD005, Leica Microsystems) in order to assess bioactive behavior of the coated samples.

Table 4. Purity and reagents quantity to prepare 1000 mL of SBF (Oyane et al., 2003).

Reagent	Purity %	Amount
<i>NaCl</i>	> 99.5	5.403 g
<i>NaHCO₃</i>	> 99.5	0.504 g
<i>Na₂CO₃</i>	> 99.5	0.426 g
<i>KCl</i>	> 99.5	0.225 g
<i>K₂HPO₄ . 3 H₂O</i>	> 99.0	0.230 g
<i>MgCl₂ . 6 H₂O</i>	> 98.0	0.311 g
<i>1.0 M HCl</i>	—	100 mL
<i>HEPES</i>	> 99.9	17.892 g
<i>CaCl₂</i>	> 95.0	0.293 g
<i>Na₂SO₄</i>	> 99.0	0.072 g
<i>1.0 M NaOH</i>	—	15 mL

3.10 Cell culture

Osteoblast progenitor cells were isolated from human femoral heads of osteoarthritic patients undergoing total hip replacement at the University Hospital Carl Gustav Carus Dresden (Germany) after informed consent (approval by the ethics commission of TU Dresden, EK 303082014). The uncoated and coated polished substrate were sterilized by gamma irradiation (minimum 29.9 KGy) (Gossia et al., 2016). The coated and uncoated samples (control) were placed in a 12-well plate and covered with 1 mL of alpha-Medium (α -MEM, Biochrom AG, Berlin, Germany) and supplemented with 9% fetal calf serum (FCS) (Biochrom AG, Berlin, Germany), 1% Penicillin/Streptomycin (LifeTechnologies), and 1% L-Glutamine (LifeTechnologies). Then, the OB10 cells were seeded in pre-incubation for 24 h at a density of 2×10^6 cells/well at 37 °C in a humidified atmosphere with 8% CO₂.

For indirect setup of the coated and uncoated polished substrates, 1×10^4 OB10 cells were seeded into 48-well tissue culture polystyrene plates in medium (α -MEM with FCS and osteogenic supplements (β -glycerophosphate/10 mM, ascorbic acid-phosphate/0,05 mM and dexamethasone/ 10^{-7} M) and cultivated for 24 h. Tissue culture polystyrene plates were used as group control. To obtain substrate extracts the samples were immersed in culture medium and kept under cell culture conditions for 24 h. After 24 h of initial incubation, 1 ml cell culture extracts from the samples was added on each sample. The experiments were performed from the first day of immersion and repeat every 3 to 4 days. After cell cultivation for 1, 7, 14 and 21 days the cells were washed with phosphate buffered saline (PBS) and stored at -80 °C for further biochemical analyses.

Direct cell culture setup was carried out directly on the coated and uncoated polished substrates. 2×10^4 cells suspended in α -MEM with FCS and osteogenic supplements were seeded into 24 wells on each coated and uncoated polished substrate. After 24 h of seeding the cell culture medium was supplemented with 10^{-7} M dexamethasone (Sigma-Aldrich GmbH), 0.05 mM β -glycerophosphate (Sigma) and 10 mM ascorbic acid 2-phosphate (Sigma). The cell culture medium was changed every 3 to 4 days. After 1, 7, 14 and 21 days the medium was removed and the substrates were washed in PBS, following freezing at -80°C until biochemistry analysis.

Biochemical analysis of alkaline phosphatase (ALP) activity, DNA content and total intracellular lactate dehydrogenase (LDH) activity of the OB10 on coated CoCr substrates were determined according to previous studies (Bernhardt et al., 2009) and polystyrene cell culture

plates were used as control group. The cell proliferation was analyzed after 4, 7, 14 and 21 days by optical microscopy (LSI, Macro Confocal, Leica, Germany).

4. Results & Discussion

4.1 Characterization of HAp powder

The identification of the crystalline phases of the HAp powder was performed using XRD, and the results are presented in Figure 12. The diffraction peaks show that no secondary phases were found and all peaks could be attributed to the HAp phase (Li et al., 2016). The main diffraction peaks characteristic of HAp were observed at 2θ values of 28.9° for reflection (002), at 31.9° (triplet) for reflections (211), (112) and (300), and at 34° for reflection (200) (Barbosa et al., 2013).

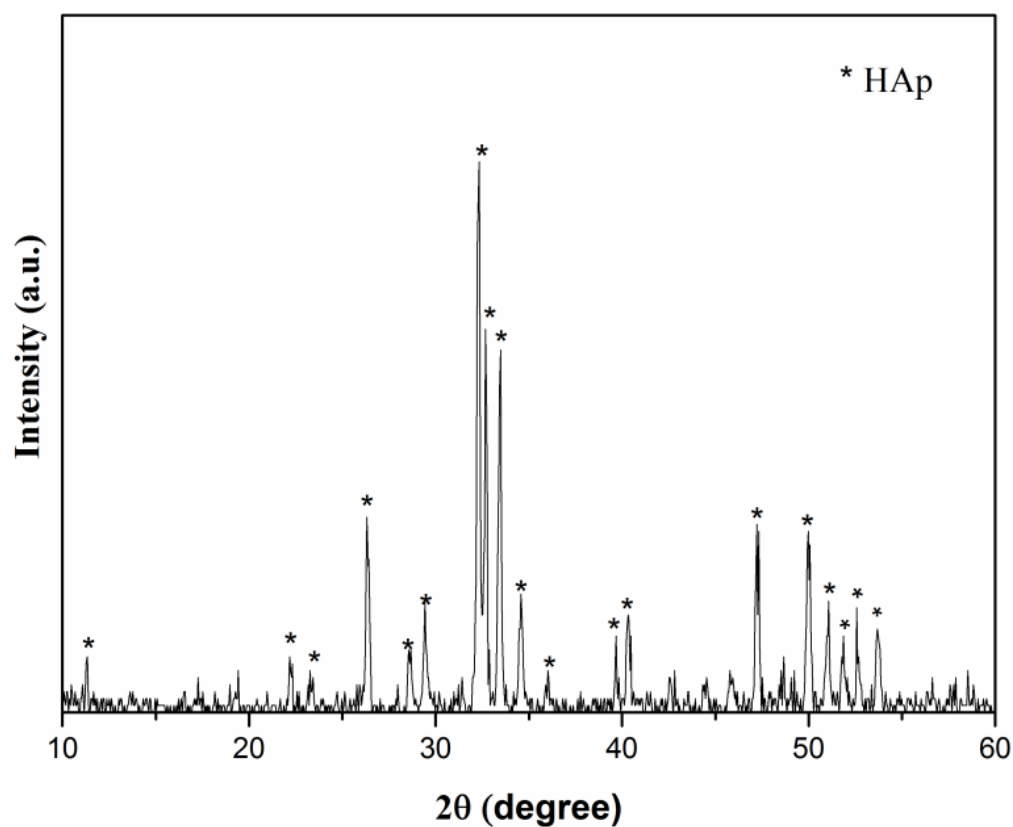


Figure 12. X-ray diffraction spectrum of HAp powder obtained by wet route and sintered at 1110°C (PDF 01-072-1243; 01-084-1998).

As observed in the FTIR spectra (Fig. 13), the bands characteristic for OH^- , PO_4^{3-} , CO_3^{2-} and H_2O are present in the sintered HAp powder at 1110°C . Absorption bands at 3433 cm^{-1} and 1639 cm^{-1} were found, correspondent to adsorbed water (Guo et al., 2013) or resulting from the

KBr matrix. The peaks around 3570 cm^{-1} and 630 cm^{-1} are characteristic peaks of stoichiometric HAp (Latifi et al., 2017). The band between 564 cm^{-1} and 604 cm^{-1} is corresponding to triplet of the phosphate group (PO_4^{3-}) (Bakan et al., 2013). Around 1094 cm^{-1} appeared a major peak of phosphate group referent to P-O stretching peak, which is the most intensified peak among the phosphate vibration modes (Wen et al., 2016). The bands between 1400 cm^{-1} and 1450 cm^{-1} correspond to stretching modes of the CO_3^{2-} ion (Shu et al., 2005; Cai et al., 2013; Chaudhuri et al., 2013).

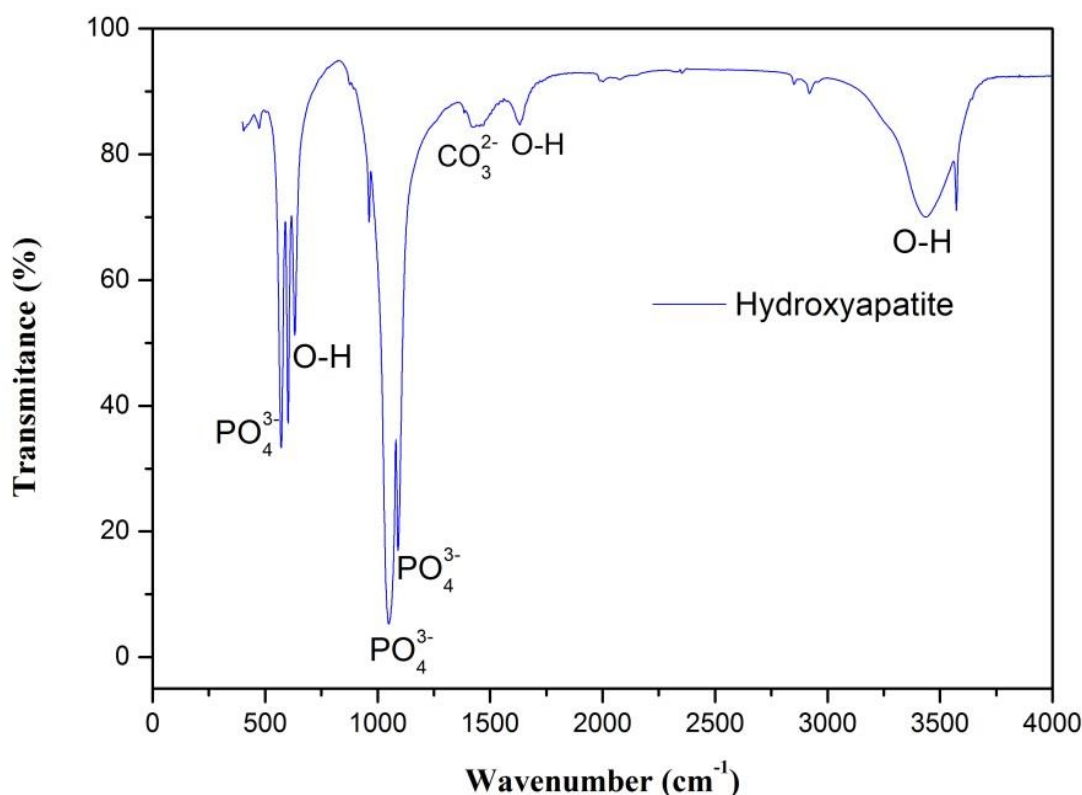


Figure 13. The FTIR spectrum of the HAp powder sintered at $1110\text{ }^{\circ}\text{C}$.

Figure 14 (A) presents the particle size distribution of the HAp powder. An average diameter for the particles of $14.82\text{ }\mu\text{m}$ was found and the presence of smaller particles were observed by evaluating the smaller peaks at around $0.8\text{ }\mu\text{m}$ and $3\text{ }\mu\text{m}$, since 10% of HAp particles revealed an average diameter of $1.66\text{ }\mu\text{m}$. The HAp powder obtained in this work showed the presence of two major peaks with different particle size ranges, which suggests agglomeration in the micrometer size range, resulting in primary agglomerations (first peak), and in the second peak the particles keep agglomerating until they reach the micrometer size range higher than $5\text{ }\mu\text{m}$ (Fig. 14 (A)). This agglomeration is related to the wet chemical methods used to produce the

HAp powder that usually produces a highly agglomerated structure, in which agglomerated sizes up to a few hundred microns can be obtained. The first peak is referent to the primary agglomeration of the HA primitive crystallites that occurs during the precipitation or aging process. The agglomeration identified in the second peak is attributed to the isothermal treatment, such as hydrothermal treatment or calcination at temperatures between 120 °C to 1100 °C up to 24 h. The SEM analysis (Fig. 14 (B)) shows that the morphology of the HAp powder is highly agglomerated and particles are composed of individual fine crystallites (Lakshmi et al., 2011).

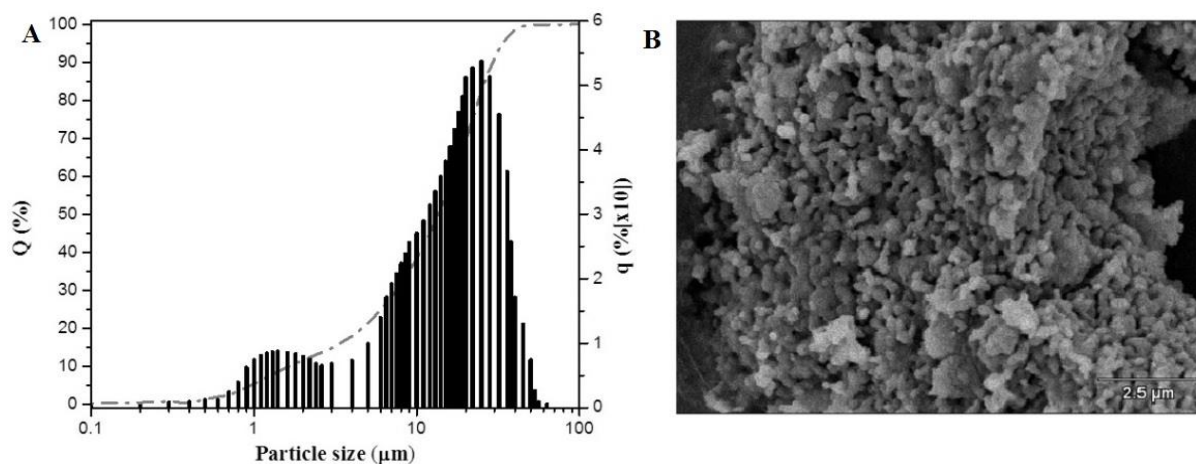


Figure 14. Particle size distributions of the HAp powder sintered at 1100 °C for 1 h (A) and appearance in scanning electron microscopy (B).

4.2 Thermal characterization of the pine oil

The thermal behavior of the PO was evaluated through TGA and DSC analyses, and these results are shown in Figures 15 and 16. Figure 15 presents the thermal stability of the PO: already at room temperature the oil began to lose mass and at 100 °C 99.3% of its mass had lost. Above 100°C, no vestiges of PO could be found due to its low viscosity and surface tension, which facilitate its evaporation (Süntar et al., 2012; Zeng et al., 2012).

Figure 16 presents the DSC thermogram of the PO, where a peak referent to the flash point is noticed at 57 °C. Thus, PO mixed with HAp will easily evaporate during the heat treatment at 800 °C.

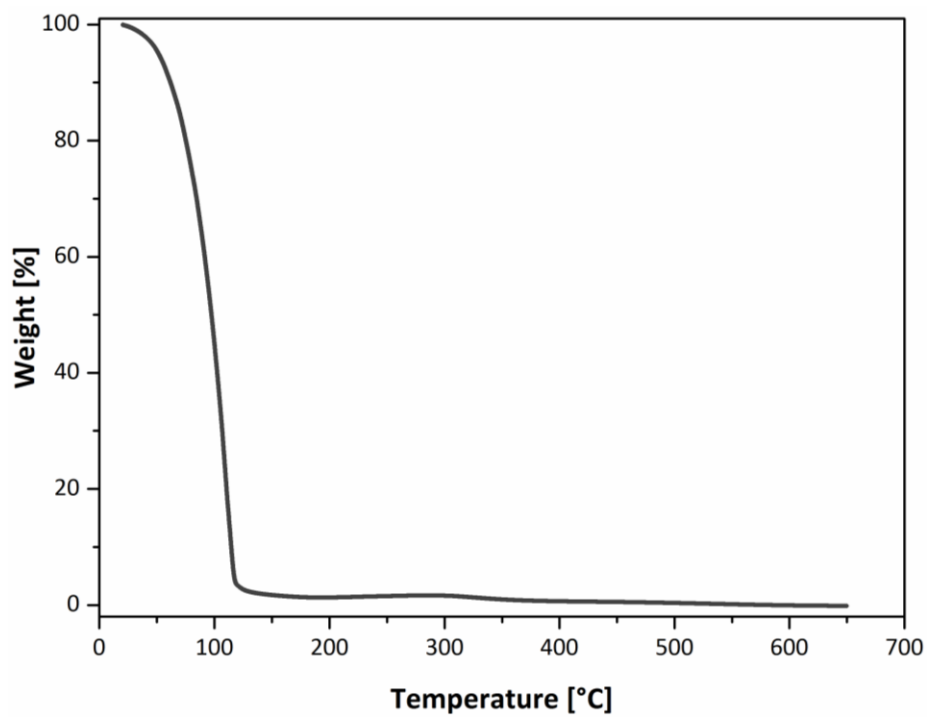


Figure 15. Weight loss of the PO (TGA).

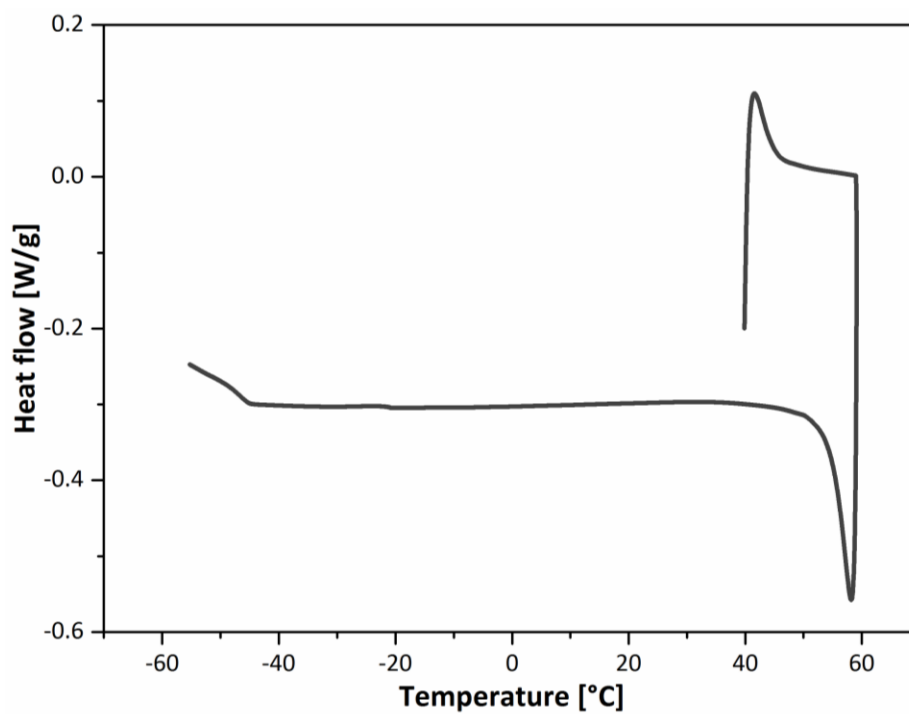


Figure 16. DSC thermogram of the PO.

4.3 Characterization of the coating surface

In order to obtain a clean surface and to allow even coating of the metal surface by the painting method, the substrates were polished to remove the oxide layer and impurities from electroerosion cut. Figure 17 shows the metallic substrate before and after complete coating with the PO/HAp slurry by brushing. It was shown that the PO allowed the HAp particles to fully disperse on the substrate, which indicates a good wettability of the substrate.

HAp coating obtained after sintering showed a homogeneous, dense and crack-free surface, however the SEM micrographs revealed the presence of micro pores (Fig. 18 (A,B)). The cross-section of the coated substrate showed that the substrate was completely covered by the coating and a close contact between the interface of substrate and coating with a layer thickness of about 20 μm can be observed, as demonstrated in Figure 19. The hydrophilic character of metallic substrate increases the wettability, allowing a better dispersion of the HAp particles and an intimate contact on the metallic surface.

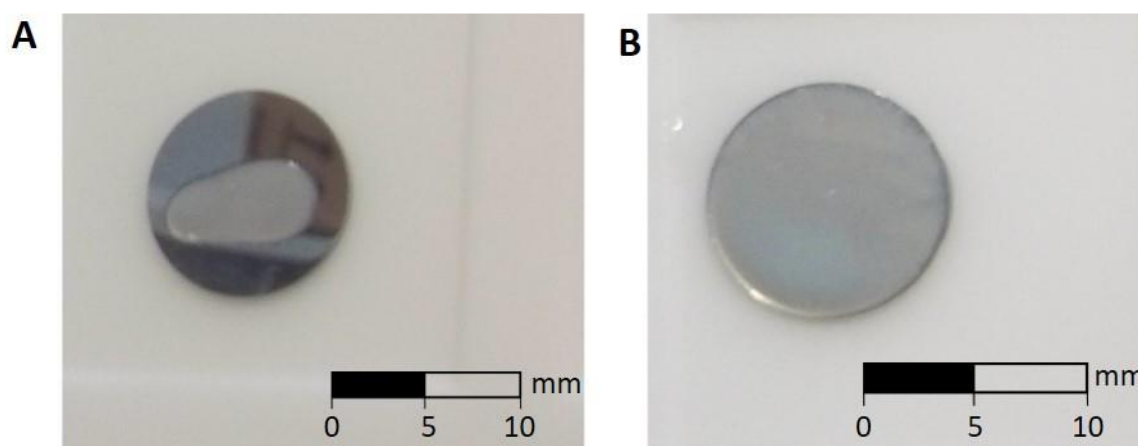


Figure 17. (A) Metallic substrate with slurry before to be fully brushed and (B) after brush coating with HAp/PO slurry.

The interaction between substrate and coating is related to hydrophilic character of PO that allows a better dispersion of HAp particles and an intimate contact with the substrate. The high surface energy of the metallic substrate improves the wettability with the PO/HAp slurry and their chemical bonds of the PO could be bind with the substrate. PO/HAp slurry coating process via brushing shows a similar behavior like other paint coatings (Fig. 17). Paint coatings are deposited on a surface as a liquid (as vehicle to deposit solid material, made of resin dissolved in a solvent) that contains a pigment. Afterwards, by drying a tough coating is formed that binds

the pigment to surface (Encyclopedia Britannica, 2018). In the present study, the slurry has a similar behavior like a paint, because the slurry is the vehicle to disperse the HAp particles in a solvent (PO) on the substrate, using brushing to coat the surface. The low surface tension of PO improves the ability of the slurry to wet the substrate and after thermal removal of the PO, the coating is bound to the surface.

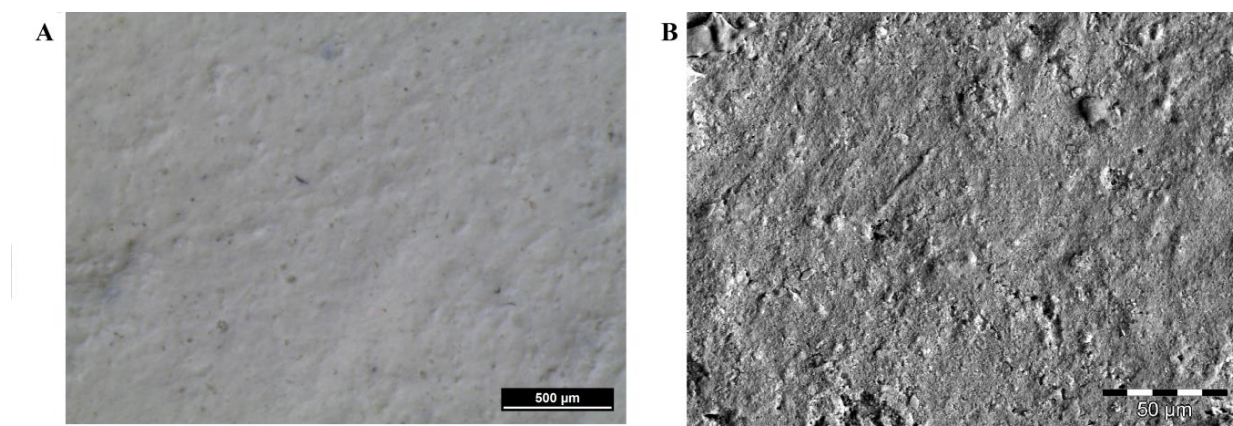


Figure 18. (A) Optical microscopy and (B) SEM images of HAp coating after sintering.

The close contact of the coating and the substrate (Fig. 19) suggests that attractive forces were developed, forming interfacial bonds (adsorption). The adsorption process occurs from molecules in the paint film wet or freely flowing over the substrate and making intimate contact with the substrate, resulting in interfacial bonds. The bonds developed from the adsorption of paint molecules on the substrate, which are resulting in attractive forces or usually designated as secondary or van der Waals forces (Materials Today, 2012), since physical adsorption or wetting happens when the molecules in the wet coating make intimate contact with the substrate (Harun et al., 2017). Figure 20 presents the coated surface after scratch test with a pencil. The results of the pencil scratch showed that HAp coating showed resistance to soft pencils. When the coating was scratched with 4H pencils the coating was completely removed, as demonstrated in Fig 20 (A). SEM revealed (Fig. 20 (B)) a complete damage of HAp coating due to intermediate coating–substrate adhesion that allowed removal of the coating by 4 H pencil, since a close contact between substrate/coating is necessary to promote adhesion bonding.

Figure 21 shows the SEM micrograph of a selected coated surface. It is observed (Fig. 21 (A)) a dense, compacted coating with some pores on the surface. The energy-dispersive X-ray spectroscopy (EDS) analysis (Fig. 21 (B)) suggests that there is coexistence of Ca, P and W, indicating inter-diffusion of the elements from the substrate (Lu et al., 2004).

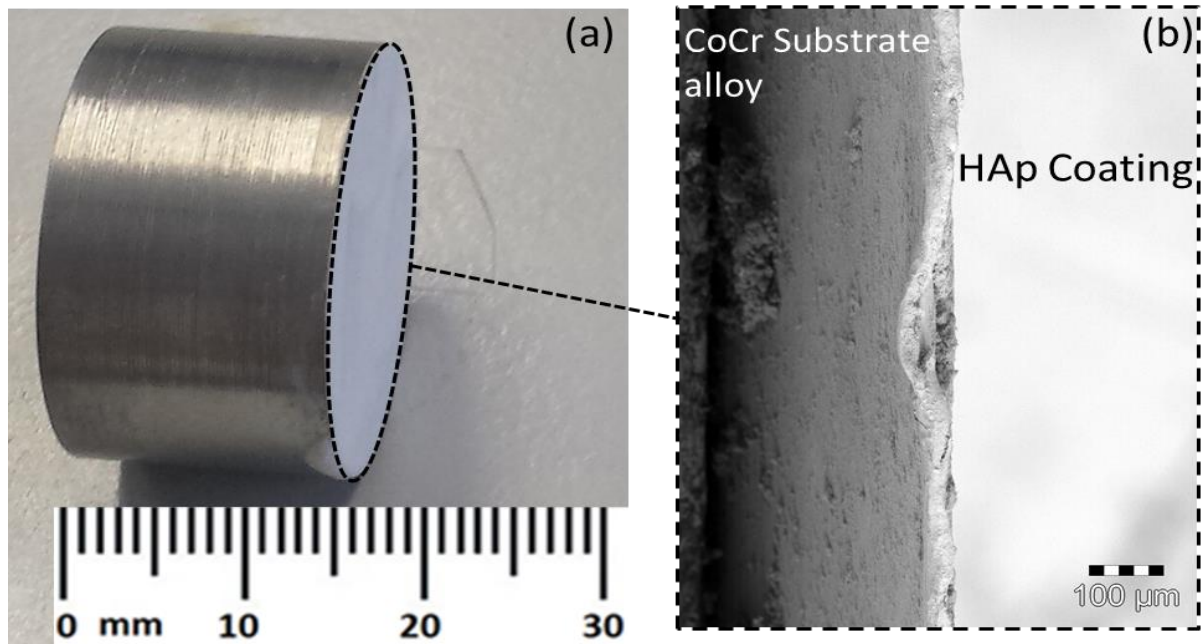


Figure 19. Coated metallic substrate (A) after sintering and (B) SEM micrograph of the cross-section.

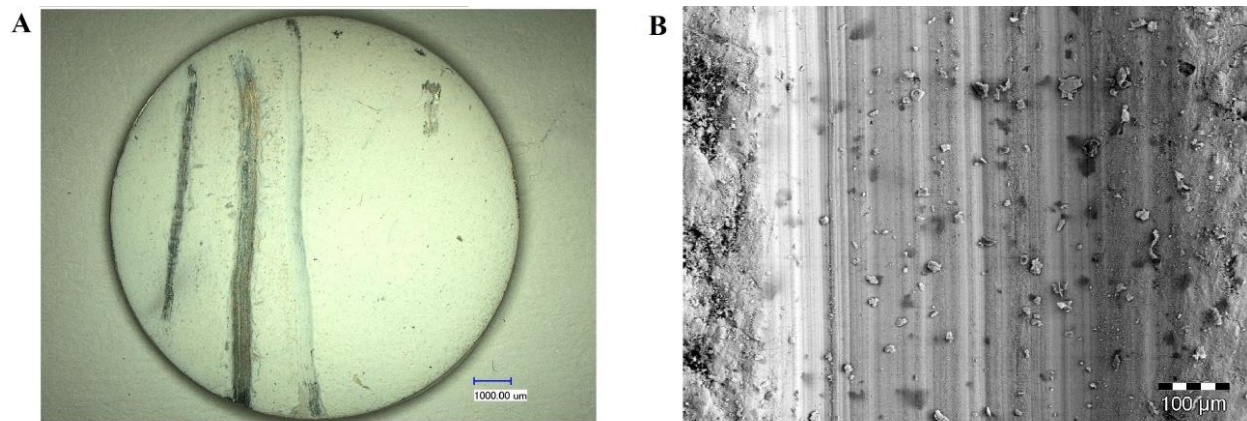


Figure 20. (A) Coated metallic substrate and (B) SEM micrograph of the coating after scratch test with 4H pencil.

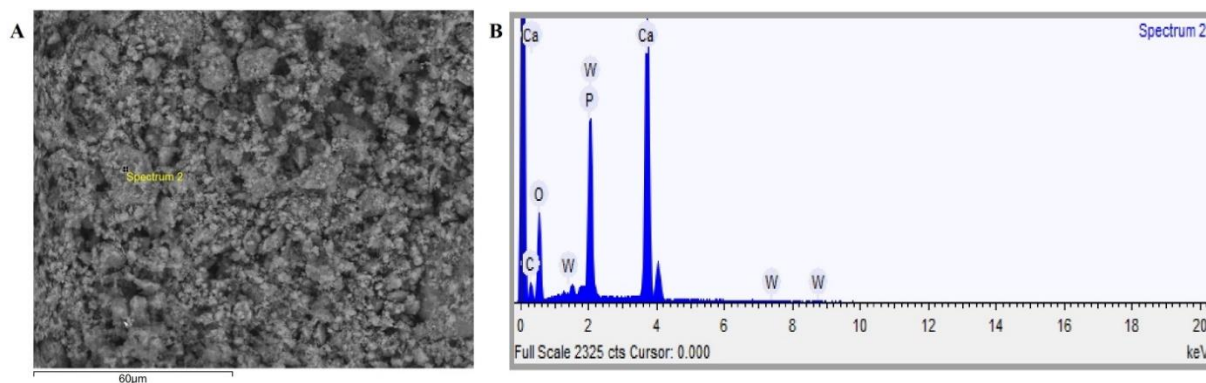


Figure 21. SEM micrograph of the HAp coating (A) and EDS spectra of the coating (B).

4.3.1 X-ray diffraction and FTIR analyses

The XRD patterns of HAp coating and dried and sintered HAp slurry are shown in Figure 22. All diffraction peaks can be ascribed to those of the HAp phase. The XRD patterns of HAp coating deposited on metallic substrate (Fig. 22) showed diffraction peaks similar to those of pure HAp, which suggested that the use of PO allowed obtaining a coated substrate with similar crystallographic properties of HAp. The diffraction peaks at $2\theta \approx 26^\circ$, 32° , 34° and 54° correspond to the (002), (211), (200) and (004) crystal planes respectively (Barbosa et al., 2013; Huang et al., 2016), confirming the absence of any other calcium phosphate phase or impurities except the Cr peaks from the substrate.

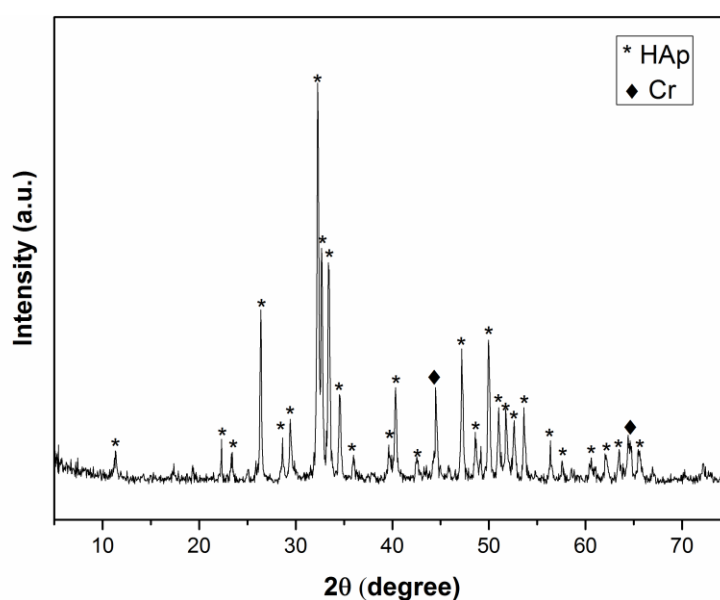


Figure 22. XRD pattern of HAp coating on CoCr alloy prepared by brushing method (PDF 01-072-1243; 01-084-1998).

Figure 23 shows FTIR spectra of the HAp/PO coating before heat treatment. Absorptions at 567 cm^{-1} , 602 cm^{-1} , 628 cm^{-1} , 957 cm^{-1} , 1045 cm^{-1} , and 1090 cm^{-1} corresponding to presence of PO_4^{3-} group from HAp were observed (Singh et al., 2011). The bands around 3578 cm^{-1} and $2913\text{--}2970\text{ cm}^{-1}$ are due to stretching vibrations of OH and C-H aliphatic groups (Duce et al., 2015; Xiao et al., 2015). The broad peak around 3400 cm^{-1} is associated to the vibration of hydrogen bonded OH groups. The peak at 1381 cm^{-1} is related to C-H bonds and at $\approx 1600\text{ cm}^{-1}$ a strong peak is attributed to aromatic rings or C=C double bonds (Liu et al., 2012). FTIR spectra before thermal treatment confirm that the groups C=C, C-H and OH are referring to chemical groups from PO. The spectra of HAp/PO coating after thermal treatment confirmed the existence of bands at 567 , 601 , 634 , 1045 cm^{-1} that can be attributed to the symmetrical stretching and bending mode of PO_4^{3-} , and band at 3569 cm^{-1} is attributed to the OH⁻ stretching mode (Zeng et al., 2012b). The bands observed between $3300\text{--}3600\text{ cm}^{-1}$ and $\approx 1628\text{ cm}^{-1}$ are referring to absorbed water. All peaks identified after the thermal treatment of the coating at $800\text{ }^{\circ}\text{C}$ correspond to HAp, which indicates the elimination of both water and organic materials, since no peak was found for PO or another chemical group from a possible PO-HAp reaction. The XRD and FTIR analysis corroborated that the pure HAp coating can be easily obtained from the precursors PO and HAp by brushing and subsequent heat treatment at $800\text{ }^{\circ}\text{C}$ for 1 h.

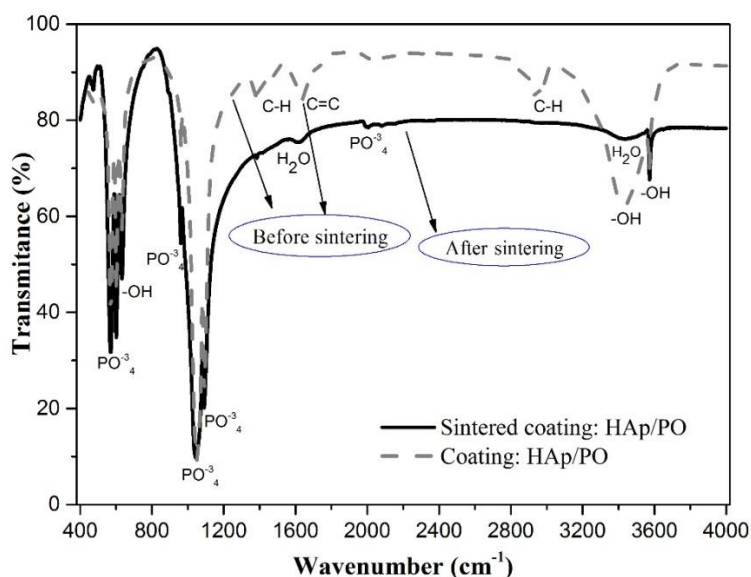


Figure 23. FTIR spectra of the HAp/PO slurry before and after sintering.

4.4 Surface properties

4.4.1 Topography, roughness and wettability

Surface roughness and wettability are key parameters to understand the adhesiveness phenomena. Physical characteristics of the substrate surface (e.g. roughness, microcavities, cracks, coatings, adsorbed layers, prior thermal or ionic cleaning etc.) can change, often dramatically, the spreading and wetting behaviors of metal-ceramic coatings (Sobczak et al., 2005). There is no doubt that roughness is a primary cause of contact angle hysteresis ($\Delta\theta$) and, on coatings, the roughness ensures a good wetting of the surface, allowing an intimate contact with the substrate.

Figure 24 depicts HAp coatings with four differently rough surfaces (passivated, polished, heat treated and uncoated). HAp coatings deposited on these different surfaces showed that it is possible to obtain a homogeneous coating for all substrates and similar and homogeneous coatings without significant differences among the samples were observed (Fig. 24). Surface topography of the uncoated and coated samples with different surface treatments characterized by profilometer can be seen in Figures 25 and 26. The untreated and heat treated uncoated samples, as expected, showed higher roughness (Fig 25 (A,B)). The first sample (untreated) is associated to fabrication process and to the spontaneous formation of a passive oxide layer. The second sample (heat treated) is attributed to heat treatment, which results in the formation of an oxide layer. The smooth nature of the polished samples was confirmed by profilometer analyses (Fig. 25 (C)) and the roughness associated to passivated sample is due to the passivation process (Fig. 25 (D)). Coated samples (Fig. 26 (A-D)) showed a similar behavior of roughness as the uncoated samples, where the rougher substrate resulted in coatings with higher roughness (Fig. 26 (A,B)) and smoother substrates had a tendency to better disperse the slurry, resulting also in a smoother coating (Fig. 26 (C,D)).

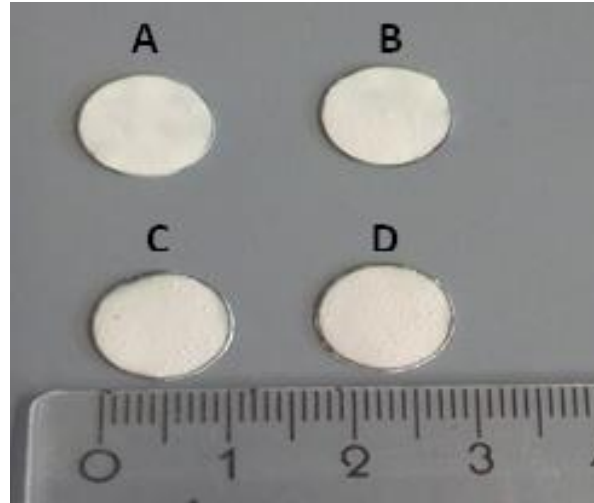


Figure 24. Image of brushing coated samples on surfaces with different treatments (passivated (A), polishing (B), heat treated (C) and untreated) (D) after heat treatment.

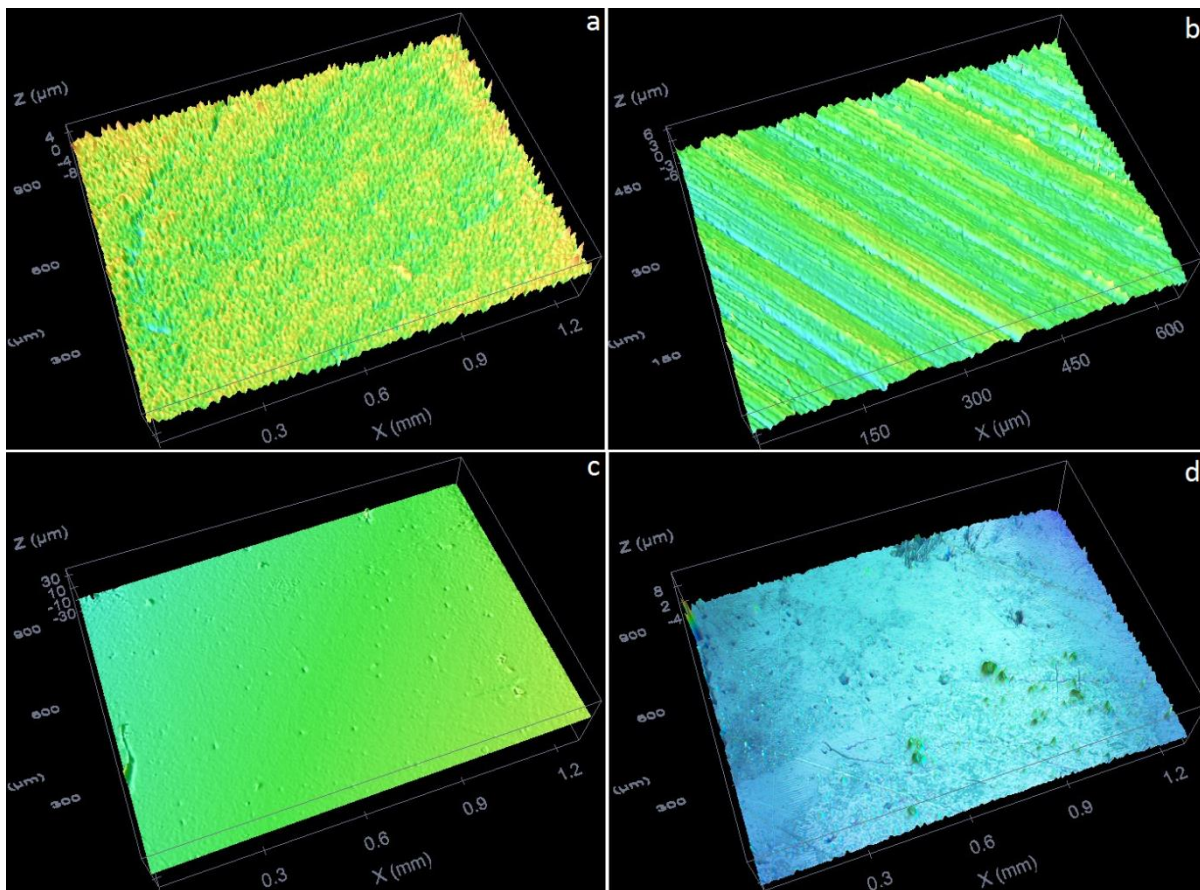


Figure 25. Surface roughness images for uncoated samples: (a) heat treated surface ($R_a = 0.825 \pm 0.060 \mu\text{m}$); (b) surface untreated ($0.550 \pm 0.009 \mu\text{m}$); (c) polished surface ($0.274 \pm 0.033 \mu\text{m}$); (d) passivated surface ($0.477 \pm 0.018 \mu\text{m}$).

The relation between the measured roughness values (R_a) and the wettability with water, PO and PO/HAp slurry of the uncoated metallic substrates are shown in Figure 27. The heat treated specimen showed rougher, more irregular surface and higher value of surface roughness (R_a 0.82 μm) is expected due to heat treatment which leads to formation of valleys. The measured roughness values (R_a) confirmed that the polished (R_a = 0.28 μm) sample showed smoother surface, because the polishing treatment was responsible to remove the oxide layer and contamination from cut and fabrication process.

Surface wettability is one the most important parameters of an implanted material and in combination with other surface characteristics, such as the micro- and nanotopography, surface energy, charge and functional groups (Rupp et al., 2014), determine a biological cascade of events responsible for example for protein adsorption, platelet adhesion/activation, blood coagulation and cell and bacterial adhesion (Xu and Siedlecki, 2007). Albrektsson et al. (Wennerberg and Albrektsson, 2009) introduced the concept of a possible role of surface finish on the biological response to an implant. Tremendous efforts have been made to understand the influence of surface topography on biological response (Rosales-Leal et al., 2010; Rupp et al., 2014). At cellular level, the surface topography is responsible to directly influence biological responses, such as the orientation and migration of cells. Also cytoskeletal arrangements are directly influenced by the surface topography (Rosales-Leal et al., 2010). According to the Wenzel model roughness added to a flat surface allows the liquid to fully wet the surface. If the contact angle on the respective flat surface is $< 90^\circ$ the roughness makes the surface become more hydrophilic, while for liquid contact angles $> 90^\circ$ the roughness makes the surface more hydrophobic and consequently there is surface repellence towards the liquid. Both processes are multiplied by the magnitude of surface roughness (Cassie and Baxter, 1944; Rodrigues et al., 2017).

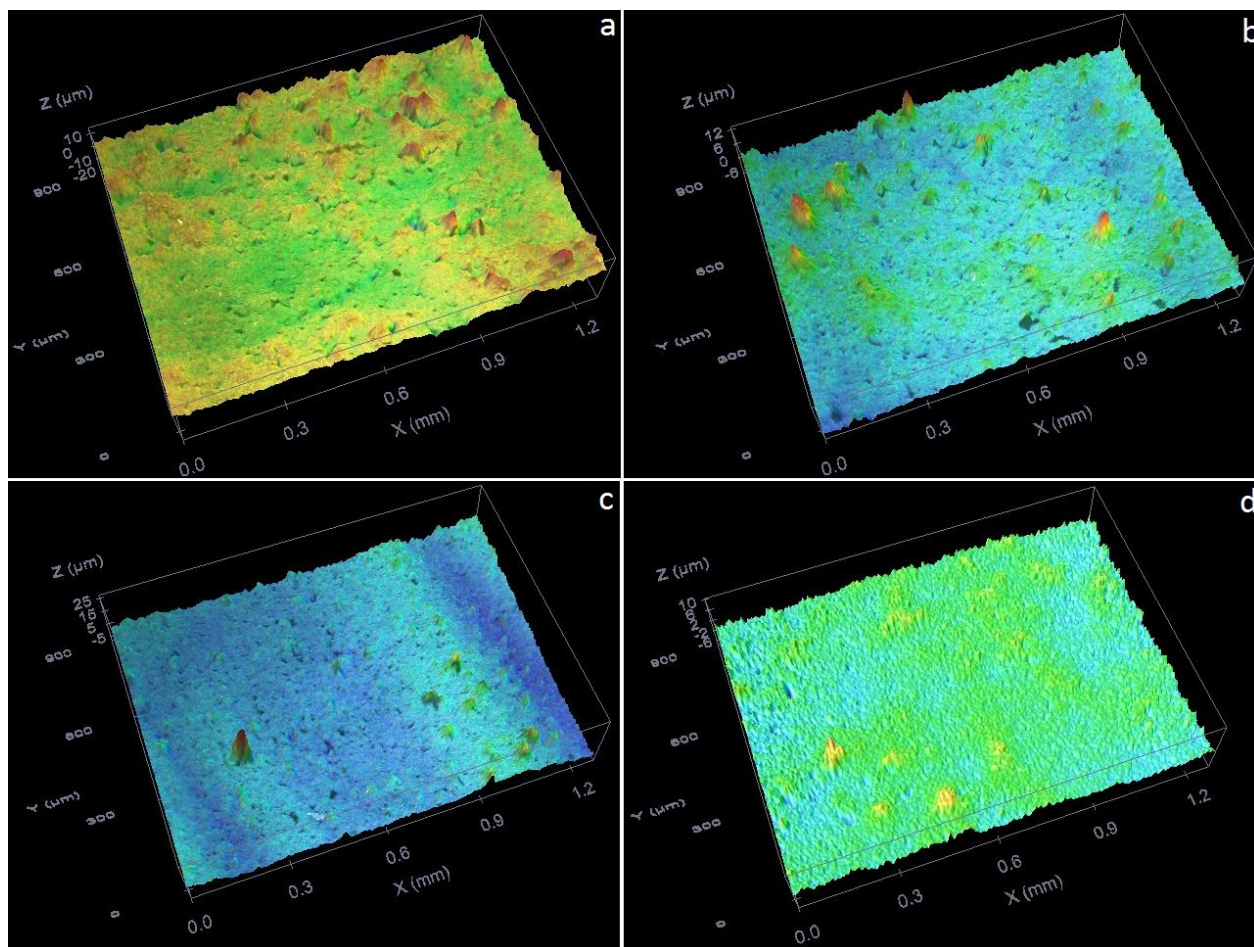


Figure 26. Surface roughness images for brush-coated samples: (a) coated heat treated surface ($R_a = 2.20 \pm 0.14 \mu\text{m}$); (b) coated untreated surface ($1.47 \pm 0.12 \mu\text{m}$); (c) coated polished surface ($1.48 \pm 0.03 \mu\text{m}$) and (d) passivated coated surface ($1.05 \pm 0.06 \mu\text{m}$).

Metallic substrates (uncoated, polished, passivated and heat treated) were tested with water, PO and HAp/PO in order to assess the wettability on differently rough substrates. All metallic substrates exhibited a more hydrophobic character (contact angle $> 90^\circ$) when measured with water (Fig. 27). A significant increase of the hydrophilic character was observed for all samples measured with PO and this is attributed to its low superficial tension, since their molecules have weak attraction to each other allowing that PO wets the surface better. Figure 27 shows that the PO allowed a better wettability on rougher surfaces (untreated $0.55 \mu\text{m}$ and heat treated $0.82 \mu\text{m}$) than smooth surfaces (polished $0.28 \mu\text{m}$ and passivates $0.48 \mu\text{m}$), but no significant differences were observed in contact angle values. HAp/PO slurry showed an improved spreading, because the PO has a lower superficial tension than water that allows an excellent wettability and a close contact of the particles with the substrate.

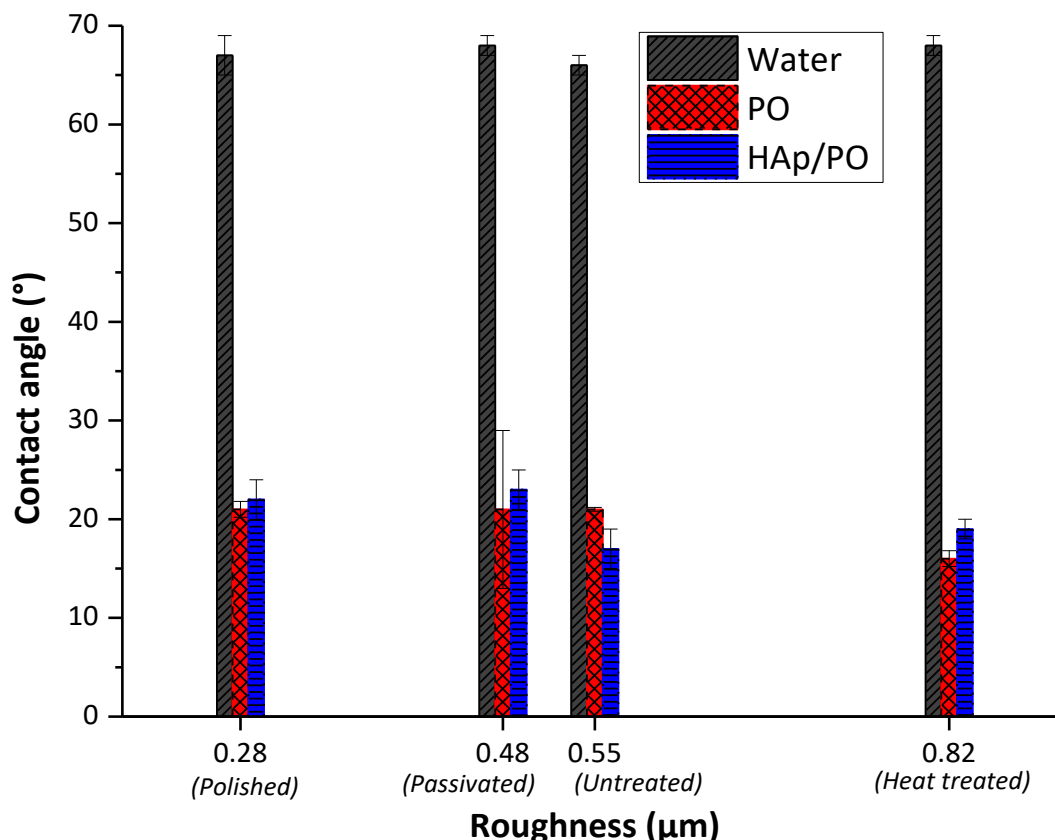


Figure 27. Evaluation of the wettability tested with different liquids (water, PO and HAp/PO) on roughness properties of the uncoated substrates: polished, passivated, untreated and heat treated.

Figure 28 presents the values and relation between contact angles measured with water and roughness of the coated samples with different surface treatments. Regarding surface interactions the adhesion of proteins on biomedical implants is mainly dependent on wettability of the biological substrates, because the hydrophobic/hydrophilic properties are the mechanism responsible for cell immobilization (Aronov et al., 2006). As expected the heat treated sample showed higher roughness values due its irregular oxide layer and no differences were observed between untreated and polished samples. However, the passivated sample showed decreased roughness and it could be associated to an adhering surface oxide formed by passivation, which creates a more homogeneous surface and allows that greater roughness promotes exposure of more surface area for interaction and dispersion of the HAp particles.

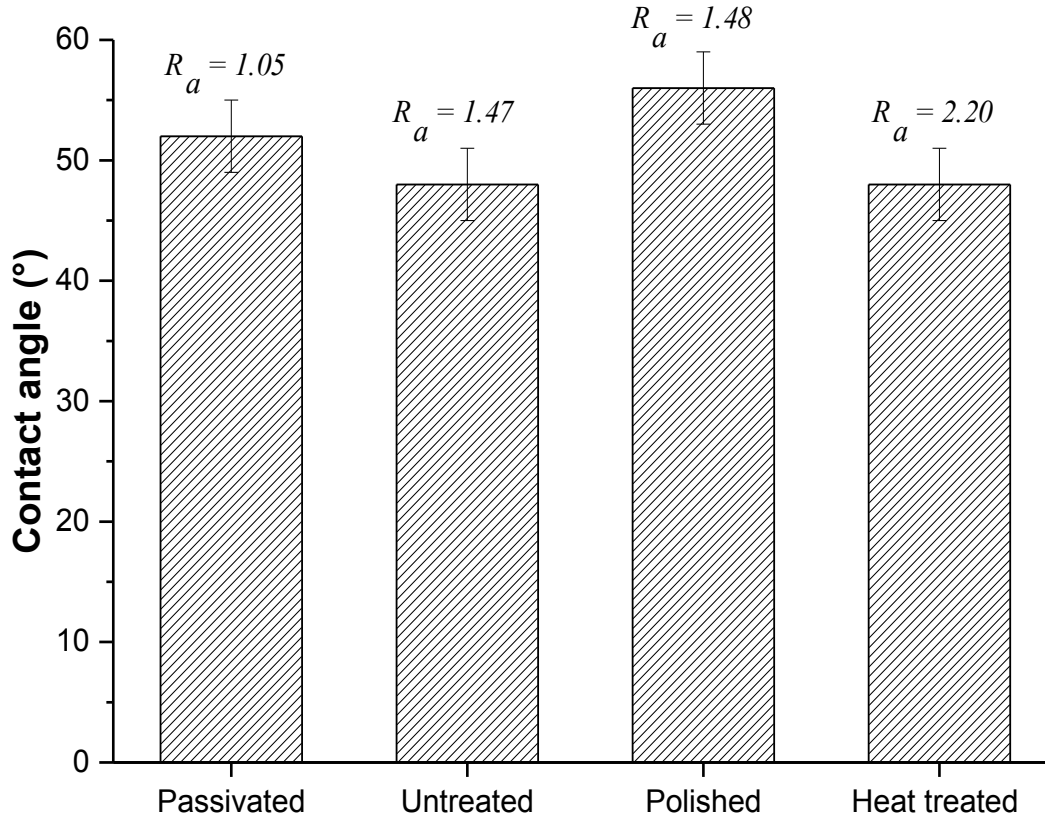


Figure 28. Effect of the different surface treatments on the contact angle values for the coated samples.

4.5 Scratch resistance of the coating

Different surface treatments (polished, passivated, heat treated and untreated) were studied by SEM to understand the influence of the roughness on the resulting coating morphology. SEM pictures (Fig. 29 (A-D)) showed that substrates were completely covered independent of the surface treatment and that the roughness influenced the morphology of the coatings. The polished and passivated substrates with lower roughness exhibited a homogenous and dense coating with similar morphologies (Fig. 29 (A,B)). The coating deposited on heat treated and untreated substrates (with higher roughness) exhibited a more porous and less homogeneous morphology.

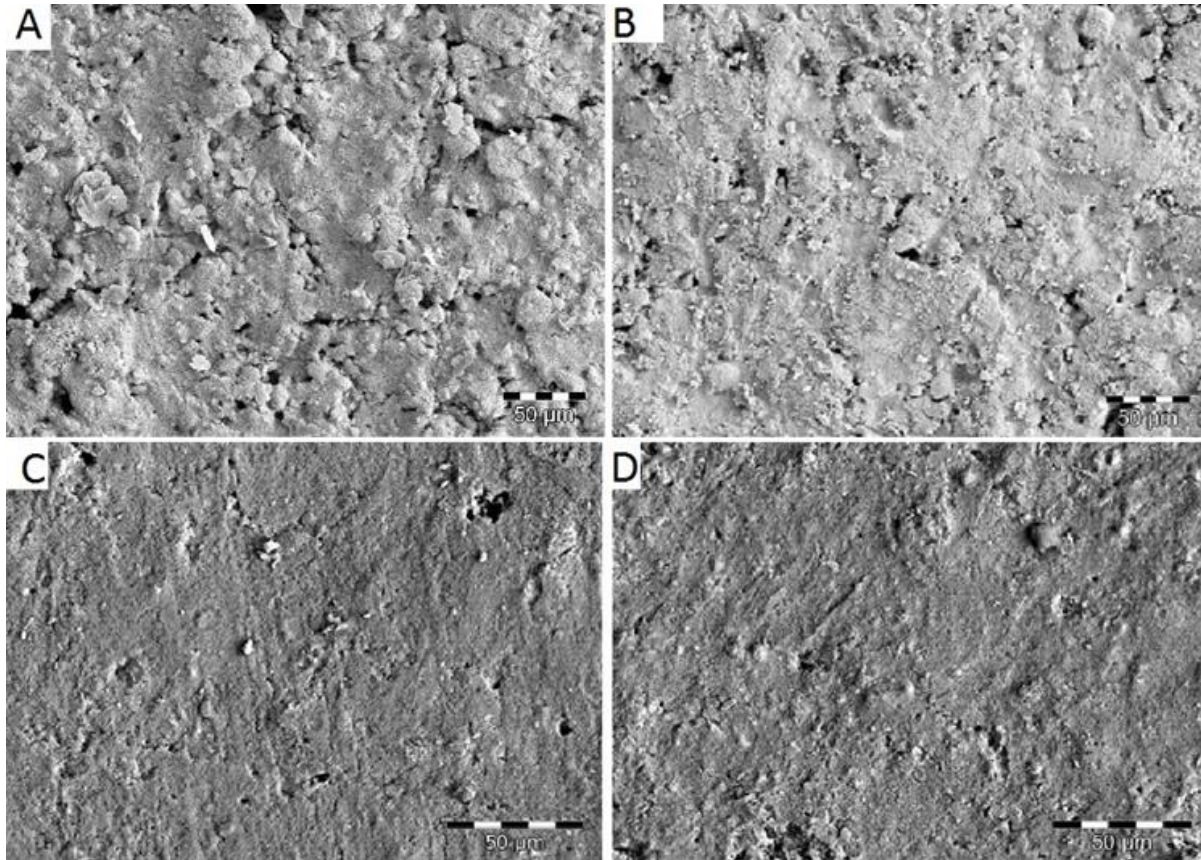


Figure 29. SEM micrographs of the coated CoCr substrates with different surface treatment: (A) heat treated, (B) untreated, (C) passivated, (D) polished.

Figure 30 (A-L) shows the coating surfaces of the polished, passivated, untreated and heat treated substrates after scratch test with a pencil. The pencil scratch test demonstrated that the HAp coatings were resistant to soft pencils and achieved a scratch resistance of up to 4H. The coating deposited on the smoothest surface (polished) showed a higher adhesion than that of the rougher surface (heat treated). Figure 30 (A,B,C) revealed increase of scratch resistance to 4H, when compared with polished (3H), untreated (3H) and heat treated (2H) substrates. As expected the heat treated substrates (Fig. 30 (J,K,L)) showed lower values of scratch resistance due to surface treatment (heat treatment) that led to formation of valleys on the surfaces. This occurs because the valleys (consisting of oxide layers) prevent a better wettability of the PO in their inner regions (rough grooves) and consequently a close contact to the surface. Thus, a poor distribution of the slurry on the surface promotes agglomeration of the HAp particles, resulting in a non-uniform coating with lower adhesion. However, such adhesiveness was achieved, because the PO allowed a good dispersion of HAp particles on the metallic substrate due to low surface tension of the PO that resulted in an increase of wettability. The HAp coating

by brushing from HAp/PO slurry suggests a similar behavior like “paints” that adhere to metals by physical, chemical or mechanical bonding.

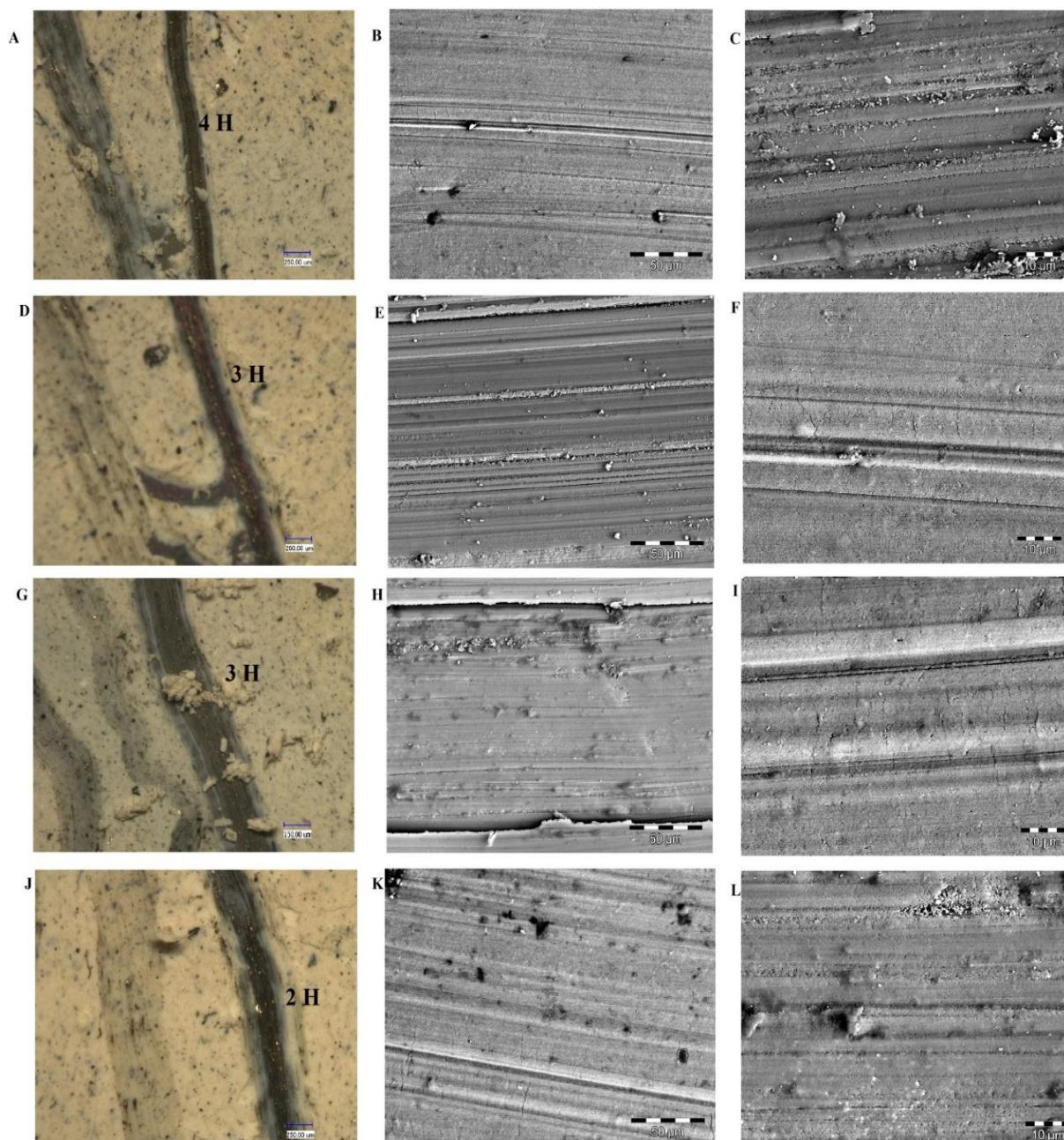


Figure 30. Optical microscopy and SEM images of surface morphology after pencil scratch with different types of surface modification: Polished (A,B,C), passivated (D,E,F), untreated (G,H,I), heat treatment (J,K,L).

The two first occur by interactions between functional groups presents in the molecules of the resins (PO) with the metal surface. For that physical adsorption or wetting to occur it is

mandatory that an intimate contact with the substrate and both the adhesive or coating promotes the bonding hydrogen atom with the substrate (electrostatic force), which lead to development of van der Waals forces between the molecules (Harun et al., 2017). Mechanical bonding is associated with one of the other two to the penetration of the coating film on the roughness of the substrate surface. The result of pencil scratch tests showed that independent of the roughness a determinate adhesiveness was observed that suggests the formation of interbonding between the coating and substrate. The close contact of the HAp/PO slurry on the metallic substrate is achieved due to interaction of groups of molecules present with the metal surface that allows the improvement of wettability.

4.6 In vitro bioactivity and morphology

In order to evaluate the degradation behavior of the coatings, the passivated and polished substrates coated by brushing method were immersed in SBF at 37 °C for 3, 7, 14, and 21 days. Figure 31 shows the coated passivated and polished substrates before soaking in SBF.

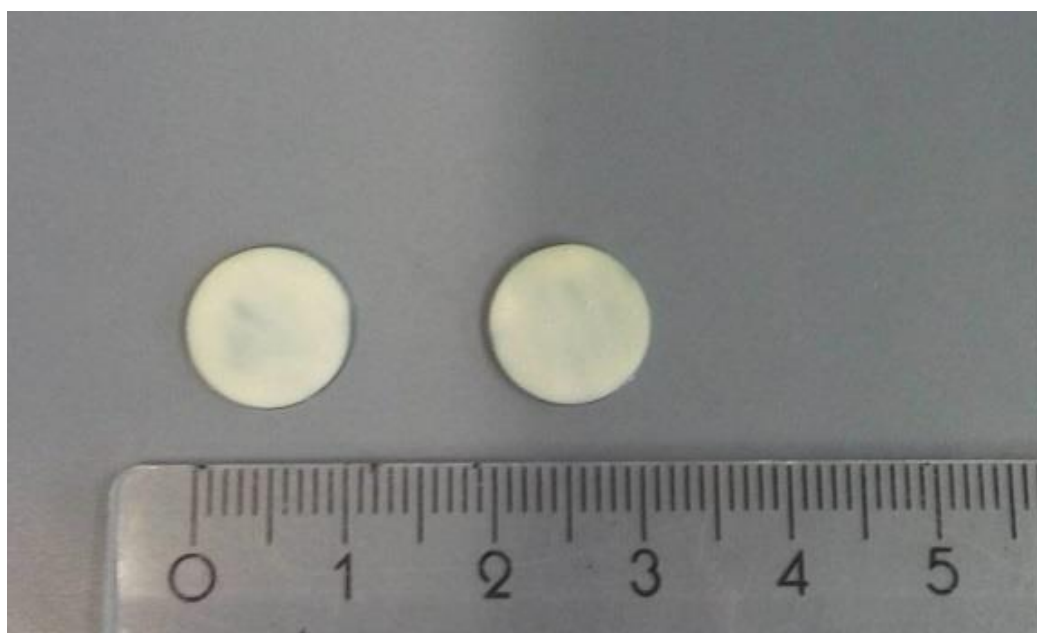


Figure 31. Coated passivated (left) and polished (right) substrate before of immersion in SBF.

In bioactivity tests, the samples presented some cracks that were not observed before. It can be associated to the non-uniform HAp particles dispersion that can promote agglomeration of the particles by brushing method. This agglomeration is related to the fine HAp particles that in presence of oil (bridging liquid) and mechanical stirring allow colliding with each other forming

agglomerates due to the interfacial tension of the oil and capillary attraction of the oil bridges between particles (Albayrak et al., 2008; Encyclopedia Britannica, 2018).

For both samples, a full coating of the substrate and cracks are observed in the microstructures. Concerning Figures 32 (A) and 33 (A), dense and homogeneous coatings were obtained and both substrates (polished and passivated) exhibited cracks, which are related to release of PO during the heat treatment. These cracks observed in the bioactivity tests samples are related to the brushing method that not allows a uniform control of the dispersion of the slurry and is influenced by particles agglomeration. This situation increases the porosity of the deposited HAp layer, and leading to higher susceptibility for crack formation. Other possibility that could influence the occurrence of the cracks is the temperature, because the PO is very volatile and already at about 22 °C the TGA confirms a weight loss. However, ceramic coatings on metallic substrates often result in cracks of the coatings as a consequence of the shrinkage occurred after process of deposition, drying and sintering. Thus, the PO may have started to evaporate before the heat treatment and the sharp shrinkage of the coating led to a tendency for crack formation (Albayrak et al., 2008).

Figure 32 shows the surface morphologies of the HAp coating on passivated substrate before and after soaking in SFB solution for 3, 7, 17 and 21 days. The morphologies of the coated surfaces after 3 days of soaking (Fig. 32 (B)) showed a homogeneous coating and a decrease of cracks can be seen. After 7 days of soaking a significant decrease of the cracks is observed. SEM analyses of the HAp coating after 21 days showed (Fig. 32 (E)) that the coating still was fully covering the surface and furthermore a significant decrease of cracks, resulting in a dense and homogeneous surface. A denser surface at later time-points of soaking suggests an increase of accumulation of an apatite-like layer or enhancement through biomineralization (Paital and Dahotre, 2009). SEM pictures of the coated polished substrate before and after soaking in SBF solution are shown in Figure 33. After three days of soaking a more homogeneous coating with fewer cracks on the surface can be observed, but an increase of dimensions of the islands between cracks were observed (Fig. 33 (C,D,E)). However, the coated polished substrate showed a reduction of cracks with increasing soaking time when compared with the samples before soaking (Fig. 33 (E)).

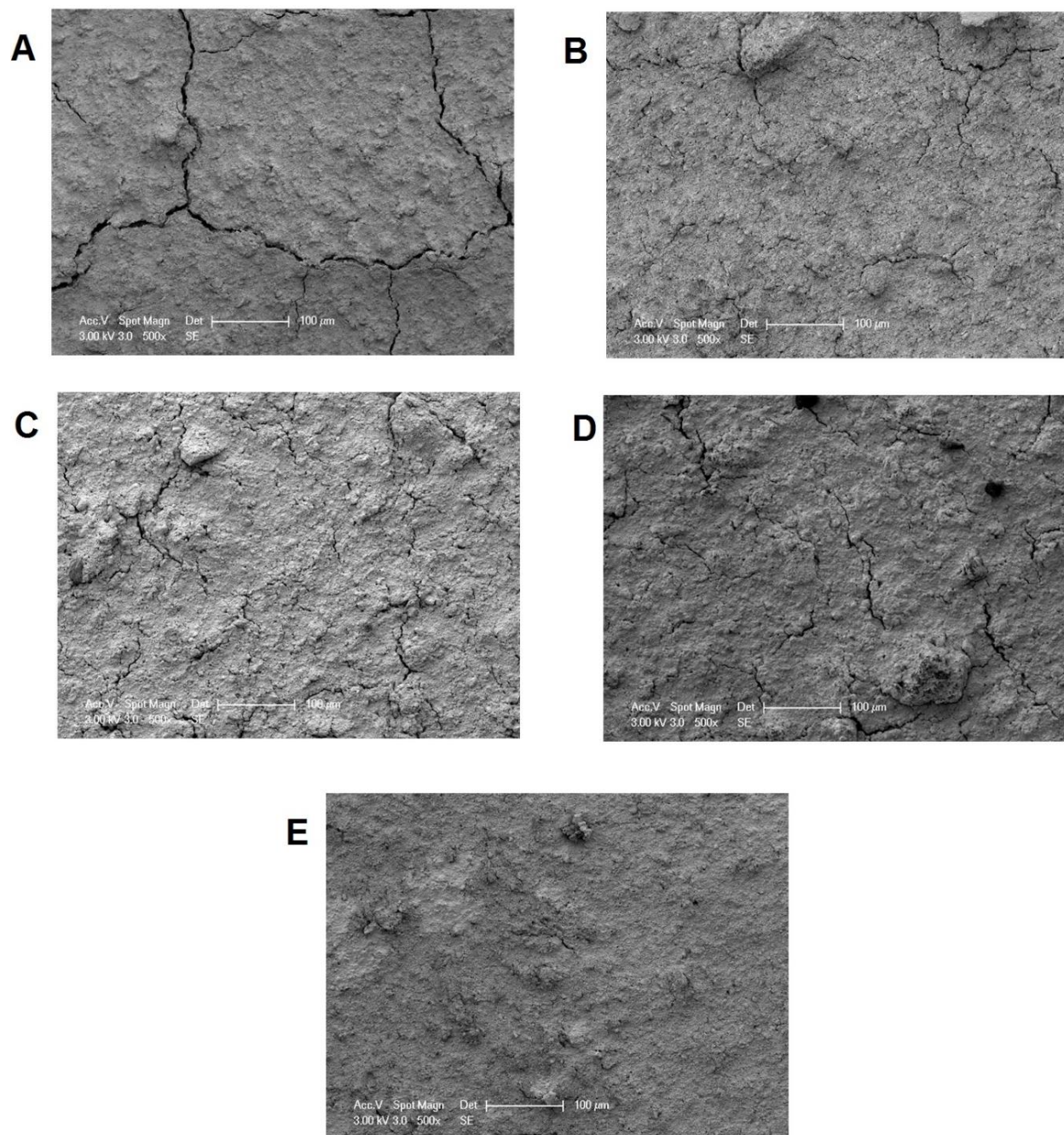


Figure 32. SEM micrographs of the coated passivated substrate before and after soaking in SBF solution: (A) before soaking, after (B) 3 days, (C) 7 days, (D) 14 days, and (E) 21 days of soaking.

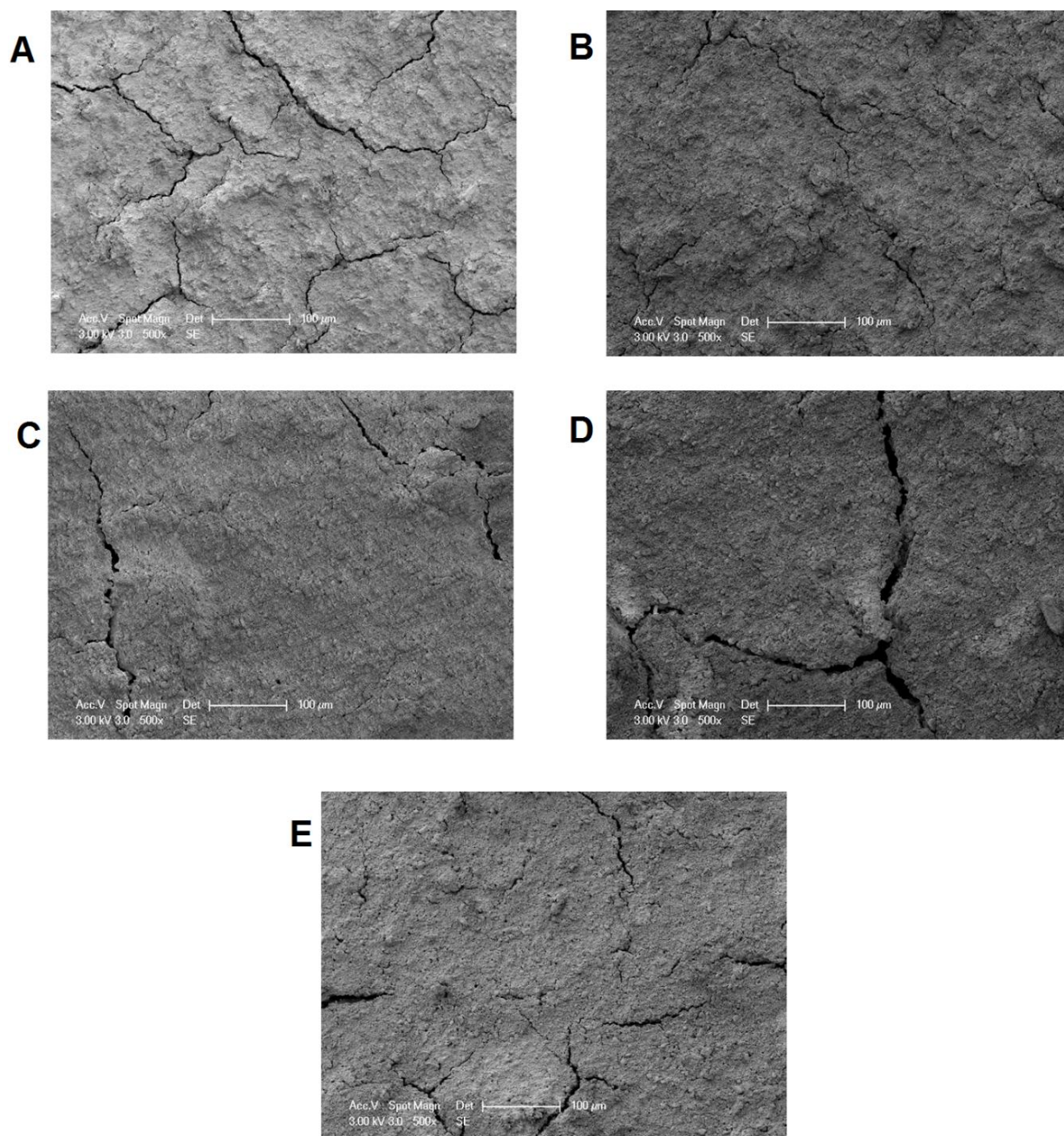


Figure 33. SEM micrographs of the coated polished substrate before and after soaking in SBF solution: (A) before soaking, after (B) 3 days, (C) 7 days, (D) 14 days, (E) 21 days of soaking.

Figure 34 depicts different morphologies of the coated passivated substrate after soaking in SBF: less porous morphology after 21 days soaking than in case of coated polished substrates was obtained. The coated polished substrate also showed a change of morphology after 3, 7, 14 and 21 days of (Fig. 35). However, after 21 days, an increase of porosity was observed, which is related to a fewer amount of cracks when compared to the passivated substrate.

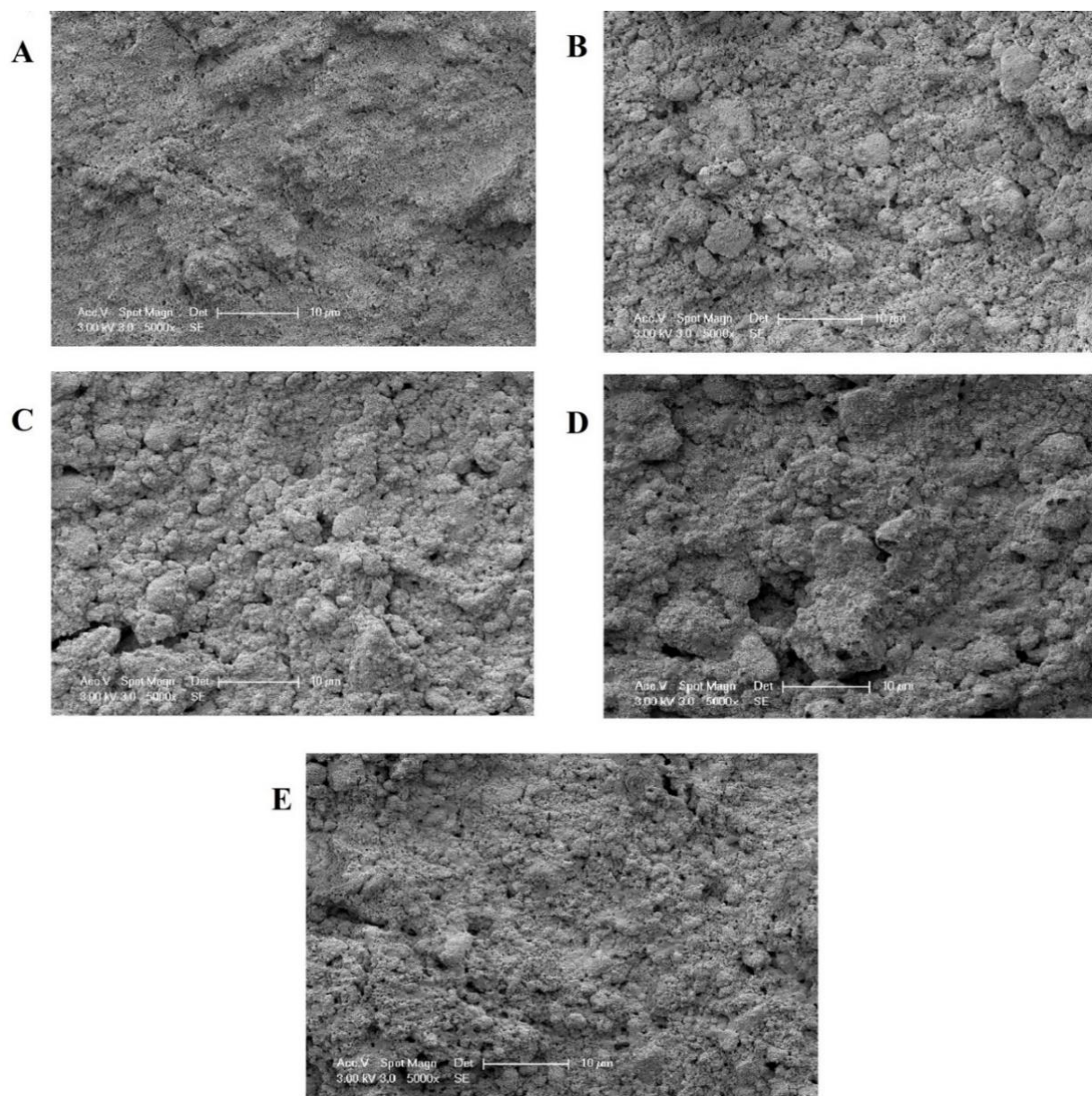


Figure 34. SEM micrographs of HAp coated passivated substrate before and after immersion in SBF: (A) before soaking, after immersion for (A) 3 days, (C) 7 days, (D) 14 days and (E) 21 days.

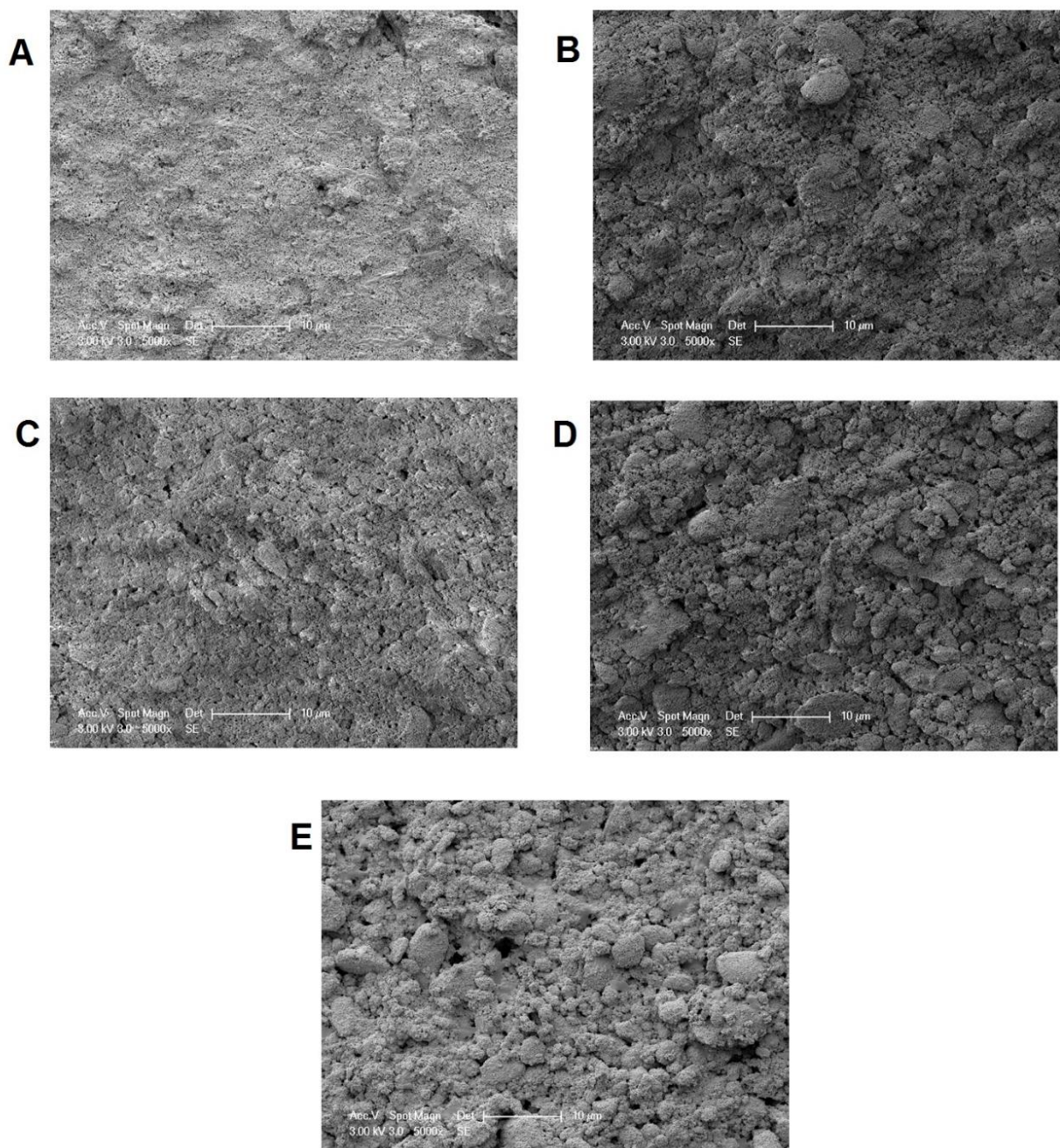


Figure 35. SEM micrographs of HAp coated polished substrate before and after immersion in SBF: (A) before soaking, after immersion for (B) 3 days, (C) 7 days, (d) 14 days and (e) 21 days.

Figures 36 and 37 depict SEM micrographs of coated passivated and polished substrates. As shown in Figure 36, the coating morphology changed after 3 days of soaking and a leaf-like structure was formed after 7 days. SEM observations allowed finding out that from the third day of soaking in SBF the surface morphology presented significant changes. After 3 days of

soaking the passivated coated substrate revealed the presence of particle agglomeration and the surface morphology became porous as the immersion period increases. Furthermore, more powder agglomeration can promote the formation of hard tissue that surrounds the implant, which is important for good implant fixation (Örnberg, 2007) . This is associated with the oxide layer formed during the passivation treatment, where the negative charge of this oxide layer adsorbs the calcium ions (positive charge) from SBF solution and then calcium ions attract phosphate ions from the SBF to form apatite on the surface (Narayanan et al., 2008).

After 7 days of soaking in SBF, apatite phases started to appear, which suggested that similar structure obtained in this work could be associated with the formation of a new apatite layer, growing over the preformed cohesive calcium phosphate coating. From 7 days of soaking the coating achieved a leaf shaped morphology and it was also observed after 14 days, as depicted in Figure 36 (C,D). A similar, leaf shaped morphology has been reached from other coating methods, but it has been named differently (e.g. flake, leaf, petal, plate and flake shape) due to a non-uniform nomenclature of HAp morphologies in the literature (Gu et al., 2004; Thanh et al., 2013b). Typical leaf-like apatite formation is expected between 5-7 days of soaking in SBF solution, and it is related with calcium and phosphate ion concentrations released from the coated surface that are still low, resulting in a preferential orientation of crystal growth. When the soaking time increase (more than 7 days), the concentration of Ca and P ions also increase due to the energy minimization principle that makes the leaf-like crystals no longer to be observed after the long times of soaking because of rapid nucleation (Thanh et al., 2013b).

Figure 36 (D, E) shows the coating surface morphology with precipitates after 14 days of soaking in SBF that are characteristic of the apatite particles that have grown on the surface (Lindahl et al., 2015). The nucleation of these precipitates tend to occur in pores or in gaps, and therefore the size of these precipitates are larger than on smooth surfaces and their amount increase with the soaking time (Lindahl et al., 2015). HAp coating was deposited on CoCr alloy by Wang and Luo , using an electrochemically-assisted deposition pretreatment followed by a chemical immersion in supersaturated calcification solution. They obtained a similar morphology in this work, named as flake-shaped surface structure that allowed the formation of a uniform coating within 2 hours of immersion and that converted to HAp within 72 hours. Lindahl et al. (Lindahl et al., 2015) prepared biomimetic HA coatings on pretreated CoCr substrates with a morphology of plate-like crystallites forming roundish flowers after 3 days of soaking. A stability test in tris (hydroxymethyl aminomethane) hydrochloric acid (Tris–HCl, pH = 7.4) solution after 28 days showed that half of the coating had dissolved.

The coated polished substrate showed before the soaking a morphology with lower porosity and homogeneity (Fig 37 (A)). After 3, 7 and 14 days agglomerated micro-structures with disordered arrangement of particles within them were observed. From Figure 37 (E) a more porous morphology than before the soaking can be seen, and the small splats indicate the growth of HAp layer after 21 days of soaking. In this study, the coated substrate showed a growing of HAp layer after 14 days of soaking in SBF and after 21 days still exhibited a fully covering coating.

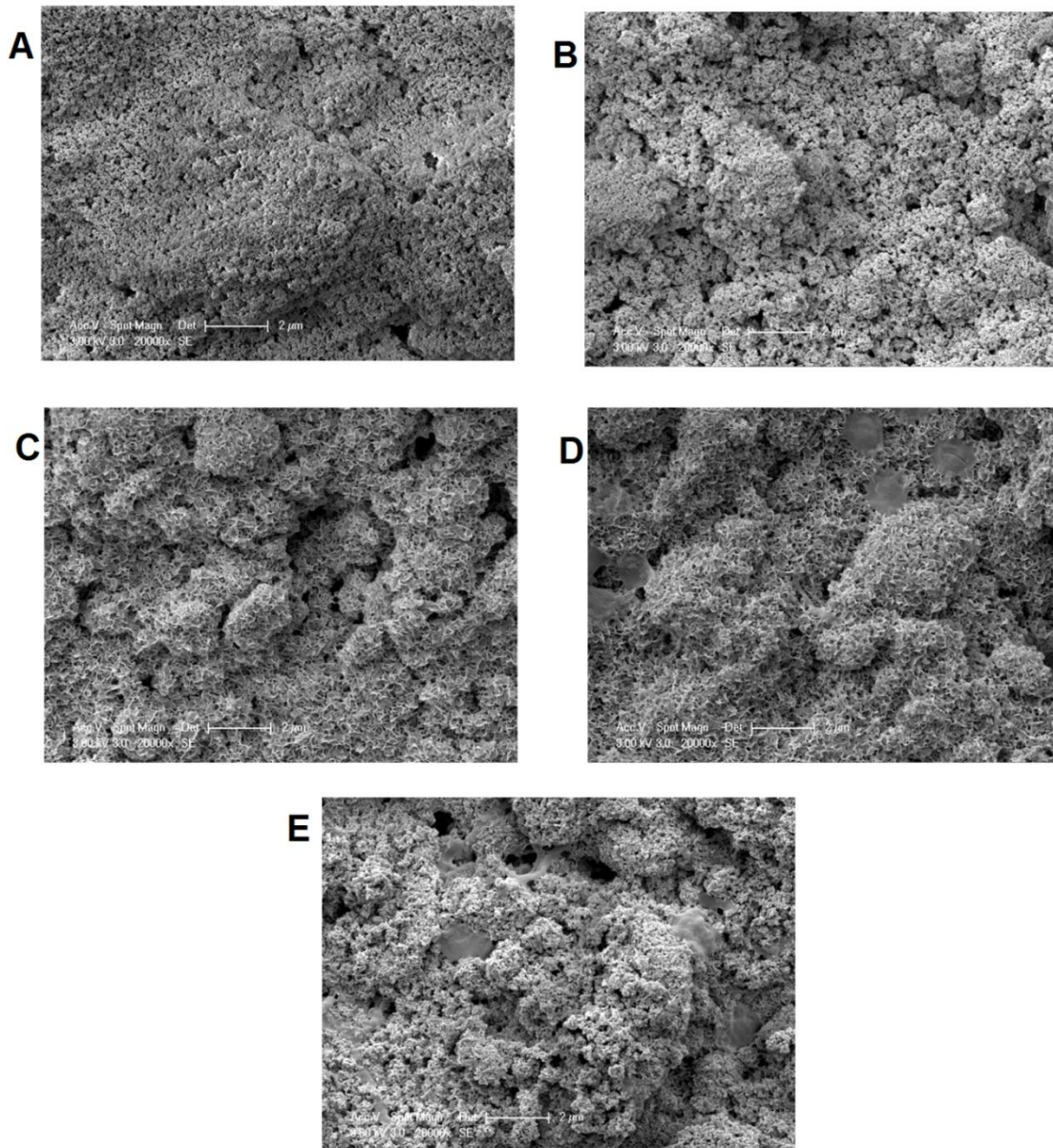


Figure 36. Surface morphologies of the coated passivated substrate before and after soaking in SBF: (A) before soaking, after soaking for (B) 3 days, (C) 7 days, (D) 14 days and (E) 21 days.

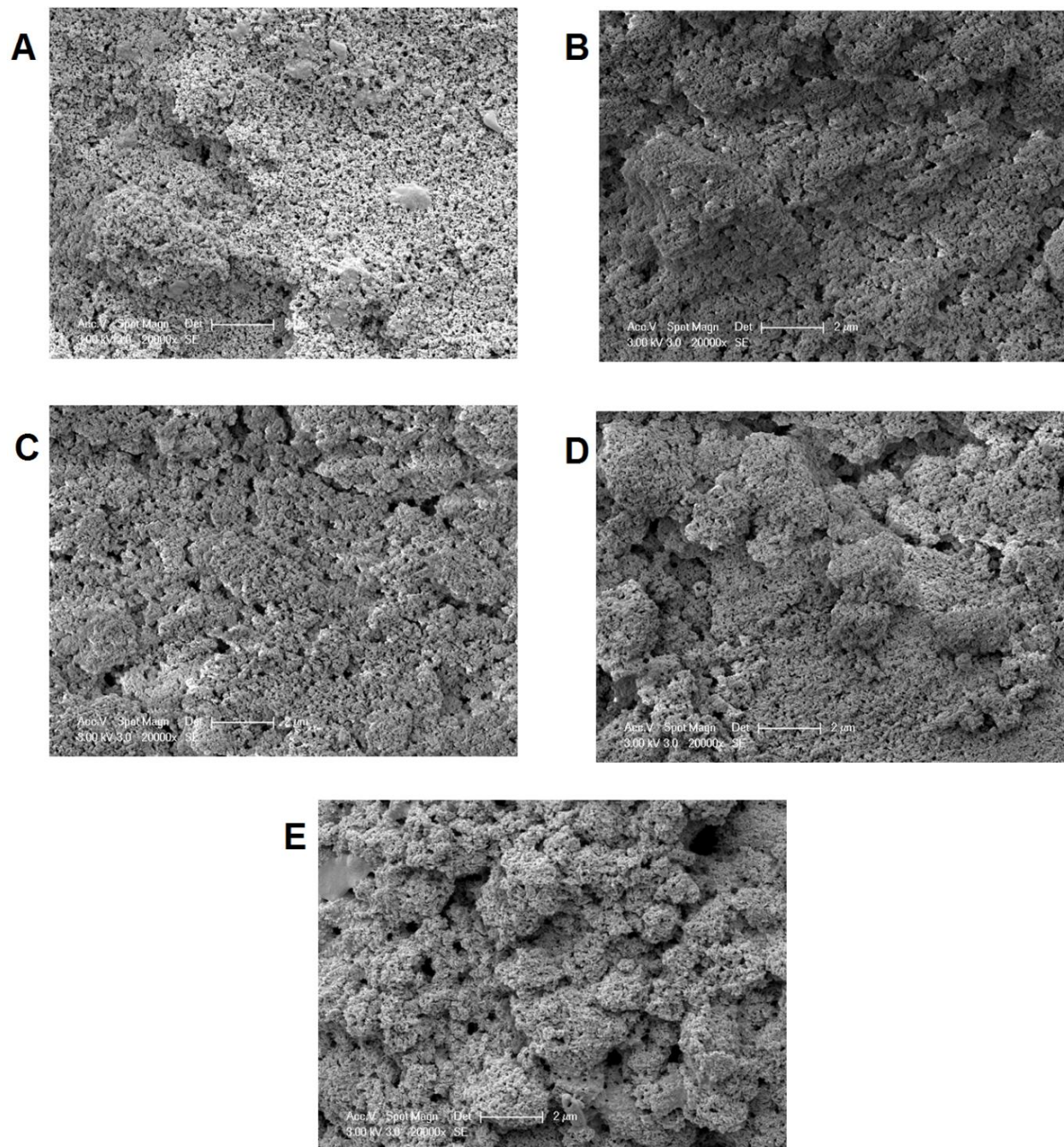


Figure 37. Surface morphologies of the coated polished substrate before and after soaking in SBF: (A) before soaking, after soaking for (B) 3 days, (C) 7 days, (D) 14 days and (E) 21 days.

4.7 Metallography of the Co-15Cr-15W-10Ni alloy

Figure 38 shows an optical micrograph of the Co-15Cr-15W-10Ni alloy microstructure as received. Co-15Cr-15W-10Ni alloy also known as L-605 super alloy is constituted of a single FCC γ -phase with alloying elements in solid solution (Favre, 2012). During manufacturing process this alloy is normally requiring heat treatment (annealing) due to its capacity to work-harden very rapidly. Thus, annealing heat treatment between 1175 °C to 1230 °C and rapid cooling are important to form complex components and to restore the best balance properties (HAYNES® 25 alloy/Principle Features, 2017).

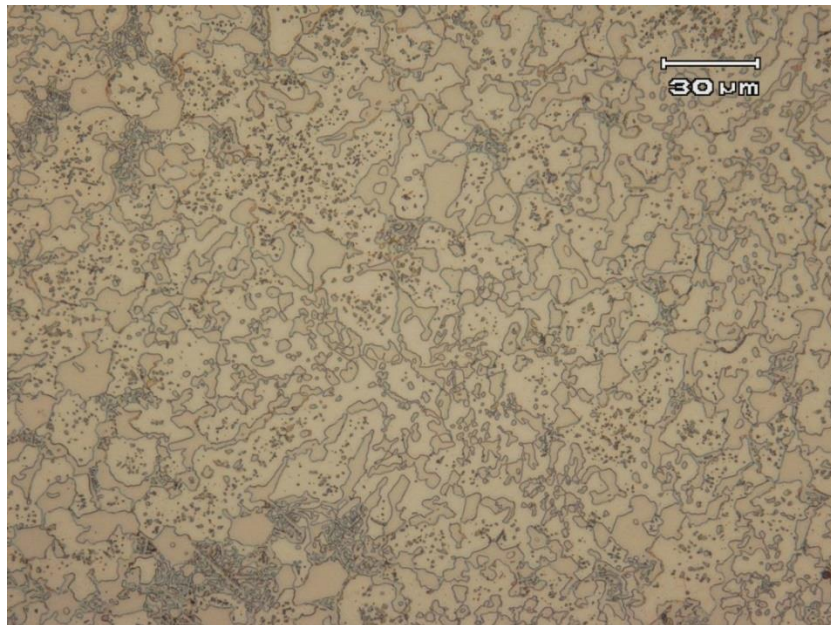


Figure 38. Optical micrograph of the untreated (as-received) Co-15Cr-15W-10Ni alloy.

The microstructure of the heat-treated alloy is shown in Figure 39. After heat treatment, a more heterogeneous microstructure can be observed with a large amount of continuous blocky precipitations inside of the grain boundaries, which suggest carbides $M_{23}C_6$ type. According to a study of J. Favre (Favre, 2012) temperatures between 700 °C and 1100 °C are expected for carbides formation. K. Euki et al. (Ueki et al., 2016) investigated the microstructure of this alloy, heat treated at 700 °C to 1000 °C and 800 °C to 1200 °C and they found the $M_{23}C_6$ and n-phase precipitate. Yucuma and Satō (K Sato., 1968) were the first to propose the currently accepted precipitation of the L-605 alloy, where they presented the precipitation at 800 °C by the follow reaction: $M_7C_3 \rightarrow M_{23}C_6 \rightarrow M_6C \rightarrow Co_2W \rightarrow \mu-Co_7W_6$.

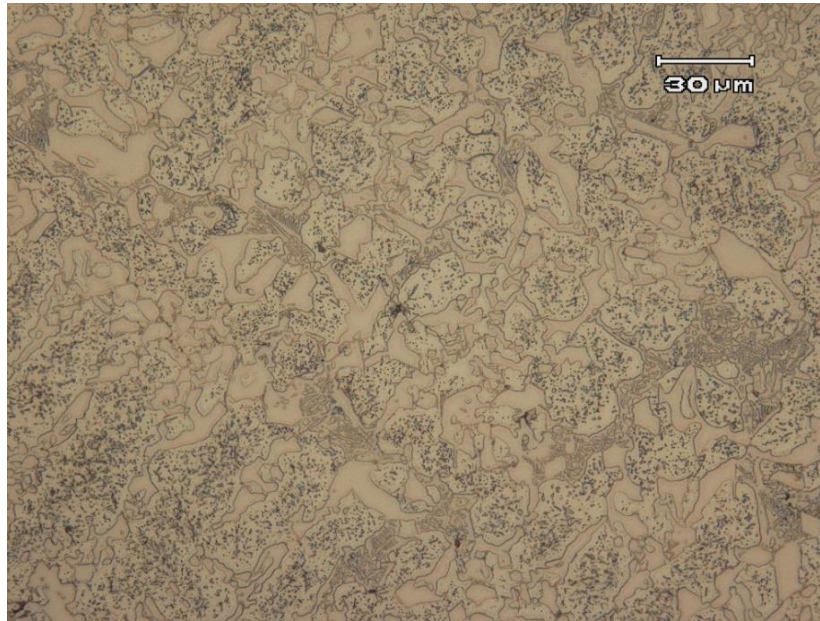


Figure 39. Optical micrograph of the Co-15Cr-15W-10Ni alloy after heat treatment at 800 °C for 1 h.

4.8 Corrosive behavior

Cyclic voltammetry is a method widely used to study the reduction process and mechanism of electron transfer on modified surfaces (Valente and Célia do Rocio, 2011). This analysis aims here to investigate the stability of the oxide layer formed during the chemical passivation. The samples investigated are described in Table 1 (section 3.8).

Firstly the expected activity of HNO_3 was investigated and the nitrogen in HNO_3 presents the $+5$ valence state (Fig. 40). When reacting with the metal surface, and releasing NO_2 and NO , the nitrogen is reduced to a lower valence state. If one element in a reaction is reduced, the conservation of electrons means that some other element needs to be oxidized. Nitric acid, which is a strong acid for dissolving metals and a powerful oxidizing agent, is ideal for oxidizing (or passivating) the surface of metals/alloys. Figure 40 shows anodic cyclic voltammetry curves recorded for the uncoated Co-15Cr-15W-10Ni alloy samples in Ringer's solution at 37°C. These are conducted in order to make (fast) oxidation reactions visible. Upon immersion in the electrolyte both sample types are spontaneously passive, therefore the anodic current densities are very low. It can also be observed that at higher anodic potential prior to the large current density, which occurs due to water decomposition, three characteristic oxidation peaks appear for the as-polished state (Pol sample). These peaks (I,II, III) may be attributed to the further

oxidation of constituent species to higher valence oxidation states, i.e. Co^{2+} to Co^{3+} ($\text{Co}(\text{OH})_3$), Ni^{2+} to $\text{Ni}^{2+/3+}$ (Ni_3O_4) or Ni^{3+} (Ni_2O_3) and Cr^{3+} to Cr^{6+} (CrO_4^{2-} or $\text{Cr}_2\text{O}_7^{2-}$). Under these conditions, tungsten W is only stable as WO_4^{2-} . After additional HNO_3 treatment the surface state is a bit more activated, i.e. anodic current densities related with these further surface oxidations are slightly higher, but peak III is not visible. Despite, both samples presented protection character against corrosion and no significant differences of potential and current densities were observed. The polished sample (Pol) has a tendency to be more resistant to corrosion.

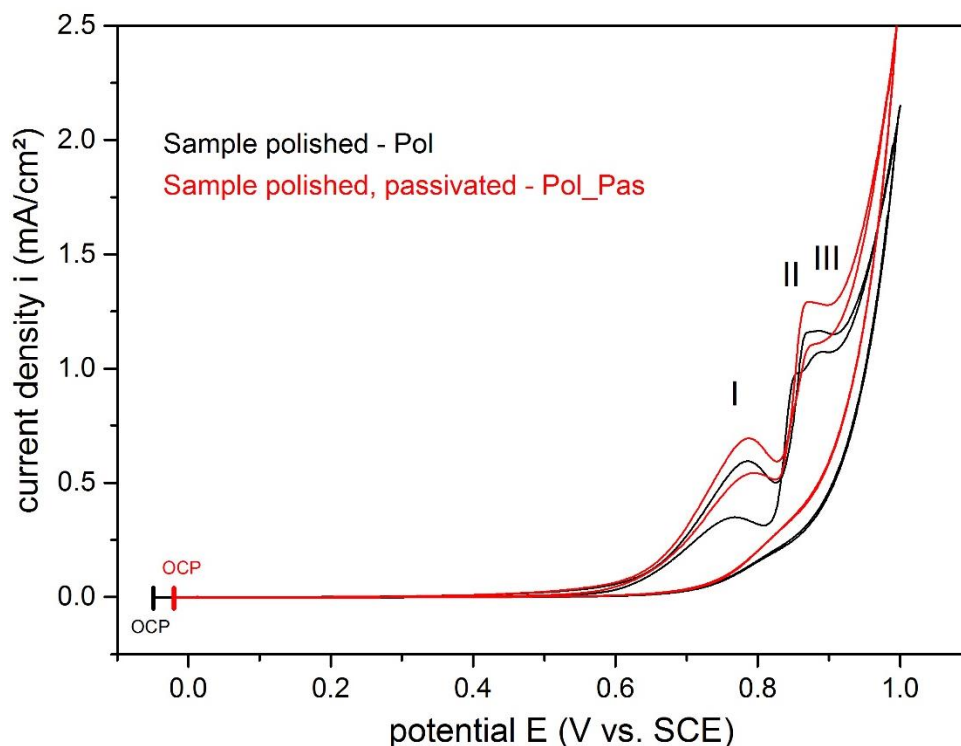


Figure 40. Comparison of cyclic voltammetry curves for Co-15Cr-15W-10Ni alloy samples in the as polished state (black) and after additional passivation in HNO_3 (red) for the valence oxide states (I,II,III peaks), recorded in Ringer's solution.

Figure 41 presents the OCP vs. time for coated and uncoated samples. As can be seen, all samples presented positives values (E: potential) in relation to the immersion potential, which is typical of passivated alloys that makes the surface more active due to the presence of a protective oxide film (Souza, 2011). In all cases, after an initial period, OCP values stabilize until they reach saturation values after 30 min. The potential value of the sample Pol demonstrated a higher value than sample Pol_Pas (polished and passivated), however, the heat treatment promoted a decrease of the potential for the Pol_coa_800 sample. From the passivation treatment, an increase on the potential (Pol_Pas_coa_800) was achieved, exhibiting a higher

corrosion resistance than Pol_coa_800 sample. The change of the surface chemistry of the Co-15Cr-15W-10Ni alloy samples due to additional acid treatment (Pol and Pol_Pas samples) is reflected in small shift of the OCP value in negative direction at about 20 mV, which indicates a slightly more active alloy state. HAp coating causes for the only “as-polished” sample (Pol) a negative shift (Pol_coa_800), whereby after passivation (Pol_Pas samples) and additional HAp coatings (Pol_Pas_coa_800 and Pol_Pas_coa_300 samples) a positive shift was observed. However, there were no significant differences between the OCP values.

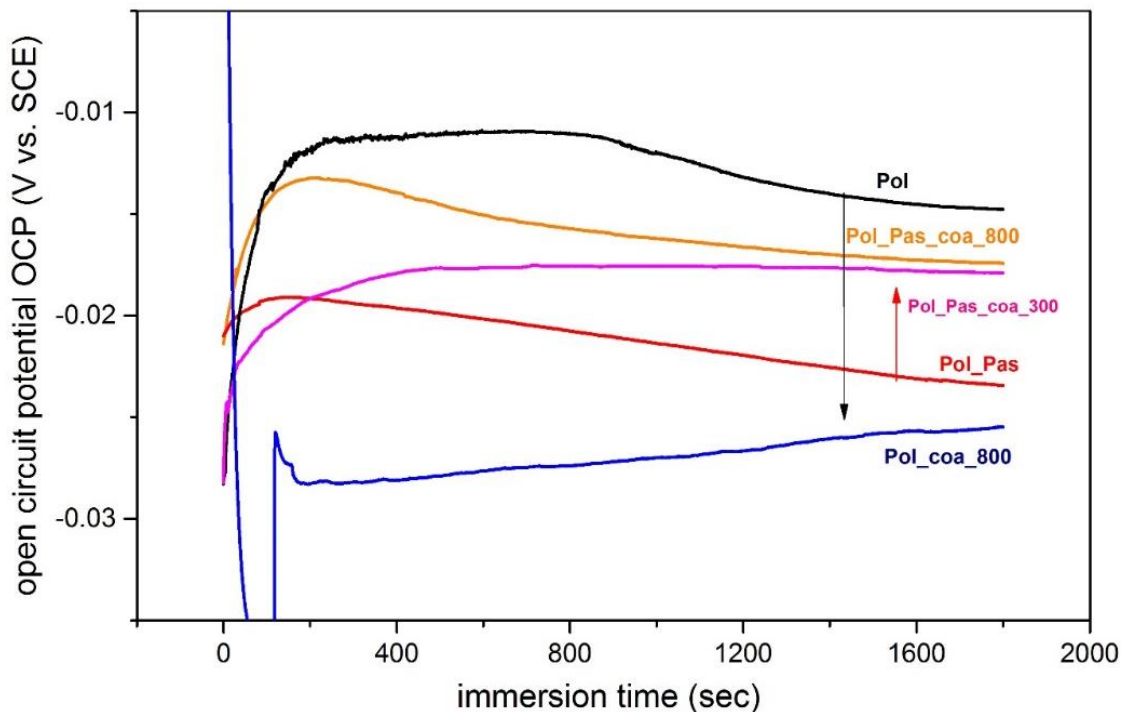


Figure 41. Comparison of open circuit potentials of Pol, Pol_Pas_coa_800, Pol_Pas_coa_300, Pol_coa_800, developing upon 30 min immersion in Ringer’s solution.

The polarization results of the passivated and polished samples (Pol and Pol_Pas) are presented in Figure 42. The results show a similar trend of the curves for both samples. The linear potentiodynamic polarization curves show that the corrosion potential E_{corr} of the passivated sample (Pol_Pas) is slightly smaller than that of the polished one (Pol), and upon anodic polarization slightly higher current densities are observed. Both are indicative for a somewhat more active surface state after acid treatment. As expected, for both alloys the corrosion current density (E_{corr}) values are very low, i.e. $<1 \mu\text{A}/\text{cm}^2$, and upon anodization, only small current densities are obtained. It is an indication that for a very low metal ion release rates

and/or, a spontaneous formation of highly protective oxide films takes place. However, sample Pol showed more positive potential values ($E_{\text{corr}} -0.019 \pm 5$) and a lower corrosion density ($i_{\text{corr}} = -0.168 \pm 5$) than Pol_Pas sample ($E_{\text{corr}} -0.028 \pm 5$ and $i_{\text{corr}} = -0.175 \pm 5$), which corroborates with OCP curves that demonstrated a better corrosion resistance of the polished sample.

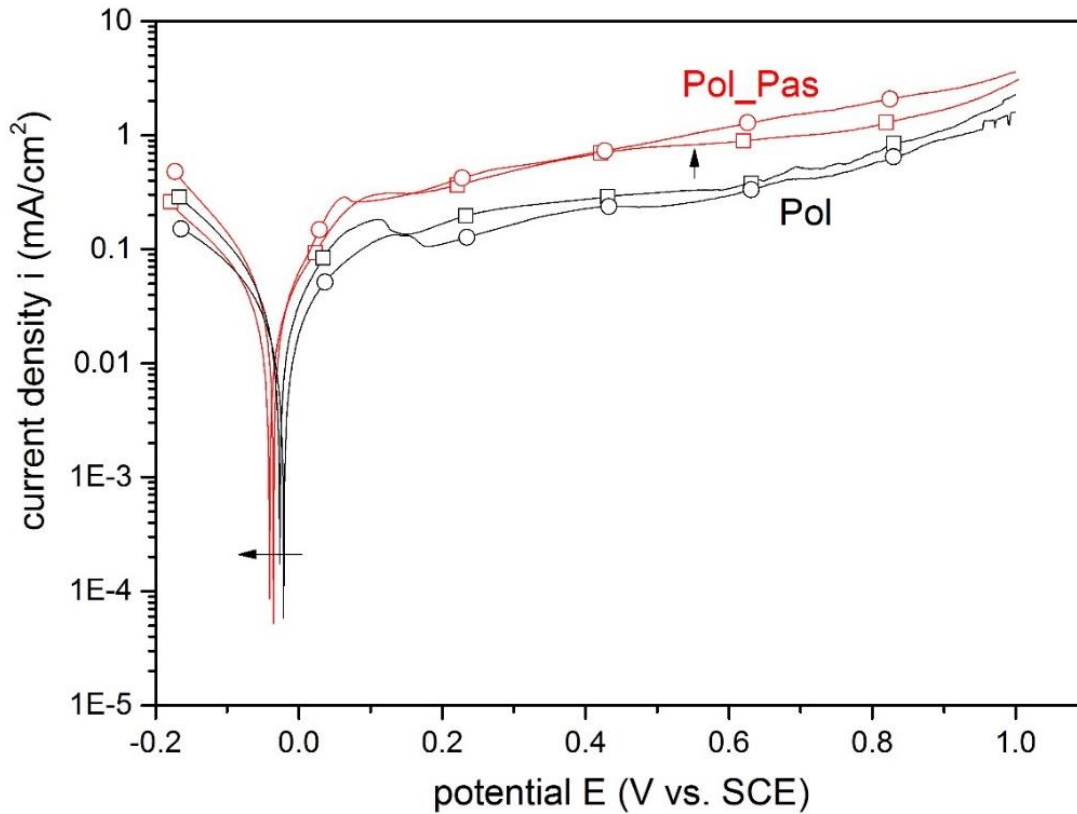


Figure 42. Linear potentiodynamic polarization plots made in duplicates for Co-15Cr-15W-10Ni alloy samples in the as polished state (Pol) and after additional passivation in HNO_3 (Pol_Pas) recorded in Ringer's solution.

4.8.1 Effect of heat treatment on corrosion resistance

In order to evaluate the influence of heat treatment on the corrosion resistance of the Co-15Cr-15W-10Ni alloy, the samples coated and heat treated (Pol_Pas_coa_300, Pol_coa_800 and Pol_Pas_coa_800) and without heat treatment/uncoated (Pol, Pol_Pas) were investigated by potentiodynamic polarization as shown in Figures 43 and 44. The effect of the heat treatment of the polished samples (Pol) before and after coating under heat treatment (Pol_coa_800) is demonstrated in Figure 43. After deposition of HAp and heat treatment (Pol_coa_800) there is a

decreasing of potential and slightly increasing of current density, which indicates a lesser corrosion protection in relation to polished samples.

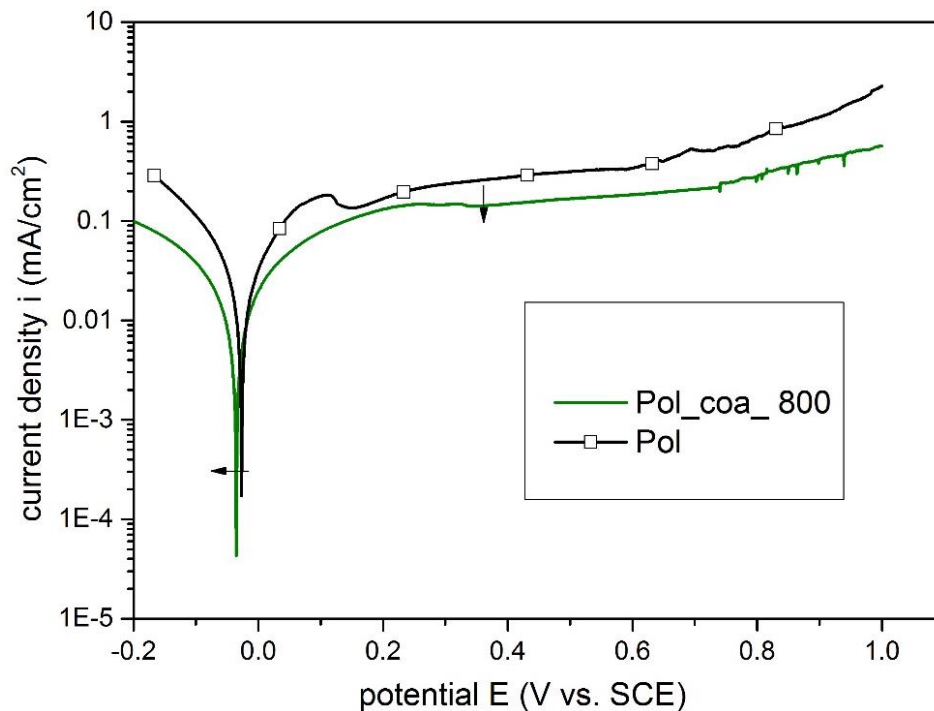


Figure 43. Linear potentiodynamic polarization plots for Co-15Cr-15W-10Ni alloy samples after HAp coating of the as polished state immersed in Ringer's solution.

Figure 44 shows the linear potentiodynamic polarization curves of the passivated samples before and after heat treatment. The sample Pol_Pas_coa_300 exhibited less negative corrosion potential (-0.024 V) than sample Pol_Pas (-0.035 V) and Pol_Pas_coa_800 (-0.028 V). The coating of (passivated) metal surface with a non-conductive ceramic like HAp will in any case decrease the surface conductivity related to the transfers of charge carriers from the metal phase to the electrolyte and therefore, the measurable current density. Tafel plots (Fig. 44) reveal very small shifts of the E_{corr} values after HAp coating corresponding to the trends observed for the OCP, shown in Figure 41. For both coatings corrosion current densities I_{corr} are lowered up to values of $\sim 0,1 \mu\text{A}/\text{cm}^2$ and anodic current densities are also visibly reduced. For the additionally acid treated sample, HAp coating and annealing at 300°C was more effective in reducing the current density level. As expected, the passivating film of the Pol_Pas_coa_300 sample showed to be more protecting than Pol_Pas_coa_800 sample due the negative influence of high temperatures on corrosion resistance. At low temperatures (up to 400°C) the

passivity of the alloy is still available and the decrease of corrosion resistance is also acceptable. However, above of 400 °C occur the formation of chromium nitride (CrN) and it is difficult to prevent. As the passivating film requires mobility to build the Cr_2O_3 layer at the surface and if the chromium is bonded to the CrN there is not enough free chromium to form the oxide film (Lutz et al., 2011). Although, the high temperatures influencing the corrosion resistance of this alloy, the linear potentiodynamic polarization plots showed that the corrosion resistance of both samples were not affected by heat treatment and the curves shifted to a nobler potential and a lower current, which indicates that the coatings have a high corrosion resistance in Ringer's solution and a low metal release rate is expected.

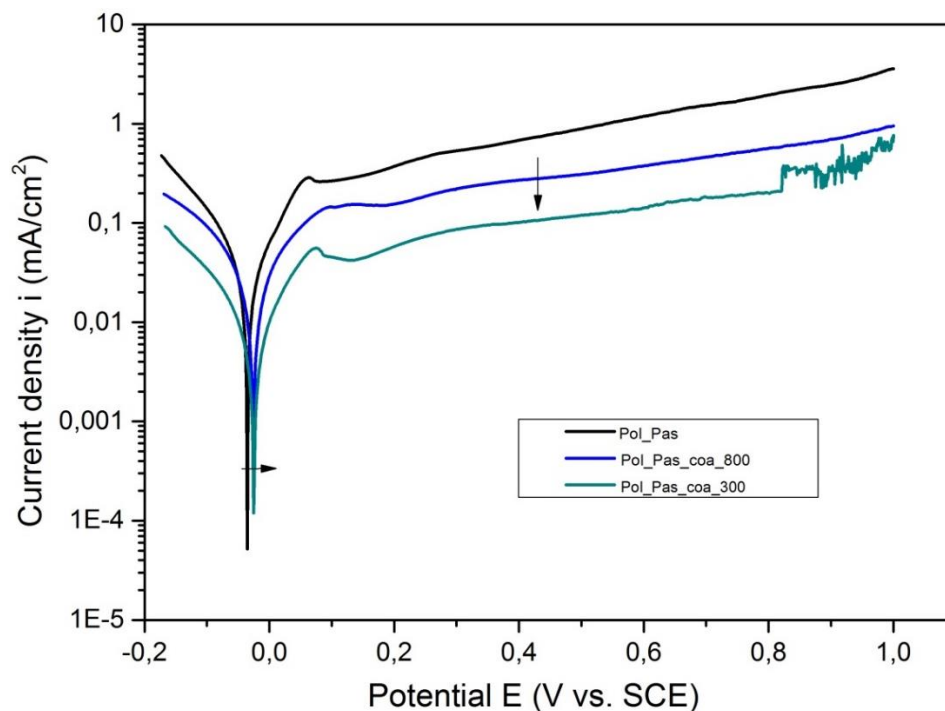


Figure 44. Linear potentiodynamic polarization plots for Co-15Cr-15W-10Ni alloy samples after HAp coating of the passivated state, measured in Ringer's solution.

4.9 Cell Proliferation and osteogenic differentiation

The proliferation of primary bone-derived cells the cells on polished uncoated and coated substrates was evaluated by determination of the cell numbers after 1, 7, 14 and 21 days using the lactate dehydrogenase (LDH) activity quantification method (Figure 45) as well as quantification of DNA content (Figure 46). The DNA content and LDH activity measurements (Figures 45 and 46) revealed that the cell number between day 1 and 21 for the uncoated

polished substrate (both direct and indirect methods) showed a better seeding efficiency than coated polished substrate. This is confirmed by determination of the LDH activity that also indicates a reduction in cell number on these samples, which shows a behavior similar with previous work of cells exposed to environments with transition metal ions like Cr, Co, Mo or Ni (Ueki et al., 2016). Anissian et al. (Anissian et al., 2002) reported that cobalt ions (above 10 μM) can result in DNA synthesis inhibition and reduced proliferation and osteoblast activity of human osteoblast-like cells. In order to overcome these issues, HAp coatings have been used as a barrier against toxic ions release, and clinical results showed an increase of coating/bone biocompatibility. However, the biological tests showed a more pronounced decrease of cell response and proliferation for the coated than the uncoated substrate. This fact is attributed to oxidation of metallic substrate during the heat treatment at 800 °C and as a result, the reaction products CoWO_4 and CoO are expected (M. E. EL-Dahshan et al., 1976). Although both coated and uncoated substrates have been shown to protect against corrosion, the coating porosity allows the cell contact with the presence of Co particles (CoWO_4 and CoO) on substrate, which affect human osteoclast and osteoblast survival and in a short-term exposure. The reduction of the cell activity in vitro has been associated to high concentrations of concentrations of cobalt²⁺ (Co^{2+}) chromium³⁺ (Cr^{3+}), and chromium⁶⁺ (Cr^{6+}) (Zheng et al., 2019). However, the uncoated substrates showed a superior biological response, because they were not subjected to any heat treatment, preserving the structural integrity of the substrate. Another explanation for their low cell response for both methods (direct and indirect) is the release of calcium phosphate from the substrate, which was reported in the in vitro bioactivity test and it may lead to change the pH of the cell culture medium.

Specific activity of the osteogenic marker enzyme alkaline phosphatase (ALP) was determined of cells cultivated on coated and uncoated polished substrates. ALP activity was normalized to cell numbers calculated both on DNA content and LDH activity and showed highest values for the direct cell seeding (Fig. 47 and 48). Specific ALP activity (normalized to DNA) by direct setup presented a higher values than cells in control group and on uncoated substrate (Fig. 47). However, ALP activity (normalized to LDH) of cells in the direct setup presented a higher value for the uncoated samples than coated (Fig. 48). In the indirect cell culture setup a high decrease overtime of the specific ALP activity was observed, where the specific ALP activity showed a lower value for cells in presence of the uncoated substrate than the coated one.

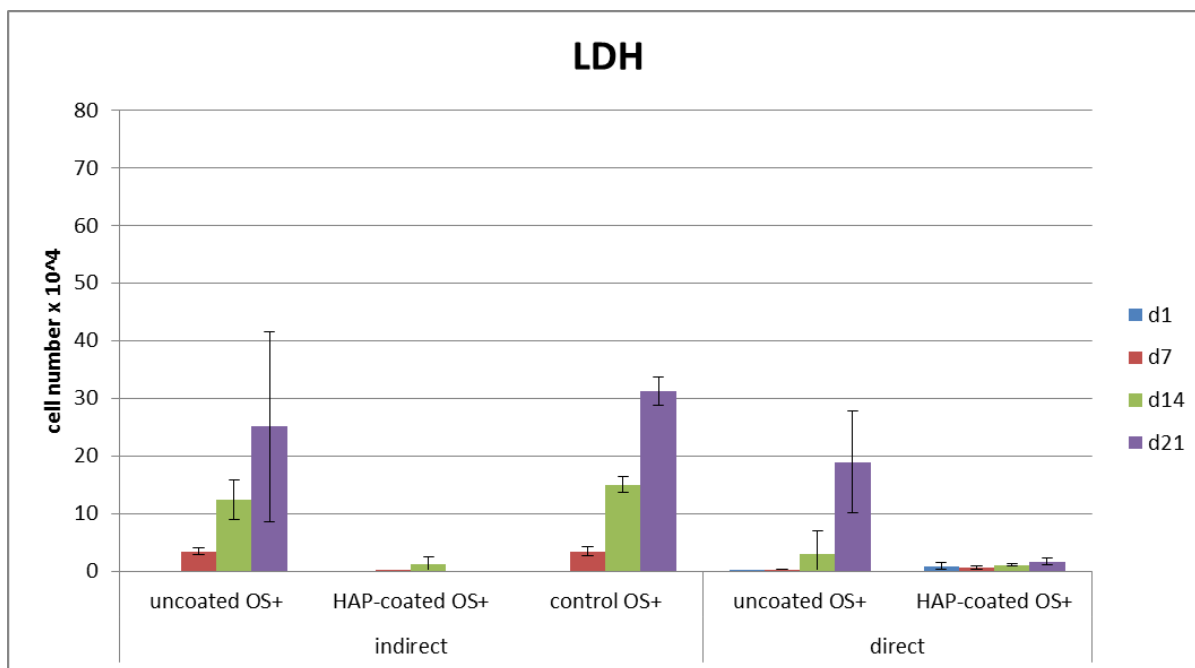


Figure 45. Development of cell numbers in indirect (left) and direct contact (right) to uncoated and coated polished substrates 1, 7, 14 and 21 days after cell seeding. Cell numbers were determined by quantification of the LDH activity.

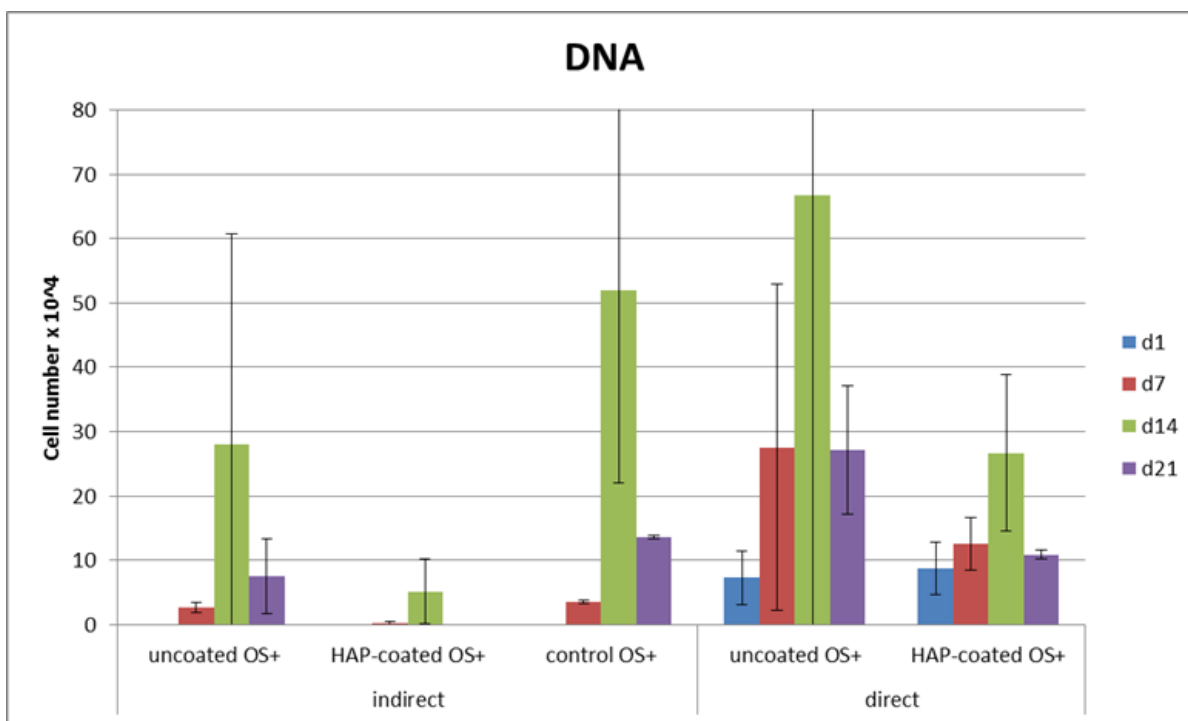


Figure 46. Cell response to the adhesion assay (DNA) on coated polished substrate after 1, 7, 14 and 21 days of culturing.

The fact that the cell numbers and proliferation rates on the coated polished substrate have decreased compared to the uncoated substrate suggests that the additional heat treatment during the coating process could have influenced cell behavior. The high temperature can lead to precipitation of Co and Cr on the surface and a decrease of the corrosion resistance (as shown in Figures 41, 43 and 44) through the protective surface layer breaks that promotes the release of the metal ions to the surrounding environment, resulting in the reduction of the cell viability. It occurs, because these metal ions bind with protein sites by displacing the original metal ions from their natural sites, which promote malfunctioning of cells and ultimately toxicity. Also, it has been reported that these metals bind to DNA and nuclear protein causing oxidative deterioration preliminary of biological macromolecules (Jaishankar et al., 2014).

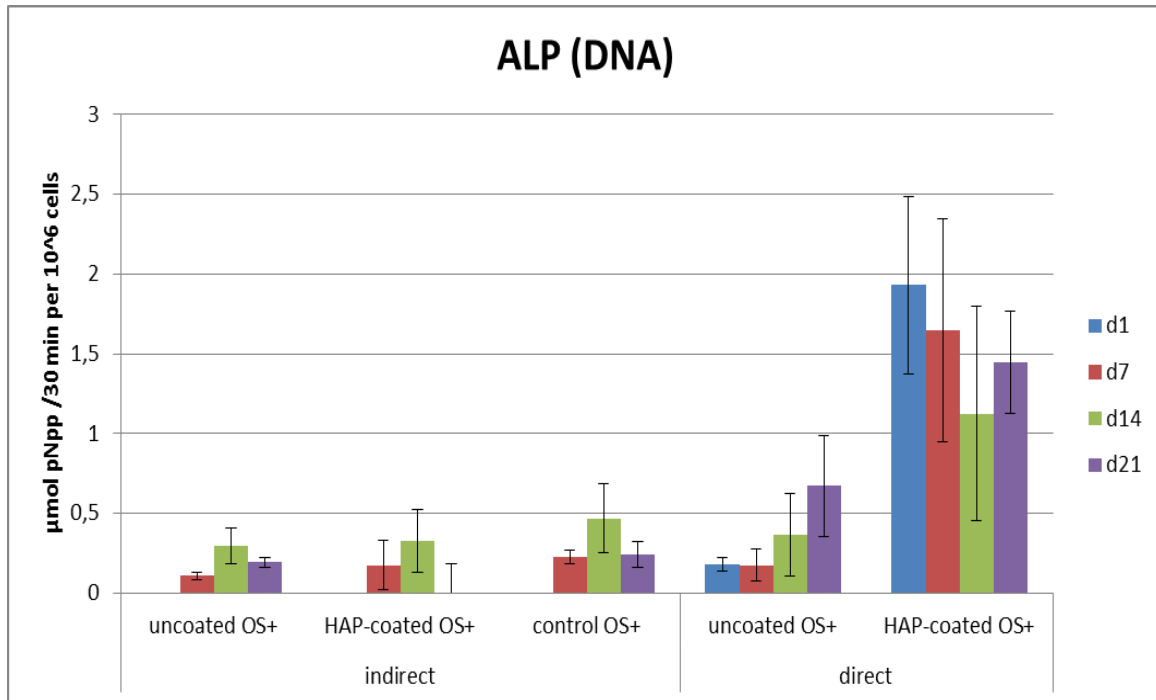


Figure 47. Specific ALP activity of cells cultivated in presence (indirect, left) or directly on (right) uncoated and coated polished substrates after 7, 14 and 21 days. Enzyme activity was normalized to the cell number using the values achieved by DNA quantification.

In order to prevent the integrity of the metallic substrate, such as oxidation and metal ion precipitation of the implanted material, the use of a controlled atmosphere in heat treatment and surface treatment showed good results concerning corrosion resistance and cell behavior. A study carried out by Yang et al. (Yang et al., 2009) proved that the use of vacuum in heat

treatment of plasma sprayed hydroxyapatite coatings improved the biological performance at 12 weeks (in vitro and in vivo results) and biological fixation in the long term clinical use. The oxidation control by application of high vacuum or inert atmosphere keep their mechanical and corrosion properties and, hence, to prevent the ion release. Therefore, it could lead to a more positive cell response. However, further biological test are required for further conclusions.

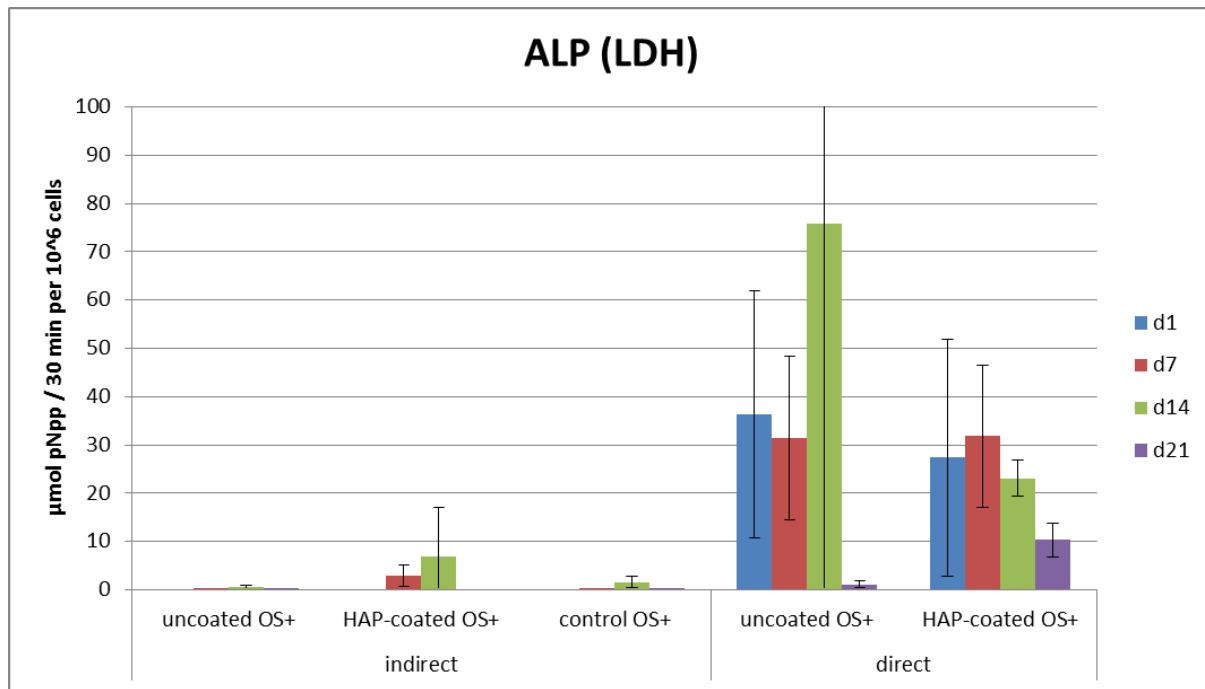


Figure 48. Cell response of the differentiation assay of ALP (LDH) activity on coated polished substrate after 7, 14 and 21 days for the indirect and direct method achieved by LDH activity quantification.

5. Conclusions

For the first time to our knowledge, pine oil as an eco-friendly material mixed with hydroxyapatite was used to coat a Co-15Cr-15W-10Ni alloy using a simple brushing method. A fully covered CoCr substrate with pure, crack free HAp coating was achieved after easily thermal removal of the PO and no evidence of impurities or other calcium phosphate phases was found in the coating by SEM, FTIR, XRD and DSC analysis after heat treatment. Wettability measurements proved that use of PO improved the wettability and distribution of the slurry on the metal alloy surface due to its low superficial tension and to functional groups that interacted with the metal, resulting in attractive forces between coating and substrate. The cross sections and pencil strength test confirmed a thickness of $\sim 20 \mu\text{m}$ and that there is a close interaction between HAp coating/substrate.

The differently rough surfaces (non-treated and altered by polishing, passivation and heat treatment) tested showed that is possible to cover all types and no significant differences were observed in the scratch resistance for the polished, passivated and non-treated substrates. The smoother substrates obtained a better scratch resistance (4H) and it suggest that smoother surfaces allow a more uniform dispersion as well as a closer contact of the HAp particles on the surfaces. However, the coated, heat treated substrate with high roughness ($R_a = 0.82 \mu\text{m}$) presented a lower scratch resistance (2H) with cracks in the coating. It is attributed to the heat treatment that promotes the formation of a non-uniform oxide layer and avoid the HAp particle distribution and a close contact to the substrate.

Bioactivity investigations in SBF solution showed a decrease of cracks after 7 days and all substrates kept covered until 21 days of soaking. SEM analysis confirms that coated passivated substrates have a better behavior than coated polished substrates due to groups formed on the substrate through the passivation treatment, which resulted after 14 days of soaking in SBF of the growth of apatite layers with leaf-like morphology. Cyclic voltammetry measurements indicated that the HAp coating deposited provide effective corrosion protection on CoCr substrate and no significant differences of the results were observed for the uncoated substrates (Pol and Pol_Pas).

The results showed that high temperature (800°C) treatment decrease corrosion resistance of the metal alloy and this could explain the decrease of the cell growth, since high temperatures without the control of oxidant atmosphere promote the breaking of passivating layer and it favors the cobalt precipitation on the surface. Overall, the good results of the interaction between

substrate and coating, corrosion resistance, morphology, wettability and degradation resistance suggests that further investigation as implant for bone replacement is very promising, but additional experiments concerning different temperatures and protective atmosphere during heat treatment are necessary in order to prevent the oxidation. With this probably the limited cytocompatibility, observed in the present study, could be overcome.

5.1 Future perspectives

In conclusion, this study allowed the deposition of HAp coating on CoCr substrates by mixing of HAp and PO, followed by a heat treatment for application as biomaterials in bone replacement. To our knowledge we are the first to study the use of PO to promote the adhesion of HAp coatings on metallic substrates. For this reason, further investigation could provide a better understanding about the interaction between substrate and coating. For a successful application as implants a deeper investigation of the cell behavior is needed using different cell types and varying temperatures for the heat treatment. Also utilization of a protective atmosphere during thermal removal of the PO and additional surfaces modifications should be explored. Furthermore, our results also suggest a possible deposition of other calcium phosphates mixed with PO, which can be investigated in combination with several metallic substrates.

6. References

- Adhesives.org. Adhesion - Cohesion. [accessed: 10/05/2017] URL: <http://www.adhesives.org/adhesives-sealants/science-of-adhesion/adhesion-cohesion>.
- Aihara H. 2009. Surface and biocompatibility study of electropolished Co-Cr alloy L605. San Jose State University, Faculty of the Department of General Engineering, Master's Thesis.
- Albayrak O, El-Atwani O, Altintas S. 2008. Hydroxyapatite coating on titanium substrate by electrophoretic deposition method: Effects of titanium dioxide inner layer on adhesion strength and hydroxyapatite decomposition. *Surf Coat Technol*, 202(11):2482–2487 DOI: 10.1016/j.surfcoat.2007.09.031.
- Allen MJ, Myer BJ, Millett PJ, Rushton N. 1997. The effects of particulate cobalt, chromium and cobalt-chromium alloy on human osteoblast-like cells in vitro. *J Bone Jt Surg Br*, 79(3):475–482 DOI: 10.1302/0301-620X.79B3.0790475.
- Al-Subai SG. 2011. Corrosion resistance of austenitic stainless steel in acetic acid solution containing bromide ions. University of Manchester, Faculty of Engineering and Physical Science, Dissertation.
- Anderson JM, Rodriguez A, Chang DT. 2008. Foreign body reaction to biomaterials. *Semin Immunol*, 20(2):86–100 DOI: 10.1016/j.smim.2007.11.004.
- Anissian L, Stark A, Dahlstrand H, Granberg B, Good V, Bucht E. 2002. Cobalt ions influence proliferation and function of human osteoblast-like cells. *Acta Orthop Scand*, 73(3):369–374 DOI: 10.1080/000164702320155400.
- APS Materials. Hydroxyapatite Coating | HA Bio-Coatings. APS Mater Inc [accessed: 01/24/2018] URL: <http://apsmaterials.com/biomedical/hydroxyapatite-coating/>.
- Aronov D, Rosen R, Ron EZ, Rosenman G. 2006. Tunable hydroxyapatite wettability: Effect on adhesion of biological molecules. *Process Biochem*, 41(12):2367–2372 DOI: 10.1016/j.procbio.2006.06.006.
- Arshanapalli SA. 2013. Fabrication of hydroxyapatite coated magnesium alloy for orthopedic bio-degradable metallic implant applications. Wichita State University, PhD Thesis.
- ASM Handbook. 2013. Introduction to Coating Design and Processing. ASM International.
- Asri RIM, Harun WSW, Hassan MA, Ghani SAC, Buyong Z. 2016. A review of hydroxyapatite-based coating techniques: Sol-gel and electrochemical depositions on biocompatible metals. *J Mech Behav Biomed Mater*, 57:95–108.

- Bai X, More K, Rouleau CM, Rabiei A. 2010. Functionally graded hydroxyapatite coatings doped with antibacterial components. *Acta Biomater*, 6(6):2264–2273 DOI: 10.1016/j.actbio.2009.12.002.
- Bakan F, Laçın O, Sarac H. 2013. A novel low temperature sol–gel synthesis process for thermally stable nano crystalline hydroxyapatite. *Powder Technol*, 233:295–302 DOI: 10.1016/j.powtec.2012.08.030.
- Bakrachevska E. 2014. Analysis of Corrosion Resistance Property of Cold Bended 316L and 6Mo Stainless Steel Pipes. University of Stavanger, Faculty of Science and Technology, Master`Thesis.
- Barbosa MC, Messmer NR, Brazil TR, Marciano FR, Lobo AO. 2013. The effect of ultrasonic irradiation on the crystallinity of nano-hydroxyapatite produced via the wet chemical method. *Mater Sci Eng C*, 33(5):2620–2625 DOI: 10.1016/j.msec.2013.02.027.
- Behl B, Papageorgiou I, Brown C, Hall R, Tipper JL, Fisher J, Ingham E. 2013. Biological effects of cobalt-chromium nanoparticles and ions on dural fibroblasts and dural epithelial cells. *Biomaterials*, 34(14):3547–3558 DOI: 10.1016/j.biomaterials.2013.01.023.
- Bernhardt A, Despang F, Lode A, Demmler A, Hanke T, Gelinsky M. 2009. Proliferation and osteogenic differentiation of human bone marrow stromal cells on alginate–gelatine–hydroxyapatite scaffolds with anisotropic pore structure. *J Tissue Eng Regen Med*, 3(1):54–62 DOI: 10.1002/term.134.
- Berstein A, Bemauer I, Marx R, Geurtsen W. 1992. Human cell culture studies with dental metallic materials. *Biomaterials*, 13(2):98–100 DOI: 10.1016/0142-9612(92)90002-6.
- Besra L, Liu M. 2007. A review on fundamentals and applications of electrophoretic deposition (EPD). *Prog Mater Sci*, 52(1):1–61 DOI: 10.1016/j.pmatsci.2006.07.001 DOI: 10.1016/j.pmatsci.2006.07.001.
- Bharati S, Sinha MK, Basu D. 2005. Hydroxyapatite coating by biomimetic method on titanium alloy using concentrated SBF. *Bull Mater Sci*, 28(6):617–621 DOI: 10.1007/BF02706352.
- Bitar D, Parvizi J. 2015. Biological response to prosthetic debris. *World J Orthop*, 6(2):172–189 DOI: 10.5312/wjo.v6.i2.172.
- Boccaccini AR, Keim S, Ma R, Li Y, Zhitomirsky I. 2010. Electrophoretic deposition of biomaterials. *J R Soc Interface*, 7(Suppl 5):S581–S613 DOI: 10.1098/rsif.2010.0156.focus.

- Boccaccini AR, Zhitomirsky I. 2002. Application of electrophoretic and electrolytic deposition techniques in ceramics processing. *Curr Opin Solid State Mater Sci*, 6(3):251–260 DOI: 10.1016/S1359-0286(02)00080-3.
- Brubaker JP. 2014. A diffusion model for cyclic voltammetry with nanostructured electrode surfaces. University of Dayton, School of Engineering, Master Thesis.
- Burnat B, Robak J, Leniart A, Piwoński I, Batory D. 2017. The effect of concentration and source of calcium ions on anticorrosion properties of Ca-doped TiO₂ bioactive sol-gel coatings. *Ceram Int* DOI: 10.1016/S1359-0286(02)00080-3.
- Cai Q, Feng Q, Liu H, Yang X. 2013. Preparation of biomimetic hydroxyapatite by biomineralization and calcination using poly(l-lactide)/gelatin composite fibrous mat as template. *Mater Lett*, 91:275–278 DOI: 10.1016/j.matlet.2012.09.101.
- Canillas M, Pena P, de Aza A, Rodríguez MA. 2017. Calcium phosphates for biomedical applications. *Bol Soc Esp Cerámica Vidr* [accessed: 09/19/2017] URL: <http://www.sciencedirect.com/science/article/pii/S0366317517300444>.
- Cao H, Liu X. 2013. Plasma-Sprayed Ceramic Coatings for Osseointegration. *Int J Appl Ceram Technol*, 10(1):1–10 DOI: 10.1111/j.1744-7402.2012.02770.x.
- Capuccini C, Torricelli P, Sima F, Boanini E, Ristoscu C, Bracci B, Socol G, Fini M, Mihailescu IN, Bigi A. 2008. Strontium-substituted hydroxyapatite coatings synthesized by pulsed-laser deposition: In vitro osteoblast and osteoclast response. *Acta Biomater*, 4(6):1885–1893 DOI: 10.1016/j.actbio.2008.05.005.
- Cassie ABD, Baxter S. 1944. Wettability of porous surfaces. *Trans Faraday Soc*, 40:546–551 DOI: 10.1039/TF9444000546.
- Chai CS, Ben-Nissan B. 1999. Bioactive nanocrystalline sol-gel hydroxyapatite coatings. *J Mater Sci Mater Med*, 10(8):465–469 DOI: 10.1023/A:1008992807888.
- Chaudhuri B, Mondal B, Modak DK, Pramanik K, Chaudhuri BK. 2013. Preparation and characterization of nanocrystalline hydroxyapatite from egg shell and K₂HPO₄ solution. *Mater Lett*, 97:148–150 DOI: 10.1016/j.matlet.2013.01.082.
- Chen Q, Thouas GA. 2015. Metallic implant biomaterials. *Mater Sci Eng R Rep*, 87(Supplement C):1–57 DOI: 10.1016/j.mser.2014.10.001.
- Chen W, Liu Y, Courtney HS, Bettenga M, Agrawal CM, Bumgardner JD, Ong JL. 2006. In vitro anti-bacterial and biological properties of magnetron co-sputtered silver-containing hydroxyapatite coating. *Biomaterials*, 27(32):5512–5517.
- Coşkun M İbrahim, Karahan İH, Yücel Y. 2014. Optimized Electrodeposition Concentrations for Hydroxyapatite Coatings on CoCrMo biomedical alloys by computational techniques. *Electrochimica Acta*, 150(Supplement C):46–54 DOI: 10.1016/j.electacta.2014.10.120.

- Crivella T. Past, Present and Future of Medical Coatings. [accessed: 01/09/2018] URL: <https://www.pfonline.com/articles/past-present-and-future-of-medical-coatings->.
- Cui FZ, Luo ZS. 1999. Biomaterials modification by ion-beam processing. *Surf Coat Technol*, 112(1):278–285 DOI: 10.1016/S0257-8972(98)00763-4.
- Demnati I, Grossin D, Errassifi F, Combes C, Rey C, Le Bolay N. 2014. Synthesis of fluor-hydroxyapatite powder for plasma sprayed biomedical coatings: Characterization and improvement of the powder properties. *Powder Technol*, 255:23–28 DOI: 10.1016/j.powtec.2013.10.022.
- Dinda GP, Shin J, Mazumder J. 2009. Pulsed laser deposition of hydroxyapatite thin films on Ti–6Al–4V: Effect of heat treatment on structure and properties. *Acta Biomater*, 5(5):1821–1830 DOI: 10.1016/j.actbio.2009.01.027.
- Disegi JA, Kennedy RL, Pilliar R. 1999. Cobalt-base Alloys for Biomedical Applications. ASTM International.
- Dorozhkin SV. 2013. A detailed history of calcium orthophosphates from 1770s till 1950. *Mater Sci Eng C*, 33(6):3085–3110 DOI: 10.1016/j.msec.2013.04.002.
- Dorozhkin SV, Epple M. 2002. Biological and medical significance of calcium phosphates. *Angew Chem Int Ed*, 41(17):3130–3146 DOI: 10.1002/1521-3773(20020902)41:17<3130::AID-ANIE3130>3.0.CO;2-1.
- Drevet R, Ben Jaber N, Fauré J, Tara A, Ben Cheikh Larbi A, Benhayoune H. 2016. Electrophoretic deposition (EPD) of nano-hydroxyapatite coatings with improved mechanical properties on prosthetic Ti6Al4V substrates. *Surf Coat Technol*, 301:94–99 DOI: 10.1016/j.surfcoat.2015.12.058.
- Duce C, Orsini S, Spepi A, Colombini MP, Tiné MR, Ribechini E. 2015. Thermal degradation chemistry of archaeological pine pitch containing beeswax as an additive. *J Anal Appl Pyrolysis*, 111:254–264 DOI: 10.1016/j.jaap.2014.10.020.
- Eliaz N, Shmueli S, Shur I, Benayahu D, Aronov D, Rosenman G. 2009. The effect of surface treatment on the surface texture and contact angle of electrochemically deposited hydroxyapatite coating and on its interaction with bone-forming cells. *Acta Biomater*, 5(8):3178–3191 DOI: 10.1016/j.actbio.2009.04.005.
- Encyclopedia Britannica. Paint | chemical product. *Encycl Br* [accessed: 05/07/2018] URL: <https://www.britannica.com/technology/paint>.
- Farrokhi-Rad M. 2018. Effect of morphology on the electrophoretic deposition of hydroxyapatite nanoparticles. *J Alloys Compd*, 741:211–222 DOI: 10.1016/j.jallcom.2018.01.101.

- Fatehi K, Moztarzadeh F, Solati-Hashjin M, Tahriri M, Rzvannia M, Ravarian R. 2008. In vitro biomimetic deposition of apatite on alkaline and heat treated Ti6Al4V alloy surface. *Bull Mater Sci*, 2008:101–108 DOI: 10.1007/s12034-008-0018-0.
- Fauchais PL, Heberlein JVR, Boulos MI. 2014. *Thermal Spray Fundamentals: From Powder to Part*. Springer Science & Business Media.
- Favre J. 2012. Recrystallization of L-605 Cobalt Superalloy during Hot-Working Process. INSA de Lyon and Tohoku University, Institute for Materials Research, Graduate School of Engineering, Tohoku University, Dissertation [accessed: 04/03/2018] URL: <http://doi.wiley.com/10.1002/9781118364987.ch32>.
- Favre J, Koizumi Y, Chiba A, Fabregue D, Maire E. 2013. Deformation Behavior and Dynamic Recrystallization of Biomedical Co-Cr-W-Ni (L-605) Alloy. *Metall Mater Trans A*, 44(6):2819–2830 DOI: 10.1007/s11661-012-1602-x.
- Fraunhofer V, Anthony J. 2012. Adhesion and Cohesion. *Int J Dent*, 2012:1–12 DOI: 10.1155/2012/951324.
- Furlong RJ, Osborn JF. 1991. Fixation of hip prostheses by hydroxyapatite ceramic coatings. *Bone Jt J*, 73-B(5):741–745 DOI: 10.1302/0301-620X.73B5.1654336.
- Giacchi JV, Morando CN, Fornaro O, Palacio HA. 2011. Microstructural characterization of as-cast biocompatible Co–Cr–Mo alloys. *Mater Charact*, 62(1):53–61 DOI: 10.1016/j.matchar.2010.10.011.
- Gomez E, Rani DA, Cheeseman CR, Deegan D, Wise M, Boccaccini AR. 2009. Thermal plasma technology for the treatment of wastes: A critical review. *J Hazard Mater*, 161(2):614–626 DOI: 10.1016/j.jhazmat.2008.04.017.
- Gossia E, Tonndorf R, Bernhardt A, Kirsten M, Hund R-D, Aibibu D, Cherif C, Gelinsky M. 2016. Electrostatic flocking of chitosan fibres leads to highly porous, elastic and fully biodegradable anisotropic scaffolds. *Acta Biomater*, 44:267–276 DOI: 10.1016/j.actbio.2016.08.022.
- Graziani G, Bianchi M, Sassoni E, Russo A, Marcacci M. 2017. Ion-substituted calcium phosphate coatings deposited by plasma-assisted techniques: A review. *Mater Sci Eng C*, 74:219–229 DOI: 10.1016/j.msec.2016.12.018.
- Gu YW, Khor KA, Cheang P. 2004. Bone-like apatite layer formation on hydroxyapatite prepared by spark plasma sintering (SPS). *Biomaterials*, 25(18):4127–4134 DOI: 10.1016/j.biomaterials.2003.11.030.
- Guo Y-J, Wang Y-Y, Chen T, Wei Y-T, Chu L-F, Guo Y-P. 2013. Hollow carbonated hydroxyapatite microspheres with mesoporous structure: Hydrothermal fabrication and drug delivery property. *Mater Sci Eng C*, 33(6):3166–3172 DOI: 10.1016/j.msec.2013.03.040.

- György E, Toricelli P, Socol G, Iliescu M, Mayer I, Mihailescu IN, Bigi A, Werckman J. 2004. Biocompatible Mn²⁺-doped carbonated hydroxyapatite thin films grown by pulsed laser deposition. *J Biomed Mater Res A*, 71A(2):353–358 DOI: 10.1002/jbm.a.30172.
- Habibovic P, Barrere F, Blitterswijk CA, Groot K, Layrolle P. 2002. Biomimetic hydroxyapatite coating on metal implants. *J Am Ceram Soc*, 85(3):517–522 DOI: 10.1111/j.1151-2916.2002.tb00126.x.
- Habraken W, Habibovic P, Epple M, Bohner M. 2016. Calcium phosphates in biomedical applications: materials for the future? *Mater Today*, 19(2):69–87 DOI: 10.1016/j.mattod.2015.10.008.
- Hallab NJ, Jacobs JJ. 2009. Biologic effects of implant debris. *Bull NYU Hosp Jt Dis*, 67(2):182–188.
- Hamdi M, Ide-Ektessabi A. 2003. Preparation of hydroxyapatite layer by ion beam assisted simultaneous vapor deposition. *Surf Coat Technol*, 163–164(Supplement C):362–367 DOI: 10.1016/S0257-8972(02)00625-4.
- Hansen DC. 2008. Metal corrosion in the human body: the ultimate bio-corrosion scenario. *Electrochem Soc Interface*, 17(2):31.
- Harun WSW, Asri RIM, Alias J, Zulkifli FH, Kadirgama K, Ghani SAC, Shariffuddin JHM. 2017. A comprehensive review of hydroxyapatite-based coatings adhesion on metallic biomaterials. *Ceram Int* DOI: 10.1016/j.ceramint.2017.10.162.
- HAYNES® 25 alloy/Principle Features. 2017. HAYNES® 25 alloy. URL: <http://haynesintl.com/docs/default-source/pdfs/new-alloy-brochures/high-temperature-alloys/brochures/25-brochure.pdf?sfvrsn=26>.
- Herrera A, Mateo J, Gil-Albarova J, Lobo-Escolar A, Ibarz E, Gabarre S, Más Y, Gracia L. 2015. Cementless Hydroxyapatite Coated Hip Prostheses. *BioMed Res Int*, 2015:1–13 DOI: 10.1155/2015/386461.
- Hiromoto S. 2008. Corrosion of metallic biomaterials in cell culture environments. *Electrochem Soc Interface*, 17(2):41.
- Huang Y, Hao M, Nian X, Qiao H, Zhang Xuejiao, Zhang Xiaoyun, Song G, Guo J, Pang X, Zhang H. 2016. Strontium and copper co-substituted hydroxyapatite-based coatings with improved antibacterial activity and cytocompatibility fabricated by electrodeposition. *Ceram Int*, 42(10):11876–11888 DOI: 10.1016/j.ceramint.2016.04.110.
- Jacobs JJ, Gilbert JL, Urban RM. 1998. Corrosion of metal orthopaedic implants. *JBJS*, 80(2):268–282 DOI: 10.2106/00004623-199802000-00015.

- Jäger M, Zilkens C, Zanger K, Krauspe R. 2007. Significance of nano-and microtopography for cell-surface interactions in orthopaedic implants. *BioMed Res Int*, 2007 [accessed: 09/18/2017] URL: <http://downloads.hindawi.com/journals/biomed/2007/069036.pdf>.
- Jaishankar M, Tseten T, Anbalagan N, Mathew BB, Beeregowda KN. 2014. Toxicity, mechanism and health effects of some heavy metals. *Interdiscip Toxicol*, 7(2) DOI: 10.2478/intox-2014-0009.
- Jove Science Education. Cyclic Voltammetry (CV) | Protocol. [accessed: 05/28/2018] URL: <https://www.jove.com/science-education/5502/cyclic-voltammetry-cv>.
- Juan-Díaz MJ, Martínez-Ibáñez M, Lara-Sáez I, da Silva S, Izquierdo R, Gurruchaga M, Goñi I, Suay J. 2016. Development of hybrid sol–gel coatings for the improvement of metallic biomaterials performance. *Prog Org Coat*, 96:42–51 DOI: 10.1016/j.porgcoat.2016.01.019.
- Jugowiec D, Łukaszczyk A, Cieniek Ł, Kowalski K, Rumian Ł, Pietryga K, Kot M, Pamuła E, Moskaiewicz T. 2017. Influence of the electrophoretic deposition route on the microstructure and properties of nano-hydroxyapatite/chitosan coatings on the Ti-13Nb-13Zr alloy. *Surf Coat Technol*, 324(Supplement C):64–79 DOI: 10.1016/j.surfcoat.2017.05.056.
- Kadlec J, Onderka F. 2013. Microstructural characterization, chemical composition and hardness of as-cast biocompatible CoCrMo alloy. *Littera Scr*, 6(2).
- Kassing R, Petkov P, Kulisch W, Popov C (eds). 2006. *Functional Properties of Nanostructured Materials*. Springer, Dordrecht.
- Kattimani VS, Kondaka S, Lingamaneni KP. 2016. Hydroxyapatite—Past, Present, and Future in Bone Regeneration. *Bone Tissue Regen Insights*, 2016(7):9–19.
- Khalid M, Mujahid M, Khan AN, Rawat RS. 2013. Dip Coating of Nano Hydroxyapatite on Titanium Alloy with Plasma Assisted γ -Alumina Buffer Layer: A Novel Coating Approach. *J Mater Sci Technol*, 29(6):557–564 DOI: 10.1016/j.jmst.2013.02.003.
- Koch CF, Johnson S, Kumar D, Jelinek M, Chrisey DB, Doraiswamy A, Jin C, Narayan RJ, Mihailescu IN. 2007. Pulsed laser deposition of hydroxyapatite thin films. *Mater Sci Eng C*, 27(3):484–494 DOI: 10.1016/j.msec.2006.05.025.
- Koju N, Sikder P, Ren Y, Zhou H, Bhaduri SB. 2017. Biomimetic coating technology for orthopedic implants. *Curr Opin Chem Eng*, 15:49–55 DOI: 10.1016/j.coche.2016.11.005.
- Kurtz S, Ong K, Lau E, Mowat F, Halpern M. 2007. Projections of primary and revision hip and knee arthroplasty in the United States from 2005 to 2030. *J Bone Jt Surg Am*:780–785 DOI: 10.2106/JBJS.F.00222.

- La FGD. 2014. A Rubric for Electrochemical Testing of Metallic Biomaterials. Faculty of California Polytechnic State University, San Luis Obispo, Master Thesis.
- Lakshmi RV, Bharathidasan T, Basu BJ. 2011. Superhydrophobic sol-gel nanocomposite coatings with enhanced hardness. *Appl Surf Sci*, 257(24):10421–10426 DOI: 10.1016/j.apsusc.2011.06.122.
- Latifi SM, Fathi M, Sharifnabi A, Varshosaz J. 2017. In vitro characterisation of a sol-gel derived in situ silica-coated silicate and carbonate co-doped hydroxyapatite nanopowder for bone grafting. *Mater Sci Eng C*, 75:272–278 DOI: 10.1016/j.msec.2017.02.078.
- Lee BS, Matsumoto H, Chiba A. 2011. Fractures in tensile deformation of biomedical Co–Cr–Mo–N alloys. *Mater Lett*, 65(5):843–846 DOI: 10.1016/j.matlet.2010.12.007.
- Li Z, Thompson BC, Dong Z, Khor KA. 2016. Optical and biological properties of transparent nanocrystalline hydroxyapatite obtained through spark plasma sintering. *Mater Sci Eng C*, 69:956–966 DOI: 10.1016/j.msec.2016.08.002.
- Lindahl C, Xia W, Engqvist H, Snis A, Lausmaa J, Palmquist A. 2015. Biomimetic calcium phosphate coating of additively manufactured porous CoCr implants. *Appl Surf Sci*, 353(Supplement C):40–47 DOI: 10.1016/j.apsusc.2015.06.056.
- Liu B, Zhang X, Xiao G, Lu Y. 2015. Phosphate chemical conversion coatings on metallic substrates for biomedical application: A review. *Mater Sci Eng C*, 47:97–104 DOI: 10.1016/j.msec.2014.11.038.
- Liu X, Bi XT, Liu C, Liu Y. 2012. Performance of Fe/AC catalyst prepared from demineralized pine bark particles in a microwave reactor. *Chem Eng J*, 193–194:187–195 DOI: 10.1016/j.cej.2012.04.039.
- Lu Y, Wu S, Gan Y, Li J, Zhao C, Zhuo D, Lin J. 2015. Investigation on the microstructure, mechanical property and corrosion behavior of the selective laser melted CoCrW alloy for dental application. *Mater Sci Eng C*, 49:517–525 DOI: 10.1016/j.msec.2015.01.023.
- Lu Y-P, Li M-S, Li S-T, Wang Z-G, Zhu R-F. 2004. Plasma-sprayed hydroxyapatite+titanium composite bond coat for hydroxyapatite coating on titanium substrate. *Biomaterials*, 25(18):4393–4403 DOI: 10.1016/j.biomaterials.2003.10.092.
- Luo X, Li X, Sun Y, Dong H. 2013. Tribocorrosion behavior of S-phase surface engineered medical grade Co–Cr alloy. *Wear*, 302(1–2):1615–1623 DOI: 10.1016/j.wear.2013.01.023.
- Luo ZS, Cui FZ, Feng QL, Li HD, Zhu XD, Spector M. 2000. In vitro and in vivo evaluation of degradability of hydroxyapatite coatings synthesized by ion beam-

- assisted deposition. *Surf Coat Technol*, 131(1):192–195 DOI: 10.1016/S0257-8972(00)00824-0.
- Lutz J, Díaz C, García JA, Blawert C, Mändl S. 2011. Corrosion behaviour of medical CoCr alloy after nitrogen plasma immersion ion implantation. *Surf Coat Technol*, 205(8–9):3043–3049 DOI: 10.1016/j.surfcoat.2010.11.017.
- M. E. EL-Dahshan, D. P. Whittle, J Stringer. 1976. The oxidation of cobalt-tungsten alloys. *Corros Sci*, 16 (2):77–82 DOI: 10.1016/0010-938X(76)90032-9.
- Mali SA, Nune KC, Misra RDK. 2016. Biomimetic nanostructured hydroxyapatite coatings on metallic implant materials. *Mater Technol*, 31(13):782–790 DOI: 10.1080/10667857.2016.1224609.
- Manso M, Jiménez C, Morant C, Herrero P, Martínez-Duart J. 2000. Electrodeposition of hydroxyapatite coatings in basic conditions. *Biomaterials*, 21(17):1755–1761 DOI: 10.1016/S0142-9612(00)00061-2.
- Marshall SJ, Bayne SC, Baier R, Tomsia AP, Marshall GW. 2010. A review of adhesion science. *Dent Mater*, 26(2):e11–e16 DOI: 10.1016/j.dental.2009.11.157.
- Materials Today. Fundamentals of Paint Adhesion. *Mater Today* [accessed: 11/21/2017] URL: <https://www.materialstoday.com/metal-finishing/features/fundamentals-of-paint-adhesion/>.
- Matković T, Matković P, Malina J. 2004. Effects of Ni and Mo on the microstructure and some other properties of Co–Cr dental alloys. *J Alloys Compd*, 366(1):293–297 DOI: 10.1016/j.jallcom.2003.07.004.
- Medicoat. Medical Coating - medicoat. [accessed: 06/01/2018] URL: <http://www.medicoat.com/coating-solutions/medical-coating/>.
- Mohseni E, Zalnezhad E, Bushroa AR. 2014. Comparative investigation on the adhesion of hydroxyapatite coating on Ti–6Al–4V implant: A review paper. *Int J Adhes Adhes*, 48:238–257 DOI: 10.1016/j.ijadhadh.2013.09.030.
- N Yukawa, K Sato. 1968. The correlation between microstructure and stress rupture properties of a Co-Cr-Ni-W (H-25) alloy. *Trans Jpn N T Met*, 9(International Conference on the Strength of Metals and Alloys, Tokyo,):680–686.
- Narayanan R, Seshadri SK, Kwon TY, Kim KH. 2008. Calcium phosphate-based coatings on titanium and its alloys. *J Biomed Mater Res B Appl Biomater*, 85B(1):279–299 DOI: 10.1002/jbm.b.30932.
- Niinomi M. 2010. *Metals for Biomedical Devices*: Elsevier.

- Niinomi M, Narushima T, Nakai M, others. 2015. Advances in metallic biomaterials. Heidelberg Springer [accessed: 09/18/2017] URL: <http://link.springer.com/content/pdf/10.1007/978-3-662-46836-4.pdf>.
- Onoki T, Hashida T. 2006. New method for hydroxyapatite coating of titanium by the hydrothermal hot isostatic pressing technique. *Surf Coat Technol*, 200(24):6801–6807 DOI: 10.1016/j.surfcoat.2005.10.016.
- Örnberg A. 2007. Study of electrochemical behaviour and corrosion resistance of materials for pacemaker lead applications. Royal Institute of Technology, School of Chemical Science and Engineering, Licentiate thesis.
- Oyane A, Kim H-M, Furuya T, Kokubo T, Miyazaki T, Nakamura T. 2003. Preparation and assessment of revised simulated body fluids. *J Biomed Mater Res*, 65A(2):188–195 DOI: 10.1002/jbm.a.10482.
- Paital SR, Dahotre NB. 2009a. Calcium phosphate coatings for bio-implant applications: Materials, performance factors, and methodologies. *Mater Sci Eng R Rep*, 66(1):1–70 DOI: 10.1016/j.mser.2009.05.001.
- Paital SR, Dahotre NB. 2009b. Wettability and kinetics of hydroxyapatite precipitation on a laser-textured Ca–P bioceramic coating. *Acta Biomater*, 5(7):2763–2772 DOI: 10.1016/j.actbio.2009.03.004.
- Pardun K, Treccani L, Volkmann E, Li Destri G, Marletta G, Streckbein P, Heiss C, Rezwan K. 2015. Characterization of Wet Powder-Sprayed Zirconia/Calcium Phosphate Coating for Dental Implants: Mixed Surface Coatings with Firm Adhesion. *Clin Implant Dent Relat Res*, 17(1):186–198 DOI: 10.1111/cid.12071.
- Paredes RSC, Amico SC, d'Oliveira ASCM. 2006. The effect of roughness and pre-heating of the substrate on the morphology of aluminium coatings deposited by thermal spraying. *Surf Coat Technol*, 200(9):3049–3055 DOI: 10.1016/j.surfcoat.2005.02.200.
- Park J, Lakes RS. 2007. *Biomaterials: an introduction*. Springer Science & Business Media.
- Patel NR, Gohil PP. 2012. A review on biomaterials: scope, applications & human anatomy significance. *Int J Emerg Technol Adv Eng*, 2(4):91–101.
- Ramesh S, Tan CY, Bhaduri SB, Teng WD. 2007. Rapid densification of nanocrystalline hydroxyapatite for biomedical applications. *Ceram Int*, 33(7):1363–1367 DOI: 10.1016/j.ceramint.2006.05.009.
- Rigo ECS, Boschi AO, Yoshimoto M, Allegrini S, König B, Carbonari MJ. 2004. Evaluation in vitro and in vivo of biomimetic hydroxyapatite coated on titanium dental implants. *Mater Sci Eng C*, 24(5):647–651 DOI: 10.1016/j.msec.2004.08.044.

- Roa JJ, Oncins G, Díaz J, Capdevila XG, Sanz F, Segarra M. 2011. Study of the friction, adhesion and mechanical properties of single crystals, ceramics and ceramic coatings by AFM. *J Eur Ceram Soc*, 31(4):429–449 DOI: 10.1016/j.jeurceramsoc.2010.10.023.
- Rodrigues SP, Alves CFA, Cavaleiro A, Carvalho S. 2017. Water and oil wettability of anodized 6016 aluminum alloy surface. *Appl Surf Sci*, 422:430–442 DOI: 10.1016/j.apsusc.2017.05.204.
- Romoni DC, Iskra J, Bele M, Demetrescu I, Milošev I. 2016. Elaboration and characterization of fluorohydroxyapatite and fluoroapatite sol- gel coatings on CoCrMo alloy. *J Alloys Compd*, 665:355–364 DOI: 10.1016/j.jallcom.2016.01.072.
- Rosales-Leal JI, Rodríguez-Valverde MA, Mazzaglia G, Ramón-Torregrosa PJ, Díaz-Rodríguez L, García-Martínez O, Vallecillo-Capilla M, Ruiz C, Cabrerizo-Vílchez MA. 2010. Effect of roughness, wettability and morphology of engineered titanium surfaces on osteoblast-like cell adhesion. *Colloids Surf Physicochem Eng Asp*, 365(1–3):222–229 DOI: 10.1016/j.colsurfa.2009.12.017.
- Royse F de S. 2010. Estudo das propriedades mecânicas e microestruturais de revestimento de liga de cobalto utilizando o processo de soldagem tig. Centro Federal de Educação Tecnológica Celso Suckow da Fonseca, Programa de Pós-Graduação em Engenharia Mecânica e Tecnologia de Materiais, Master Thesis.
- Rupp F, Gittens RA, Scheideler L, Marmur A, Boyan BD, Schwartz Z, Geis-Gerstorfer J. 2014. A review on the wettability of dental implant surfaces I: Theoretical and experimental aspects. *Acta Biomater*, 10(7):2894–2906 DOI: 10.1016/j.actbio.2014.02.040.
- Savarino L, Granchi D, Ciapetti G, Stea S, Donati ME, Zinghi G, Fontanesi G, Rotini R, Montanaro L. 1999. Effects of metal ions on white blood cells of patients with failed total joint arthroplasties. *J Biomed Mater Res A*, 47(4):543–550 DOI: 10.1002/(SICI)1097-4636(19991215)47:4<543::AID-JBM11>3.0.CO;2-G.
- Schmalz G, Garhammer P. 2002. Biological interactions of dental cast alloys with oral tissues. *Dent Mater*, 18(5):396–406 DOI: 10.1016/S0109-5641(01)00063-X.
- Shadanbaz S, Dias GJ. 2012. Calcium phosphate coatings on magnesium alloys for biomedical applications: a review. *Acta Biomater*, 8(1):20–30 DOI: 10.1016/j.actbio.2011.10.016.
- Shi D. 2006. Introduction to Biomaterials. World Scientific, London.
- Shojaee P, Afshar A. 2015. Effects of zirconia content on characteristics and corrosion behavior of hydroxyapatite/ZrO₂ biocomposite coatings codeposited by

- electrodeposition. *Surf Coat Technol*, 262:166–172 DOI: 10.1016/j.surfcoat.2014.12.044.
- Shu C, Yanwei W, Hong L, Zhengzheng P, Kangde Y. 2005. Synthesis of carbonated hydroxyapatite nanofibers by mechanochemical methods. *Ceram Int*, 31(1):135–138 DOI: 10.1016/j.ceramint.2004.04.012.
- Siddiqui K, Bawazeer N, Scaria Joy S. 2014. Variation in Macro and Trace Elements in Progression of Type 2 Diabetes. *Sci World J*, 2014 DOI: 10.1155/2014/461591.
- Silva-Bermudez P, Rodil SE. 2013. An overview of protein adsorption on metal oxide coatings for biomedical implants. *Surf Coat Technol*, 233(Supplement C):147–158 DOI: 10.1016/j.surfcoat.2013.04.028.
- Singh G, Singh S, Prakash S. 2011. Surface characterization of plasma sprayed pure and reinforced hydroxyapatite coating on Ti6Al4V alloy. *Surf Coat Technol*, 205(20):4814–4820 DOI: 10.1016/j.surfcoat.2011.04.064.
- Sobczak N, Singh M, Asthana R. 2005. High-temperature wettability measurements in metal/ceramic systems – Some methodological issues. *Curr Opin Solid State Mater Sci*, 9(4–5):241–253 DOI: 10.1016/j.cossms.2006.07.007.
- Sojitra P, Engineer C, Raval A, Kothwala D, Jariwala A, Kotadia H, Adeshara S, Mehta G. 2009. Surface enhancement and characterization of L-605 cobalt alloy cardiovascular stent by novel electrochemical treatment. *Artif Organs India*, 23(2):55–64.
- Song YW, Shan DY, Han EH. 2008. Electrodeposition of hydroxyapatite coating on AZ91D magnesium alloy for biomaterial application. *Mater Lett*, 62(17):3276–3279 DOI: 10.1016/j.matlet.2008.02.048.
- Souza K dos S. 2011. Estudo eletroquímico de ligas à base de cobalto-cromo e níquel-cromo. Universidade de São Paulo, text DOI: 10.11606/D.46.2011.tde-13102011-095002.
- Süntar I, Tumen I, Ustün O, Keleş H, Küpeli Akkol E. 2012. Appraisal on the wound healing and anti-inflammatory activities of the essential oils obtained from the cones and needles of *Pinus* species by in vivo and in vitro experimental models. *J Ethnopharmacol*, 139(2):533–540 DOI: 10.1016/j.jep.2011.11.045.
- Surmenev RA. 2012. A review of plasma-assisted methods for calcium phosphate-based coatings fabrication. *Surf Coat Technol*, 206(8–9):2035–2056 DOI: 10.1016/j.surfcoat.2011.11.002.
- Surmenev RA, Surmeneva MA, Ivanova AA. 2014. Significance of calcium phosphate coatings for the enhancement of new bone osteogenesis – A review. *Acta Biomater*, 10(2):557–579 DOI: 10.1016/j.actbio.2013.10.036.

- Tan H. 2016. In vivo surface roughness evolution of a stressed metallic implant. *J Mech Phys Solids*, 95:430–440 DOI: 10.1016/j.jmps.2016.05.025.
- Tanaka Y, Kurashima K, Saito H, Nagai A, Tsutsumi Y, Doi H, Nomura N, Hanawa T. 2009. In vitro short-term platelet adhesion on various metals. *J Artif Organs*, 12(3):182–186.
- Thanh DTM, Nam PT, Phuong NT, Que LX, Anh NV, Hoang T, Lam TD. 2013a. Controlling the electrodeposition, morphology and structure of hydroxyapatite coating on 316L stainless steel. *Mater Sci Eng C*, 33(4):2037–2045 DOI: 10.1016/j.msec.2013.01.018.
- Thanh DTM, Nam PT, Phuong NT, Que LX, Anh NV, Hoang T, Lam TD. 2013b. Controlling the electrodeposition, morphology and structure of hydroxyapatite coating on 316L stainless steel. *Mater Sci Eng C*, 33(4):2037–2045 DOI: 10.1016/j.msec.2013.01.018.
- Tiwari A, Wang R, Wei B. 2016. *Advanced Surface Engineering Materials*. John Wiley & Sons.
- Tsui YC, Doyle C, Clyne TW. 1998. Plasma sprayed hydroxyapatite coatings on titanium substrates Part 2: optimisation of coating properties. *Biomaterials*, 19(22):2031–2043 DOI: 10.1016/S0142-9612(98)00104-5.
- Ueki K, Ueda K, Narushima T. 2016. Microstructure and Mechanical Properties of Heat-Treated Co-20Cr-15W-10Ni Alloy for Biomedical Application. *Metall Mater Trans A*, 47(6):2773–2782 DOI: 10.1007/s11661-016-3488-5.
- Vahabzadeh S, Roy M, Bandyopadhyay A, Bose S. 2015. Phase stability and biological property evaluation of plasma sprayed hydroxyapatite coatings for orthopedic and dental applications. *Acta Biomater*, 17:47–55 DOI: 10.1016/j.actbio.2015.01.022.
- Valente J de, Célia do Rocio. 2011. Crescimento e reconstrução de óxidos de titânio em meios que simulam fluidos corpóreo. Universidade Federal do Paraná, Programa de pós-graduação em engenharia e ciências dos materiais, Master Thesis.
- Vasilescu C, Drob P, Vasilescu E, Demetrescu I, Ionita D, Prodana M, Drob SI. 2011. Characterisation and corrosion resistance of the electrodeposited hydroxyapatite and bovine serum albumin/hydroxyapatite films on Ti-6Al-4V-1Zr alloy surface. *Corros Sci*, 53(3):992–999 DOI: 10.1016/j.corsci.2010.11.033.
- Vogler EA. 1998. Structure and reactivity of water at biomaterial surfaces. *Adv Colloid Interface Sci*, 74(1):69–117 DOI: 10.1016/S0001-8686(97)00040-7.
- Vundelinckx BJ, Verhelst LA, De Schepper J. 2013. Taper Corrosion in Modular Hip Prostheses: Analysis of Serum Metal Ions in 19 Patients. *J Arthroplasty*, 28(7):1218–1223 DOI: 10.1016/j.arth.2013.01.018.

- Wang C, Ma J, Cheng W, Zhang R. 2002. Thick hydroxyapatite coatings by electrophoretic deposition. *Mater Lett*, 57(1):99–105 DOI: 10.1016/S0167-577X(02)00706-1.
- Wang Z, Yan Y, Qiao L. 2017. Protein adsorption on implant metals with various deformed surfaces. *Colloids Surf B Biointerfaces*, 156:62–70 DOI: 10.1016/j.colsurfb.2017.05.015.
- Wegman RF, Twisk JV. 2012. *Surface Preparation Techniques for Adhesive Bonding*. William Andrew.
- Wei M, Ruys AJ, Milthorpe BK, Sorrell CC, Evans JH. 2001. Electrophoretic deposition of hydroxyapatite coatings on metal substrates: a nanoparticulate dual-coating approach. *J Sol-Gel Sci Technol*, 21(1):39–48 DOI: 10.1023/A:1011201414651.
- Wen Z, Wang Z, Chen J, Zhong S, Hu Y, Wang J, Zhang Q. 2016. Manipulation of partially oriented hydroxyapatite building blocks to form flowerlike bundles without acid-base regulation. *Colloids Surf B Biointerfaces*, 142:74–80 DOI: 10.1016/j.colsurfb.2016.02.016.
- Wennerberg A, Albrektsson T. 2009. On Implant Surfaces: A Review of Current Knowledge and Opinions. *Int J Oral Maxillofac Implants*, 25(1):63–74.
- Wilson CJ, Clegg RE, Leavesley DI, Percy MJ. 2005. Mediation of Biomaterial–Cell Interactions by Adsorbed Proteins: A Review. *Tissue Eng*, 11(1–2):1–18 DOI: 10.1089/ten.2005.11.1.
- Xiao S, Gao R, Lu Y, Li J, Sun Q. 2015. Fabrication and characterization of nanofibrillated cellulose and its aerogels from natural pine needles. *Carbohydr Polym*, 119:202–209 DOI: 10.1016/j.carbpol.2014.11.041.
- Xiao XF, Liu RF. 2006. Effect of suspension stability on electrophoretic deposition of hydroxyapatite coatings. *Mater Lett*, 60(21):2627–2632 DOI: 10.1016/j.matlet.2006.01.048.
- Xu L-C, Siedlecki CA. 2007. Effects of surface wettability and contact time on protein adhesion to biomaterial surfaces. *Biomaterials*, 28(22):3273–3283 DOI: 10.1016/j.biomaterials.2007.03.032.
- Yang C-Y, Yang C-W, Chen L-R, Wu M-C, Lui T-S, Kuo A, Lee T-M. 2009. Effect of vacuum post-heat treatment of plasma-sprayed hydroxyapatite coatings on their in vitro and in vivo biological responses. *J Med Biol Eng*, 29:296–302.
- Yang Y, Kim K-H, Ong JL. 2005. A review on calcium phosphate coatings produced using a sputtering process—an alternative to plasma spraying. *Biomaterials*, 26(3):327–337 DOI: 10.1016/j.biomaterials.2004.02.029.

- Yao MX, Wu JBC, Xie Y. 2005. Wear, corrosion and cracking resistance of some W- or Mo-containing Stellite hardfacing alloys. *Mater Sci Eng A*, 407(1):234–244 DOI: 10.1016/j.msea.2005.06.062.
- Yunpeng. J et al. 2013. Current research in the pathogenesis of aseptic implant loosening associated with particulate wear debris. *Acta Orthop Belg*, 79:1–9.
- Zeng W-C, He Q, Sun Q, Zhong K, Gao H. 2012a. Antibacterial activity of water-soluble extract from pine needles of *Cedrus deodara*. *Int J Food Microbiol*, 153(1–2):78–84 DOI: 10.1016/j.ijfoodmicro.2011.10.019.
- Zeng W-C, He Q, Sun Q, Zhong K, Gao H. 2012b. Antibacterial activity of water-soluble extract from pine needles of *Cedrus deodara*. *Int J Food Microbiol*, 153(1):78–84 DOI: 10.1016/j.ijfoodmicro.2011.10.019.
- Zhang LC, Kiat ECS, Pramanik A. 2009. A Briefing on the Manufacture of Hip Joint Prostheses. *Adv Mater Res*, 76–78:212–216 DOI: 10.4028/www.scientific.net/AMR.76-78.212.
- Zheng Y, Xu X, Xu Z, Cai H, Wang J-Q. 2017. *Metallic Biomaterials: New Directions and Technologies*. John Wiley & Sons.
- Zheng Y, Yang Y, Deng Y. 2019. Dual therapeutic cobalt-incorporated bioceramics accelerate bone tissue regeneration. *Mater Sci Eng C*, 99:770–782 DOI: 10.1016/j.msec.2019.02.020.
- Zhitomirsky I, Gal-Or L. 1997. Electrophoretic deposition of hydroxyapatite. *J Mater Sci Mater Med*, 8(4):213–219 DOI: 10.1023/A:1018587623231.

Acknowledgements

I would like to express my gratitude to Prof. Dr. Michael Gelinsky and Prof. Luís Alberto Loureiro dos Santos for their guidance and kind support to promote this joint PhD between the two institutions. I would like especially to thank my German supervisor Prof. Dr. Michael Gelinsky for his patient supervision and his precious suggestions and meetings. After these great years in his group, I had opportunities to experience new challenges and improve my knowledge about biomaterials. Today, I am a new and better person and I will never forget all his efforts to help me to achieve my goals.

I am very grateful to my Brazilian supervisor Prof. Luís Alberto dos Santos for the opportunity and for encouraging me to performing this research. A special thank goes to Dr.-Ing. Matthias Schumacher, who was determinant for this research and helped me with a lot of patience in the introduction of cell tests, experiments and thesis corrections. I am profoundly grateful for his suggestions and kind support in all my difficulties and mainly for teaching me to move on even in the hardest moments.

I am grateful to all my colleagues from Centre for Translational Bone, Joint and Soft Tissue Research (TFO) and Laboratory of Biomaterials (Labiomat) for these years of support and friendship. I would especially like to thank my colleagues: Camila Escobar, Wilbur Trajano, Junio Augusto Rodrigues Pasqual, David Killian, Mandy Quade and Ulrike Weißflog for their support; you always were promptly available to help me mainly when I was working outside Brazil or Germany to accomplish this Bilateral PhD.

A special thanks to Dr.-Ing. Axel Spickenheuer from Leibniz-Institut für Polymerforschung Dresden (IPF) for the opportunity to join his group that was of great value during my PhD. Moreover, my special thanks to IPF Dresden for the given Fellowship.

I sincerely thank my colleague Nathália Oderich Muniz, who was one of my greatest supporters over the years. Another special thanks to my dear colleague Tilman Ahlfeld for his suggestions and corrections of this thesis. Many thanks for sharing great ideas in the materials science field.

I thank very much Prof. Dr. Telmo Strohaecker (*in memoriam*) for his kind comprehension and to open the doors of the Physical Metallurgy Laboratory (LAMEF) for using his facilities and equipment. I especially acknowledge Rogério Mendonça Soares and Anderson Pelufa for their kind help with samples cutting by electroerosion and metallography at LAMEF. I am very grateful to Prof. Dr. Kuroschi Rezwan for welcoming me in his group at the Advanced Ceramics Group at the University of Bremen, where I had a great opportunity to perform important experiments for this thesis.

I would like also to thank Dr. Annett Gebert from Leibniz Institute for Solid State and Materials Research (IFW) for her precious explanation about corrosion of metallic biomaterials and corrosion experiments. Also, I would like to thank Robby Unger for his help and attention during the corrosion experiments.

I am also very grateful to Fort Wayne Metals for the courtesy of the CoCr alloy and especially Ms. Patricia Wasserman for her kind assistance in providing the samples. I thank very much Prof. Dr. Moises Matos Dias and Prof. Dr. Halston Mozetic for their incentive, constructive discussion about materials science and engineering.

I would like to give an especial dedication to Dr. José Humberto dos Santos Almeida, my boyfriend, for his unconditional support and motivation. His fascination for the science was a great inspiration for I always give my best.

I am grateful to my best friend Janaina Fontative, friends and family for all support that I received during these years, especially in the difficult moments.

I would like to thank Coordination of Superior Level Staff Improvement (CAPES), ERAMUS and The Association of Friends and Sponsors of TU Dresden for their financial support provided to perform this research.

Last, but no least, I would like to express my gratitude to my parents for all their efforts and unconditional love.

Declarations

Technische Universität Dresden

Medizinische Fakultät Carl Gustav Carus

Promotionsordnung vom 24. Juli 2011

Erklärungen zur Eröffnung des Promotionsverfahrens

1. Hiermit versichere ich, dass ich die vorliegende Arbeit ohne unzulässige Hilfe Dritter und ohne Benutzung anderer als der angegebenen Hilfsmittel angefertigt habe; die aus fremden Quellen direkt oder indirekt übernommenen Gedanken sind als solche kenntlich gemacht.

2. Bei der Auswahl und Auswertung des Materials sowie bei der Herstellung des Manuskripts habe ich Unterstützungsleistungen von folgenden Personen erhalten: Dr. Matthias Schumacher, Dr. Annett Gebert.

3. Weitere Personen waren an der geistigen Herstellung der vorliegenden Arbeit nicht beteiligt. Insbesondere habe ich nicht die Hilfe eines kommerziellen Promotionsberaters in Anspruch genommen. Dritte haben von mir weder unmittelbar noch mittelbar geldwerte Leistungen für Arbeiten erhalten, die im Zusammenhang mit dem Inhalt der vorgelegten Dissertation stehen.

4. Die Arbeit wurde bisher weder im Inland noch im Ausland in gleicher oder ähnlicher Form einer anderen Prüfungsbehörde vorgelegt.

5. Die Inhalte dieser Dissertation wurden in folgender Form veröffentlicht:

- **Vechietti, F.A.**, Muniz., O.N., Rezwan, K., Schumacher, M., Gelinsky, M., Santos, L.A.L. Influence of cobalt chromium alloy surface modification on the roughness and wettability behavior of pine oil/hydroxyapatite as coating. Materials Research Express, v.6, p. 1-15, 2018.
- **Vechietti, F.A.**, Santos, L.A.L. Process of coating on substrate with bioceramic and substrate with surface coating with bioceramic, Patent number: BR10201701516, 2017.
- **Vechietti, F.A.**, Santos, L.A.L., Muniz, N.O., Marques, D. Fibers Obtaining and Characterization Using Poly (Lactic-co-Glycolic Acid) and Poly (Isoprene) Containing Hydroxyapatite and α -TCP Calcium Phosphate by Electrospinning Method. Key Engineering Materials, v. 631, p.173 – 178, 2014.
- Muniz, N. O., **Vechietti, F.A.**, Santos, L.A.L. Effect of Variation of Dispersant and Fluid in the Rapid Prototyping of Alumina. Key Engineering Materials, v.631, p.275 - 279, 2014.

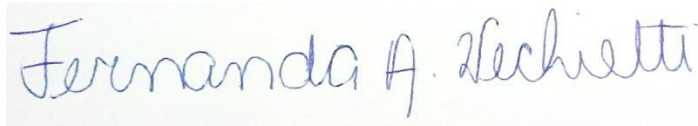
6. Ich bestätige, dass es keine zurückliegenden erfolglosen Promotionsverfahren gab.

7. Ich bestätige, dass ich die Promotionsordnung der Medizinischen Fakultät der Technischen Universität Dresden anerkenne.

8. Ich habe die Zitierrichtlinien für Dissertationen an der Medizinischen Fakultät der Technischen Universität Dresden zur Kenntnis genommen und befolgt.

Dresden, 10.07.2019

Unterschrift des Doktoranden:

A handwritten signature in blue ink that reads "Fernanda A. Lechietti". The signature is written in a cursive style with a clear, legible font.

**Hiermit bestätige ich die Einhaltung der folgenden aktuellen gesetzlichen
Vorgaben im Rahmen meiner Dissertation**

☐ das zustimmende Votum der Ethikkommission bei Klinischen Studien, epidemiologischen Untersuchungen mit Personenbezug oder Sachverhalten, die das Medizinproduktegesetz betreffen

Aktenzeichen der zuständigen Ethikkommission

.....303082014.....

☐ Die Einhaltung der Bestimmungen des Tierschutzgesetzes

Aktenzeichen der Genehmigungsbehörde zum Vorhaben/zur Mitwirkung

.....

☐ die Einhaltung des Gentechnikgesetzes
Projektnummer ...55-8811.71/135.....

☐ die Einhaltung von Datenschutzbestimmungen der Medizinischen Fakultät und des Universitätsklinikums Carl Gustav Carus.

Dresden, den 10.07.2019